PROCESS MODELING ASPECTS OF CHEMICAL-LOOPING WITH OXYGEN UNCOUPLING AND CHEMICAL-LOOPING COMBUSTION FOR SOLID FUELS

by

Asad Hasan Sahir

A dissertation submitted to the faculty of
The University of Utah
in partial fulfillment of the requirements for the degree of

Doctor of Philosophy

Department of Chemical Engineering

The University of Utah

August 2013

The University of Utah Graduate School

STATEMENT OF DISSERTATION APPROVAL

The dissertation of **Asad Hasan Sahir**

has been approved by the following supervisory committee members:

JoAnn S. Lighty	, Chair	**April 29,2013** Date Approved
Hong Yong Sohn	, Member	**April 29,2013** Date Approved
Terry A. Ring	, Member	**April 29,2013** Date Approved
Milind D. Deo	, Member	**April 29,2013** Date Approved
Kevin J. Whitty	, Member	**April 29,2013** Date Approved

and by **Milind D. Deo** , Chair of

the Department of **Chemical Engineering**

and by Donna M. White, Interim Dean of The Graduate School.

ABSTRACT

Chemical-looping combustion (CLC) is one of the candidate technologies that is currently being explored to reduce the energy penalty associated with capturing CO_2 from coal-fired power plants. In CLC, the fuel is burnt in the presence of oxygen supplied by an oxygen carrier circulating between two reactors, instead of atmospheric air. This dissertation investigates the requisite process modeling aspects for CLC for solid carbonaceous fuels, in particular focusing on chemical-looping with oxygen uncoupling (CLOU). In CLOU, gaseous phase oxygen is released by the decomposition of a metal oxide (e.g. CuO) in which the solid fuel burns to form CO_2. This contrasts with CLC, where the solid fuel has to be gasified initially to form syngas which subsequently reacts with the circulating oxygen carrier to form CO_2.

As a first step, the significance of the Law of Additive Reaction Times in identifying the controlling regime (internal/external mass transfer or chemical reaction) for CLC systems was explored. Two reported experimental studies for copper oxidation reaction in air reactor were reanalyzed. The methodology developed was applied to analyze the CuO decomposition and Cu_2O oxidation reaction for CLOU.

A rate analysis of the reported bench-scale batch fluidized-bed CLOU experimental data was performed to determine the kinetics of the CuO decomposition,

Cu_2O oxidation, and petcoke oxidation reactions. The obtained kinetics were subsequently utilized in the development of a fluidized-bed model to evaluate the oxygen and carbon dioxide concentration trends, and the results were validated against independently obtained experimental data reported in literature.

The kinetics obtained from the rate analysis of the CLOU reactions were employed in the development of a process model using ASPEN PLUS. Material and energy balance scenarios were developed for solid fuel combustion using a copper-based oxygen carrier for CLOU, and compared with CLC employing an iron-based oxygen carrier. The conceptual design principles will be employed in future investigations on a process development unit based on the CLOU process currently under construction at the University of Utah.

In memory of Prof. Adel F. Sarofim (1934-2011), Presidential Professor,
Chemical Engineering, University of Utah

TABLE OF CONTENTS

ACKNOWLEDGEMENTS

As Nobel Laureate and physicist, Albert Einstein strongly acknowledged, "It is the supreme art of the teacher to awaken joy in creative expression and knowledge." It has been my honor to be a graduate student at the University of Utah and be guided by outstanding academicians in my academic journey who embody Einstein's observation.

I express my sincere gratitude to Prof. JoAnn S. Lighty, my doctoral dissertation advisor, who had given me the opportunity to work on a topic in the area of chemical-looping combustion (CLC). Her continuous support and guidance throughout the course of my work has encouraged me to envision the larger picture associated with CLC. Under her supervision, I not only acquired the courage to navigate technical ambiguities associated with research, but I also learned the importance of effective technical and oral communication. Her insights were very valuable for a student who belongs to the first batch of chemical-looping combustion graduate researchers at the University of Utah.

Prof. Adel F. Sarofim, to whom this dissertation is dedicated, served as a major inspiration. He always encouraged his students to appreciate the importance of technology for serving society. His wisdom, vision, and wealth of knowledge on fuel combustion were invaluable in the development of an initial framework. As an international student at the University of Utah, he instilled in me not only the importance of the philosophy of conceptual design, but also provided insights on academic life in the United States

as my co-advisor until his death on December 4, 2011.

It was an honor and privilege for me to learn about gas-solid reactions and modeling of fluidized bed reactors from Prof. Hong Yong Sohn. In this work, with his help and guidance, I have been able to understand and apply some of the aspects on the topic to chemical-looping combustion (CLC) systems.

Professors Terry Ring, Kevin Whitty, and Milind Deo, as my supervisory committee members, have helped me in building the requisite intellectual foundation during technical discussions on various concepts in Chemical Engineering.

I wish to express my heartfelt gratitude to Prof. Henrik Leion at Chalmers University for providing the experimental data which enabled me to appreciate the seminal work on chemical-looping with oxygen uncoupling (CLOU) on solid fuels, and fostered scientific understanding.

Artur Cadore, James Dansie, and Nicholas Tingey, undergraduate students at the University of Utah, deserve a special mention as their hard work contributed in building the process modeling concepts.

I convey my gratitude to the chemical-looping combustion working group members at the University of Utah for their insightful suggestions and thoughtful comments during the group meetings. I am also thankful to the administrative staff at the Institute of Clean and Secure Energy and the Department of Chemical Engineering who contributed to my well-being.

This material is based upon work supported by the Department of Energy under Award Number DE-NT0005015. The author gratefully acknowledges their support.

CHAPTER 1

INTRODUCTION

1.1. Background

Coal is an important energy resource which contributed to 42% of the global electricity production in 2010.[1] In the United States, about 42% of the electricity was generated by coal in 2011.[2] The burning of fossil fuels constituted about 43% of the CO_2 emissions worldwide in 2010.[3] According to the Intergovernmental Panel on Climate Change (IPCC) "Most of the observed increase in global average temperatures since the mid-20th century is very likely due to the observed increase in anthropogenic greenhouse gas concentrations."[4] Davis et al.[5] have calculated cumulative future emissions of 496 gigatonnes of CO_2 (282 to 701 in lower- and upper-bounding scenarios) from combustion of fossil fuels by existing infrastructure between 2010 and 2060, contributing to forcing mean warming of 1.3°C (1.1° to 1.4°C) above the pre-industrial era, and atmospheric concentrations of CO_2 less than 430 parts per million.

The data on the U.S. energy-related CO_2 emissions determined on a sector basis indicate that the combustion of coal contributes to approximately 75% of the CO_2 emissions in the United States resulting from electric power generation.[6] The possibility of developing CO_2 capture technologies which will not only help in addressing environmental impact, but also facilitate in value addition to existing energy and chemical supply chains has invited significant research attention in the past decade. The generated CO_2 could be utilized for injecting into depleted oil wells to recover untapped oil.[7] The pursuit of identifying economic and environmentally friendly technologies for the exploitation and recycling of CO_2 is also an emerging area of active research interest.[8]

Three technology routes are being currently considered for carbon dioxide capture.[9,10] CO_2 can either be captured from the flue gas (i.e. end-products of combustion)

termed as 'postcombustion carbon capture', or the CO_2 concentration could be enhanced by burning a fuel in an oxygen-rich environment instead of air known as 'oxy-fuel combustion'. Another class of carbon capture processes exists where CO_2 can be captured before the fuel is burnt called 'precombustion'. The processes in the 'precombustion' category constitute those where the solid carbonaceous fuel (e.g. coal, petcoke) is gasified to form syngas, which is subsequently converted to a mixture of CO_2 and H_2 by a shift reaction. The CO_2 could be recovered from the CO_2-H_2 gas mixture by a gas separation process. The objective of all the three categories of carbon capture processes ('postcombustion', 'precombustion' and 'oxy-fuel') is to obtain a high-purity stream of CO_2 which is suitable for sequestration and subsequent utilization. These processes are energy intensive, and the energy requirements are derived from the power plant resulting in an efficiency loss. This efficiency loss for carbon capture processes is currently estimated to be of the order of 10% which is in addition to the efficiency penalty of 1-2% associated with pollutant removal.[10]

Coal plays a major role in powering anthropogenic activity worldwide. However, the possibility of the looming threat of a global climate change exists due to increase in temperatures resulting from greenhouse gas emissions, mostly from CO_2 generated from fossil fuel combustion. This scenario provides an adequate perspective for the scientific and engineering community to proactively explore innovative approaches to help humankind address the challenge of fostering sustainable economic growth, along with environmental protection for societal benefit.

According to Rubin et al.[11], about 60% of the breakdown of the energy penalty associated with supercritical and IGCC power plants is attributed to carbon capture (e.g.

thermal energy for solvent regeneration in "postcombustion" carbon capture, loss in water gas shift reaction in "precombustion" carbon capture, or electricity requirements for oxy-combustion). Approximately 30% of the energy penalty incurred is associated with CO_2 compression and about 10% of the remaining energy penalty breakdown is the requirement for operating fans and pumps. Thus, a technology possessing the potential to reduce the energy penalty associated with carbon capture will provide impetus to the development of carbon capture utilization and storage (CCUS) technologies.

1.2. Chemical-looping combustion (CLC)

Chemical-looping combustion(CLC) is a two-step combustion process in which the mixing of fuel and air is completely avoided.[12] The term "chemical-looping" has been used to define a cyclic process that uses a solid material, typically a metal oxide, as an oxygen carrier containing the oxygen required for the conversion of the fuel. To complete the loop, the oxygen depleted solid material must be re-oxidised to initiate a new cycle.[13] CLC can also be defined as an indirect combustion strategy in which a metal oxide serves as an oxygen carrier and a combustion intermediate between the air and the fuel.[14] CLC offers the promise to attain a significant reduction in energy penalty for solid fuels. In an ideal operational scenario, CLC shall require energy for CO_2 compression only, which accounts for an energy penalty of approximately 2.5% units.[15]

A typical CLC system consists of two reactors, a fuel reactor where the fuel combustion occurs, and an air reactor where the oxygen-depleted solid material is re-oxidised in contact with atmospheric air to initiate a new cycle. Figure 1.1 represents a conceptual schematic of a CLC process which consists of a fuel reactor and an air reactor.

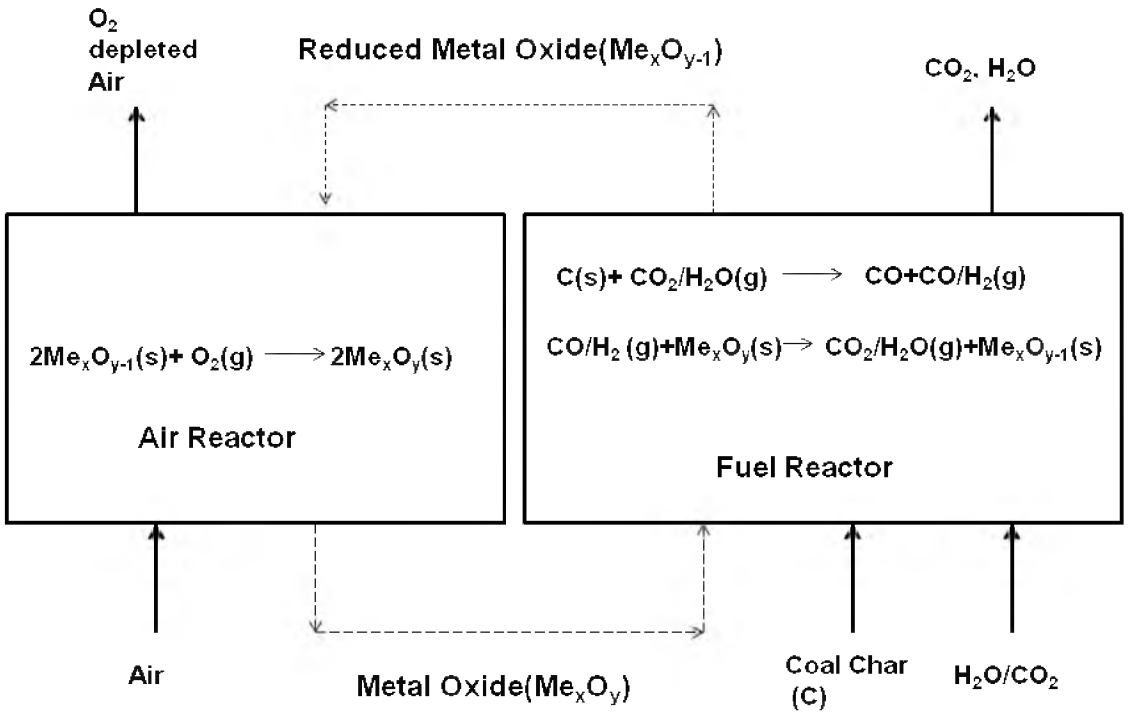

Figure 1.1 Schematic of a chemical-looping combustion(CLC) process for solid fuels (Based on nomenclature of Berguerand and Lyngfelt[16])

In the first step, the solid fuel to be burnt represented by C (for simplicity of analysis) is introduced in the fuel reactor. As no solid-solid coal char oxygen carrier reaction is expected to occur, the solid fuel is typically gasified using a gasification agent like CO_2 or H_2O.[16] The generated syngas subsequently reacts with the circulating oxygen carrier, typically a metal oxide represented by Me_xO_y.

The following reactions represent the processes which occur in a chemical-looping combustion system.

The general reactions (1.1) and (1.2) represent the processes which occur in the fuel reactor of a chemical-looping combustion system.

$$C(s) + CO_2/H_2O\ (g) \rightarrow CO(g)+CO/H_2(g) \quad (1.1)$$

$$CO/H_2(g)+ Me_xO_y(s) \rightarrow CO_2/H_2O(g)+ Me_xO_{y-1}(s) \quad (1.2)$$

The volatiles represented by C_nH_{2m} react through the general reaction (1.3) in the fuel reactor.

$$C_nH_{2m} + (2n+m)Me_xO_y \leftrightarrow nCO_2 + mH_2O + (2n+m)Me_xO_{y-1} \quad (1.3)$$

The reduced metal oxide Me_xO_{y-1} is regenerated in the air reactor through the general reaction (1.4).

$$O_2 + 2Me_xO_{y-1} \leftrightarrow 2Me_xO_y \quad (1.4)$$

The overall reaction in the air and fuel reactor is the same, as conventional combustion. The concept of chemical-looping was pioneered by Lewis and Gilliland in the 1950s at MIT.[17,18] The patents mention the production of carbon dioxide by using an iron oxide (US Patent 2,665,971) and copper oxide (US Patent 2,665,972). Richter and Knoche proposed that oxygen carriers could be utilized to reduce the loss in exergy associated with a highly irreversible combustion process by facilitating intermediate chemical reactions (Exergy has been defined as the maximum work output of any thermodynamic system or process which could be obtained, if the material in the system or the working fluid in the process is brought into equilibrium with the environment reversibly).[19]

Ishida, Zheng, and Akehata[20] proposed the concept of incorporating a loop of chemical reactions to reduce the exergy loss caused by the conversion of fuel energy to thermal energy in conventional LNG power plants, and introduced the term "chemical-looping combustion". Based on energy utilization diagrams, Ishida and Jin[21] in 1994 proposed the use of the loop of chemical reactions to reduce the exergy destruction caused by combustion and heat exchange processes; to recover the water used in the system; and to

recover CO_2 easily from the exhaust gas of the turbine. Thus, it was envisaged that CLC could be utilized potentially as a CO_2 capture process.

Lyngfelt, Leckner, and Mattisson[22] in 2001 proposed the first design of a 10 MW_{th} combustor based on the two interconnected fluidized bed concept consisting of a high velocity riser and a low velocity bubbling bed. After 2001, numerous studies have been reported in the areas of oxygen carrier characterization and development, reactor design and process development on chemical-looping combustion involving gaseous, liquid, and solid fuels.[13-15,23-25]

Table 1.1 outlines the chemical looping processes for CO_2 capture for solid fuel combustion as discussed by Adanez et al.[13] It is important to point out that the chemical-looping concept has also been utilized for developing process concepts to explore hydrogen production, co-production of hydrogen and electricity, and poly-generation applications.[24] The emphasis in this chapter shall be on understanding the broader process engineering challenges associated with solid fuels, which will be elaborated upon in later chapters of this dissertation.

1.3. Chemical-looping combustion: Challenges for solid fuels

According to Lyngfelt,[15] the following aspects comprise the major engineering challenges associated with the development of a CLC technology for solid fuels.

Firstly, the reaction between the circulating oxygen-carrier and char remaining after devolatilization is not direct, but requires an intermediate gasification step. In this context, the minimization of unconverted gases like H_2, CO, CH_4 in conjunction with a high solid fuel conversion leading to a significant CO_2 capture is an important design consideration.

Table 1.1 Chemical-looping combustion processes for CO_2 capture for combustion of solid fuels (Adapted from Adanez et al.[13])

Goal	Primary fuel	Process	Salient features
Combustion	Solid	Syngas-chemical-looping combustion	Solid fuel needs to be gasified in a gasification reactor and the syngas subsequently reacts with the oxygen carrier.
	Solid	In situ gasification and chemical-looping combustion	The solid fuel has to be gasified inside the fuel reactor and the syngas subsequently reacts with the oxygen carrier.
	Solid	Chemical-looping with oxygen uncoupling (CLOU)	The oxygen carrier has the property to release oxygen, which reacts with the fuel introduced.

Secondly, gasification of char requires a sufficient residence time, which necessitates minimization of char carryover to the air reactor.

Thirdly, high conversion of volatiles shall require reactor designs facilitating fuel and oxygen carrier contact. For in situ gasification and chemical-looping combustion, as the gasification of the fuel to form syngas occurs in the same reactor as the reaction with oxygen carrier, the location of fuel feed plays an important role in design of a CLC system for solid fuels.

Fourthly, the presence of ash in a solid fuel affects the lifetime of an oxygen carrier, resulting in loss of the material.

Lastly, the choice of oxygen carriers is not only restricted by high reactivity with fuel and oxygen, but also by their ability to convert fuel to CO_2 and H_2O with low fragmentation and attrition. The considered oxygen carriers should have a sufficient oxygen transfer capacity. Cost and environmental friendliness are also important attributes which oxygen carriers should also possess.

Table 1.2 outlines the operational experience in CLC units operated on solid fuels. As can be seen, there is interest in investigating materials based on iron, copper, manganese, nickel, and calcium for solid fuel combustion. Universities and industrial research organizations have played an important role in spearheading the development of chemical-looping combustion (CLC) for solid fuels till date.

Table 1.2 Chemical-looping combustion units for solid fuels (Based on Lyngfelt et al. [15] and Kim et al.[26])

Location	Size	Fuel	Oxides proposed/tested
ALSTOM	3 MW_{th}	coal	$CaSO_4$
ALSTOM (under ÉCLAIR program)	1 MW_{th}	coal	Naturally occurring ilmenite and composite copper oxide
University of Utah	100-200 kW_{th}	coal/natural gas	Oxygen carrier is under consideration for CLOU and CLC operation
Chalmers	100 kW_{th}	coal	ilmenite
Ohio-State	25 kW_{th}	coal	composite iron-based material
Chalmers	10 kW_{th}	coal, petcoke	ilmenite, Mn ore
Nanjing	10 kW_{th}	coal, biomass	NiO, Fe_2O_3
Nanjing	1 kW_{th}	coal, biomass	Fe_2O_3
CSIC	0.5 kW_{th} and 1.5 kW_{th}	coal	Ilmenite, CuO, Fe_2O_3

1.4. Chemical-looping with oxygen uncoupling (CLOU)

Chemical-looping with oxygen uncoupling (CLOU) is a variant of chemical-looping combustion (CLC) which exploits the property of certain metal oxides to release and capture oxygen at suitable temperatures and oxygen partial pressures, such as CuO/Cu_2O, Mn_2O_3/Mn_3O_4 and Co_3O_4/CoO.[27] As a consequence, the decomposition of the oxygen carrier to release oxygen and the combustion of the fuel in the fuel reactor proceeds through the reactions (1.5) and (1.6).

$$2Me_xO_y(s) \leftrightarrow 2Me_xO_{y-1}(s) + O_2(g) \quad (1.5)$$

$$C_nH_{2m} + (n+m/2)O_2(g) \leftrightarrow nCO_2(g) + mH_2O(g) \quad (1.6)$$

The oxygen carrier is regenerated in the air reactor by reaction with atmospheric air through reaction (1.7).

$$O_2(g) + 2Me_xO_{y-1}(s) \leftrightarrow 2Me_xO_y(s) \quad (1.7)$$

Figure 1.2 represents a schematic of the CLOU process which represents the reactions and the reactor scheme. In terms of potential oxygen carriers for CLOU, natural Cu ores,[28] Mn-based particles supported on Fe_2O_3 and NiO,[29,30] and perovskite-based ($CaMn_xTi_{1-x}O_3$)[31] have also been investigated. Copper oxide as an oxygen carrier has attracted significant research interest in CLOU studies as it has a higher reactivity, high oxygen transport capacity, and the thermodynamic limitation for complete combustion of fuel is absent.[32]

Figure 1.3 represents the equilibrium partial pressure of O_2 versus temperature for CuO-Cu_2O system. As can be observed from the figure, the equilibrium oxygen partial

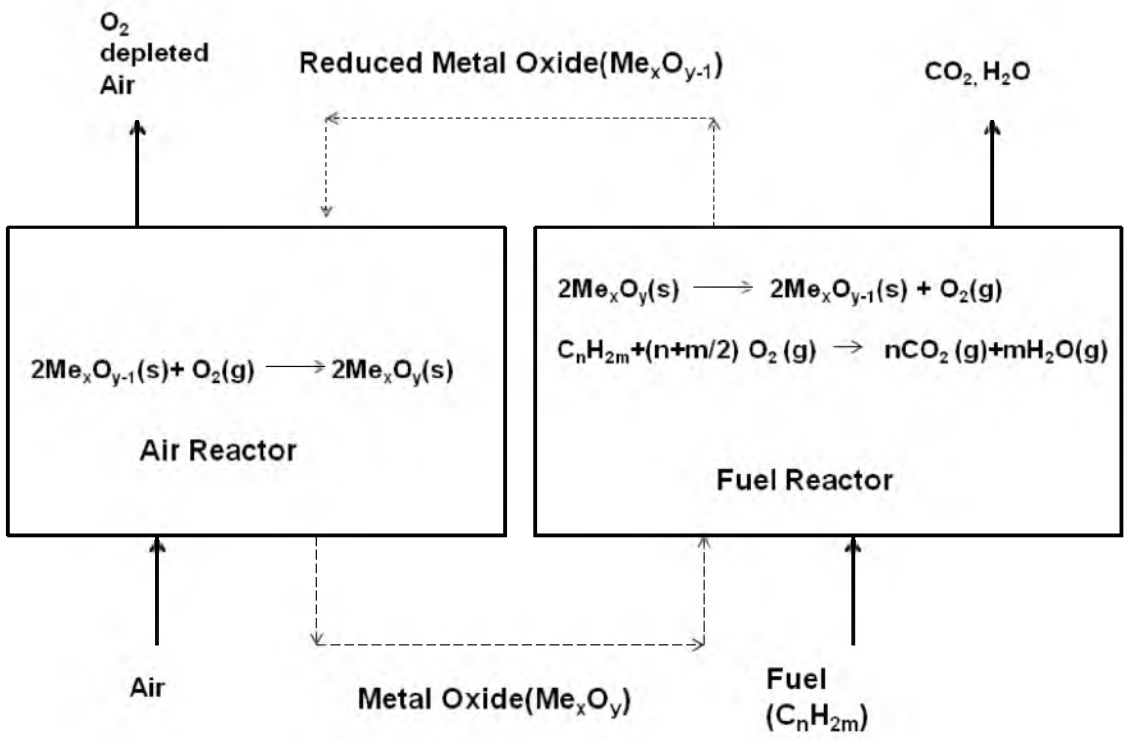

Figure 1.2 Schematic representing the CLOU process (Based on nomenclature of Mattisson et al.[33])

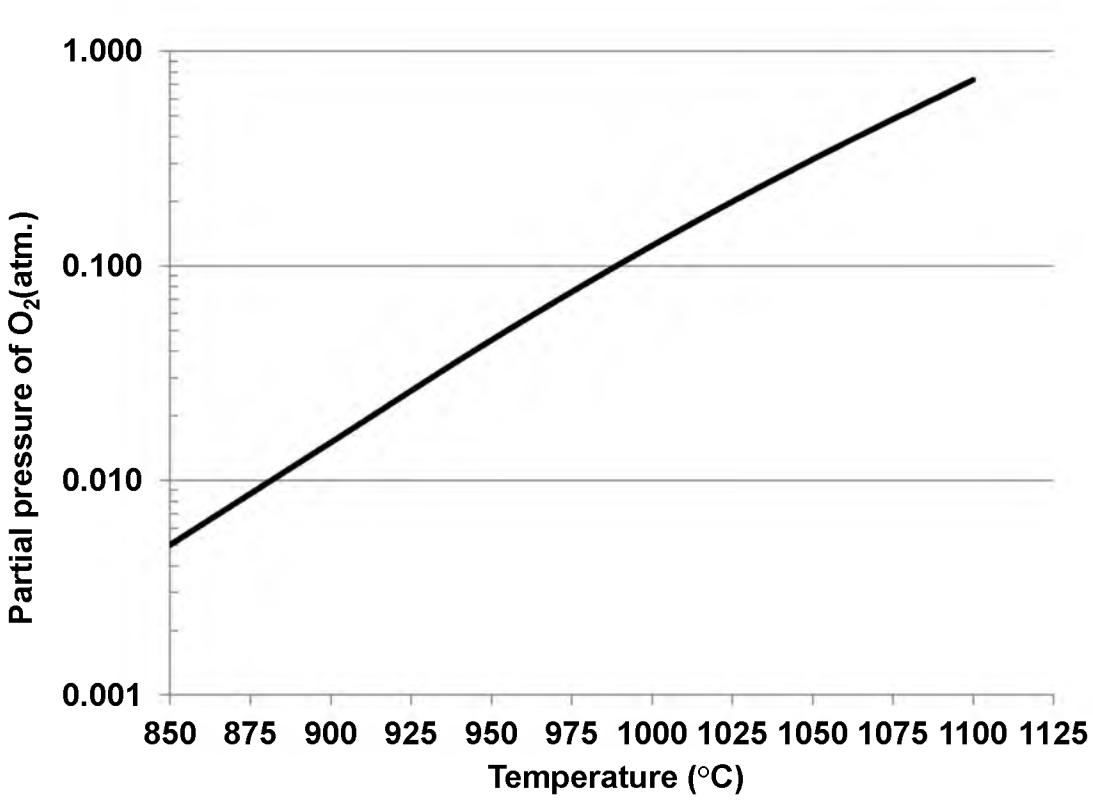

Figure 1.3 Partial pressure of gaseous phase oxygen over the metal oxide system CuO/Cu_2O (Based on the data of Mattisson et al.[27])

pressure for CuO varies between 0.005 atm. and 0.045 atm. between the temperature range of 850-950°C.

The CuO decomposition to Cu_2O in the fuel reactor is represented by chemical reaction (1.8).

$$4CuO(s) \leftrightarrow 2Cu_2O(s) + O_2(g); \qquad \Delta H_{R,900^\circ C} = 262.1 \text{ kJ/mol } O_2 \text{[34]} \qquad (1.8)$$

The Cu_2O is oxidized to CuO in the air reactor by the chemical reaction represented by (1.9).

$$2Cu_2O(s) + O_2(g) \leftrightarrow 4CuO(s); \qquad \Delta H_{R,850^\circ C} = -263.2 \text{ kJ/mol } O_2 \text{[27]} \qquad (1.9)$$

Lewis, Gilliland, and Sweeney[17] conducted experiments with gasification of carbon by CuO supported on silica gel, where the importance of O_2 release by CuO decomposition for the oxidation of carbonaceous particles was recognized. This phenomenon has also been discussed in a related patent (US Patent 2,665,972).[18] On investigations with CuO supported on Al_2O_3, de Diego et al.[35] concluded that oxygen carriers with CuO content greater than 20 wt.% always agglomerated in fluidized bed experiments. With Al_2O_3 as a support, partial loss of CuO through the formation of copper (II) aluminate – $CuAl_2O_4$ and copper (I) aluminate – $CuAlO_2$ occurs, which should be avoided for CLOU applications for retaining CuO as an active phase.[36]

Experiments in laboratory fluidized beds were performed in Chalmers[33,37,38] using 40% CuO on ZrO_2 as an oxygen carrier. Recent investigations on CuO with $MgAl_2O_4$[32,36,39,40] have been reported which indicate the suitability of CuO as a oxygen carrier. Table 1.3 lists the oxygen carriers that have been explored for the CLOU process

Table 1.3 CuO-based oxygen carriers investigated for CLOU with solid fuels

Investigators	Metal Oxides	Support Material	Size	Reacting Fuel
Lewis et al. (1951) [17]	10-15% CuO	Silica Gel	20-200 mesh (75-850 μm)	Metallurgical koppers-type coke
Leion et al. (2008)[41]	40% CuO	ZrO_2	125-180 μm	Lignite
Mattisson et al. (2009) [27,33]	40% CuO	ZrO_2	125-180 μm	Petroleum coke
Abad et al.(2012)[34] and Adanez-Rubio et al.(2013)[42]	60% CuO	$MgAl_2O_4$	100-200 μm	Anthracite, low volatile bituminous coal, medium volatile bituminous coal, lignite
Arjmand et al. (2012)[32]	40% CuO	$MgAl_2O_4$	125-180 μm	Devolatilized wood char

with solid fuels. A major advantage of CLOU over CLC is the large reduction in the time needed to convert solid carbonaceous fuels in the fuel reactor, as CLOU facilitates combustion instead of gasification, a property especially important for low reactivity fuels. In studies of CLC and CLOU in a batch reactor,[27,33,41,43,44] it was determined that, for a low reactivity solid, such as petroleum coke, the times for reaction of the coke with CO_2 were impractically long (50 minutes to reach 95% conversion at 950°C for the injection of 0.2 g of coke in 20 g of fluidized carrier composed of 60% Fe_2O_3 and 40% $MgAl_2O_4$, compared to 8 minutes when steam was added to produce an atmosphere of 50% H_2O) in batch fluidized bed experiments for CLC.[44] These times can be compared with a time of 30 s required to react 0.1 g of petroleum coke completely in 15 g of fluidized CuO/ZrO_2 at 955°C for CLOU experiments.[33] Abad et al. (2012), in their experiments on a continuously operated 1.5 kW_{th} CLC unit, have reported a sixty fold increase in the conversion rates of a bituminous coal with CLOU using a CuO-based oxygen carrier as compared to CLC using ilmenite.[34] It is hoped that the reduced reaction times for solid fuels achievable with CLOU will result in reductions in the size for the fuel reactor and the total amount of oxygen carrier.

A second advantage of CLOU relative to CLC is that the reactions in both the fuel and air reactors are exothermic. The circulation rate of the oxygen carrier in CLOU can therefore be determined solely on the basis of providing the oxygen to the fuel in the air reactor. In contrast, the circulation rate in CLC reactors is determined by the need to transfer energy from the air reactor to supply the endothermic reactions in the fuel reactor. This fact has been investigated in detail in Chapter 5 of this dissertation.

A third advantage is that the fuel reactor is overall oxidizing so that sulfur compounds released by high sulfur fuels will be in the form primarily of SO_2. This has the

advantage of eliminating problems with sulphide formation by the oxygen carrier. The formation of $CuSO_4$ is also not favored thermodynamically with unrealistically high concentrations of SO_x, in excess of 30,000 ppm, required to form the sulfate at 600°C, and the concentration needed increases rapidly as temperature is increased.[41]

1.5. Objective of this work

The necessity of exploring a process which can address CO_2 capture from coal-fired power plants with reduced energy penalty makes chemical-looping combustion a promising candidate. The potential offered in exploiting the release of gas phase oxygen to facilitate combustion reactions in chemical-looping with oxygen uncoupling (CLOU), as an alternative to slower gasification reactions, encourages further investigation. The objective of the dissertation is to investigate process design principles through rate analysis, material and energy balances, and reactor modeling which will advance the understanding of key aspects in developing CLOU for a pilot-scale process development unit.

1.6. Organization of the dissertation

This dissertation has been divided into five chapters. In the next chapter, the utility of the Law of Additive Reaction Times in identifying the role of chemical reaction (or rapid pore diffusion), internal, and external mass transfer control for reactions in chemical-looping combustion (CLC) systems has been investigated. The role of particle size and its effect on the controlling regime has been illustrated with the help of previously reported experimental data on Cu oxidation in the air reactor of a CLC system as an illustrative example.

In the third chapter, a rate analysis of CLOU experiments for CuO/ZrO_2 particles with Mexican Petcoke as a fuel conducted by Leion[37] has been performed. The insights gathered on identifying the relative importance of chemical reaction and mass transfer in

CLC reactions discussed in the previous chapter have been applied to the rate analysis for the CLOU experimental data of Leion.[27,33,37]

The fourth chapter discusses the development of a bubbling fluidized bed model for the fuel reactor based on the rate analysis for CLOU with CuO/ZrO_2 particles as discussed in Chapter 3.

The fifth chapter consists of a procedure to determine the optimum circulation rate and residence time utilizing insights gathered from rate analysis for CLOU with CuO/ZrO_2 particles. These calculations lay the foundation to perform a material and energy balance using ASPEN PLUS for the CLOU process for solid fuels. The results of the CLOU process are compared with a process model for CLC with a 60% Fe_2O_3 supported on Al_2O_3 as an oxygen carrier using coal as a fuel.

1.7. References

1. IEA, Power Generation from Coal- Measuring and Reporting Efficiency Performance and CO_2 Emissions. International Energy Agency: 2010. http://www.iea.org/ciab/papers/power_generation_from_coal.pdf (accessed January 18, 2013).

2. EIA Electricity Explained :Electricity in the United States. http://www.eia.gov/energyexplained/index.cfm?page=electricity_in_the_united_states (accessed January 18, 2013).

3. IEA Statistics CO_2 emissions from fuel combustion Highlights. International Energy Agency: 2012. http://www.iea.org/publications/freepublications/publication/name,32870,en.html (accessed January 18, 2013).

4. IPCC, *Summary for Policymakers.In Climate Change 2007: The Physical Science Basis. Contribution of Working Group I to the Fourth Assessment Report of the Intergovernmental Panel on Climate Change,* Cambridge University Press,Cambridge, United Kingdom and New York, NY, USA, 2007.

5. Davis, S. J.; Caldeira, K.; Matthews, H. D., Future CO_2 Emissions and Climate Change from Existing Energy Infrastructure. *Science* **2010,** *329* (5997), 1330-1333.

6. Annual Energy Outlook 2012 with Projections to 2035,DOE/EIA-0383. www.eia.gov/forecasts/aeo (accessed September 13, 2012).

7. McConnell, C., Adding "utilization" to Carbon Capture and Storage. http://energy.gov/articles/adding-utilization-carbon-captureand-storage (accessed September 13, 2012).

8. Peters, M.; Köhler, B.; Kuckshinrichs, W.; Leitner, W.; Markewitz, P.; Müller, T. E., Chemical technologies for exploiting and recycling carbon dioxide into the value chain. *ChemSusChem* **2011,** *4* (9), 1216-1240.

9. Markewitz, P.; Kuckshinrichs, W.; Leitner, W.; Linssen, J.; Zapp, P.; Bongartz, R.; Schreiber, A.; Müller, T. E., Worldwide innovations in the development of carbon capture technologies and the utilization of CO_2. *Energy and Environmental Science* **2012,** *5* (6), 7281-7305.

10. Riensche, E.; Nazarko, J.; Schiebahn, S.; Weber, M.; Zhao, L.; Stolten, D., Capture options for coal power plants. In *Efficient Carbon Capture for Coal Power Plants*, Stolten, D., Scherer, V., Ed. Wiley VCH: 2011.

11. Rubin, E. S.; Mantripragada, H.; Marks, A.; Versteeg, P.; Kitchin, J., The outlook for improved carbon capture technology. *Progress in Energy and Combustion Science* **2012,** *38* (5), 630-671.

12. Kolbitsch, P., *Chemical looping combustion for 100% carbon capture Design operation and modeling of a 120 kW pilot rig*. Sudwestdeutscher Verlag fur Hochschulschriften: 2009.

13. Adanez, J.; Abad, A.; Garcia-Labiano, F.; Gayan, P.; de Diego, L. F., Progress in Chemical-Looping Combustion and Reforming technologies. *Progress in Energy and Combustion Science* **2012,** *38* (2), 215-282.

14. Fan, L. S., *Chemical Looping Systems for Fossil Energy Conversions*. Wiley-AIChE: Hoboken, New Jersey, 2010.

15. Lyngfelt, A., Chemical-looping combustion of solid fuels-status of development. In *2nd International Conference on Chemical Looping*, Darmstadt, Germany, 2012.

16. Berguerand, N.; Lyngfelt, A., Chemical-looping combustion of petroleum coke using ilmenite in a 10 kW_{th} unit-high-temperature operation. *Energy Fuels* **2009,** *23* (10), 5257-5268.

17. Lewis, W. K.; Gilliland, E. R.; Sweeney, M. P., Gasification of Carbon, Metal Oxides in a Fluidized Powder Bed. *Chem. Eng. Prog.* **1951,** *47*, 251-256.

18. Lewis, W. K.; Gilliland, E. R., Production of pure carbon dioxide. U.S. Patent 2,665,971 and U.S. Patent 2,665,972, January 12,1954.

19. Richter, H. J.; Knoche, K. F., Reversibility of combustion process. *ACS Symposium Series* **1983,** *235* (235), 71-85.

20. Ishida, M.; Zheng, D.; Akehata, T., Evaluation of a chemical-looping-combustion power-generation system by graphic exergy analysis. *Energy* **1987,** *12* (2), 147-154.

21. Ishida, M.; Jin, H., A new advanced power-generation system using chemical-looping combustion. *Energy* **1994,** *19* (4), 415-422.

22. Lyngfelt, A.; Leckner, B.; Mattisson, T., A fluidized-bed combustion process with inherent CO_2 separation; Application of chemical-looping combustion. *Chemical Engineering Science* **2001,** *56* (10), 3101-3113.

23. Hossain, M. M.; de Lasa, H. I., Chemical-looping combustion (CLC) for inherent CO_2 separations-a review. *Chemical Engineering Science* **2008,** *63* (18), 4433-4451.

24. Moghtaderi, B., Review of the Recent Chemical Looping Process Developments for Novel Energy and Fuel Applications. *Energy Fuels* **2011,** *26* (1), 15-40.

25. Lyngfelt, A., Oxygen carriers for chemical-looping combustion 4000 h of operational experience. *Oil & Gas Science and Technology - 4000 h of operational experience* **2011,** *66* (2), 161-172.

26. Kim, H. R.; Wang, D.; Zeng, L.; Bayham, S.; Tong, A.; Chung, E.; Kathe, M. V.; Luo, S.; McGiveron, O.; Wang, A.; Chen, D.; Fan, L.-S., Coal direct chemical looping combustion process: Design and operation of a 25-kW_{th} sub-pilot unit. *Fuel* **2013**,*108*,370-384.

27. Mattisson, T.; Lyngfelt, A.; Leion, H., Chemical-looping with oxygen uncoupling for combustion of solid fuels. *International Journal of Greenhouse Gas Control* **2009,** *3* (1), 11-19.

28. Wen, Y.; Li, Z..; Xu, L.; Cai, N., Experimental Study of Natural Cu Ore Particles as Oxygen Carriers in Chemical Looping with oxygen uncoupling (CLOU). *Energy Fuels* **2012,** *26* (6), 3919-3927.

29. Shulman, A.; Cleverstam, E.; Mattisson, T.; Lyngfelt, A., Manganese/iron, manganese/nickel, and manganese/silicon oxides used in chemical-looping with oxygen uncoupling (CLOU) for combustion of methane. *Energy Fuels* **2009,** *23* (10), 5269-5275.

30. Azimi, G.; Leion, H.; Rydén, M.; Mattisson, T.; Lyngfelt, A., Investigation of Different Mn–Fe Oxides as Oxygen Carrier for Chemical-Looping with Oxygen uncoupling (CLOU). *Energy Fuels* **2012,** *27* (1), 367-377.

31. Rydén, M.; Lyngfelt, A.; Mattisson, T., $CaMn_{0.875}Ti_{0.125}O_3$ as oxygen carrier for chemical-looping combustion with oxygen uncoupling (CLOU)-Experiments in a continuously operating fluidized-bed reactor system. *International Journal of Greenhouse Gas Control* **2011,** *5* (2), 356-366.

32. Arjmand, M.; Keller, M.; Leion, H.; Mattisson, T.; Lyngfelt, A., Oxygen Release and Oxidation Rates of $MgAl_2O_4$-Supported CuO Oxygen Carrier for Chemical-looping combustion with oxygen uncoupling (CLOU). *Energy Fuels* **2012,** *26* (11), 6528-6539.

33. Mattisson, T.; Leion, H.; Lyngfelt, A., Chemical-looping with oxygen uncoupling using CuO/ZrO_2 with petroleum coke. *Fuel* **2009,** *88* (4), 683-690.

34. Abad, A.; Adánez-Rubio, I.; Gayán, P.; García-Labiano, F.; de Diego, L. F.; Adánez, J., Demonstration of chemical-looping with oxygen uncoupling (CLOU) process in a 1.5 kW_{th} continuously operating unit using a Cu-based oxygen-carrier. *International Journal of Greenhouse Gas Control* **2012,** *6*, 189-200.

35. de Diego, L. F.; Gayán, P.; García-Labiano, F.; Celaya, J.; Abad, A.; Adánez, J., Impregnated CuO/Al_2O_3 oxygen carriers for chemical-looping combustion: Avoiding fluidized bed agglomeration. *Energy Fuels* **2005,** *19* (5), 1850-1856.

36. Arjmand, M.; Azad, A.-M.; Leion, H.; Lyngfelt, A.; Mattisson, T., Prospects of Al_2O_3 and $MgAl_2O_4$-Supported CuO Oxygen Carriers in Chemical-Looping Combustion (CLC) and Chemical-Looping with oxygen uncoupling (CLOU). *Energy Fuels* **2011,** *25* (11), 5493-5502.

37. Leion, H., Chemical-Looping Combustion with Solid Fuels. Ph.D. Dissertation, Chalmers University of Technology, Göteborg, Sweden, 2007.

38. Leion, H.; Mattisson, T.; Lyngfelt, A., Using chemical-looping with oxygen uncoupling (CLOU) for combustion of six different solid fuels. *Energy Procedia* **2009,** *1* (1), 447-453.

39. Adánez-Rubio, I.; Gayán, P.; García-Labiano, F.; de Diego, L. F.; Adánez, J.; Abad, A., Development of CuO-based oxygen-carrier materials suitable for Chemical-looping with oxygen uncoupling (CLOU) process. *Energy Procedia* **2011,** *4* (0), 417-424.

40. Gayán, P.; Adánez-Rubio, I.; Abad, A.; de Diego, L. F.; García-Labiano, F.; Adánez, J., Development of Cu-based oxygen carriers for Chemical-looping with oxygen uncoupling (CLOU) process. *Fuel* **2012,** *96* (0), 226-238.

41. Leion, H.; Mattisson, T.; Lyngfelt, A., Combustion of a German Lignite Using Chemical-looping with oxygen uncoupling (CLOU). In *The 33rd International Technical Conference on Coal Utilization & Fuel Systems*, Clearwater, FL, 2008.

42. Adánez-Rubio, I.; Abad, A.; Gayán, P.; de Diego, L. F.; García-Labiano, F.; Adánez, J., Performance of CLOU process in the combustion of different types of coal with CO_2 capture. *International Journal of Greenhouse Gas Control* **2013,** *12* (0), 430-440.

43. Leion, H.; Mattisson, T.; Lyngfelt, A., Solid fuels in chemical-looping combustion. *International Journal of Greenhouse Gas Control* **2008,** *2* (2), 180-193.

44. Leion, H.; Mattisson, T.; Lyngfelt, A., The use of petroleum coke as fuel in chemical-looping combustion. *Fuel* **2007,** *86* (12-13), 1947-1958.

CHAPTER 2

KINETICS OF COPPER OXIDATION IN THE AIR REACTOR OF A CHEMICAL LOOPING COMBUSTION SYSTEM USING THE LAW OF ADDITIVE REACTION TIMES

Asad H. Sahir, JoAnn S. Lighty
Department of Chemical Engineering
The University of Utah
Salt Lake City, Utah, 84112-9203

Hong Yong Sohn
Department of Metallurgical Engineering
The University of Utah
Salt Lake City, Utah, 84112

Reprinted with permission from (Sahir, A.H.; Lighty, J.S.; Sohn, H.Y. Kinetics of Copper Oxidation in the Air Reactor of a Chemical Looping Combustion System using the Law of Additive Reaction Times. *Ind. Eng. Chem. Res,* 2011, 50 (23), 13330–13339).

I&EC research
Industrial & Engineering Chemistry Research

ARTICLE

pubs.acs.org/IECR

Kinetics of Copper Oxidation in the Air Reactor of a Chemical Looping Combustion System using the Law of Additive Reaction Times

Asad H. Sahir* and JoAnn S. Lighty

Department of Chemical Engineering, University of Utah, Salt Lake City, Utah, 84112-9203

Hong Yong Sohn

Department of Metallurgical Engineering, University of Utah, Salt Lake City, Utah, 84112

ABSTRACT: Chemical looping combustion (CLC) is one of the promising technologies for fuel combustion which has the potential to reduce the energy penalty associated with the CO_2 capture process. A CLC system typically consists of two interconnected fluidized beds that act as a fuel and an air reactor, with a recirculating metal/metal-oxide system acting as the carrier of oxygen from the latter to the former. Insights to the design and optimization of an air reactor in a CLC process could be obtained by analyzing the oxidation kinetics by the Law of Additive Reaction Times. The law offers an approximate closed form solution for a gas−solid reaction in which structural changes on reaction can be neglected. It takes into account the pore diffusion of gaseous species in the interior of the porous oxygen carrier. This is in contrast to shrinking-core model, which assumes the occurrence of the reaction along a well-defined sharp reaction interface that progresses into the solid as the reaction occurs; when applied to an initially porous solid, this model is only appropriate when pore diffusion is controlling. This law provides a convenient and realistic means for analyzing the oxidation process in an air reactor of a CLC system.

1. INTRODUCTION

Chemical looping combustion (CLC) is one of the alternative technologies currently being investigated for fuel combustion which has the promise of reducing both the energy penalty and the cost associated with the capture of CO_2. The CLC process involves the use of a metal/metal-oxide system that recirculates between the fuel and the air reactors. The required oxygen for fuel combustion is supplied by an oxygen carrier, which is reduced in the fuel reactor. Metal oxide is regenerated by oxidation with air in the air reactor. The advantage of the CLC process is that an undiluted stream of CO_2 can be obtained from the combustion process, which can subsequently be sequestered.[1,2] A number of metal−metal oxide systems have been investigated for the CLC of various fossil fuels.[2]

Copper is one of the candidate metals that are being considered for a CLC system either in its elemental form or in its lower oxide form, Cu_2O, to achieve oxidation to CuO. Numerous studies on the development, characterization and reactivity under reducing and oxidizing conditions of copper-based oxygen carriers have been reported in the literature.[3−25] The various engineering aspects related to the utilization of copper based oxygen carriers in CLC have also been investigated, which include identification of the range of operating conditions,[26] pressure effects,[27] solid waste management,[28] and the effect of sulfur[29] and light hydrocarbons[30] on their performance. Recent studies of CLC systems using copper-based oxygen carriers have addressed the formulation and solution of mathematical model equations at the single particle[31,32] and at the reactor scale.[33,34] A variant of the CLC system based on the transition from CuO to Cu_2O in the fuel reactor to release oxygen, known as Chemical looping with oxygen uncoupling (CLOU), is of significant interest in solid fuel combustion owing to its promise in increasing solid fuel combustion rates.[35−37] The use of copper has also been investigated as a potential candidate for Chemical looping hydrogen (CLH) generation process.[38]

Out of the many studies reported on CLC with copper based oxygen carriers, few studies have focused on modeling the oxidation process of Cu in air reactors. The kinetics of the copper oxidation reaction in CLC systems has been investigated by Garcia-Labiano et al.[4] for a 10 wt % CuO alumina supported oxygen carrier prepared by impregnation. Another important study is that by Chuang et al.[17] who have reported on the modeling aspects of copper oxidation in a CLC system using a 82.5 wt % CuO supported on a 17.5 wt % Al_2O_3 carrier. The analysis on the oxidation of copper in air reactor is of significant importance as it provides a quantitative basis for the design and optimization of the air reactor.

In the study, the process of copper oxidation for application to CLC has been analyzed using the method developed for porous solids by Sohn and Szekely[39,40] and Sohn.[41] As a result of this work, a closed-form equation for the relationship between the conversion of solid reactant and time, known as the Law of Additive Reaction Times, was formulated.[41] The law is applicable for isothermal reactions in which the effective diffusivity of the solid remains constant during the reaction.[42] Conceptually, the

Received: July 20, 2011
Accepted: October 12, 2011
Revised: September 21, 2011
Published: October 12, 2011

law states that

[The time required to attain a certain conversion]
≅ [The time required to attain the same conversion under the conditions of rapid pore diffusion]
+ [The time required to attain the same conversion under the rate control by pore diffusion and external mass transfer]
(1)

Mathematically, eq 1 is expressed as

$$t_g^* \cong g_{F_g}(X) + \tilde{\sigma}^2\left(p_{F_p}(X) + \frac{4X}{N_{Sh}^*}\right) \quad (2)$$

Equation 2 is a dimensionless relationship between conversion and time expressed in terms of a conversion function for chemical reaction control, a conversion function for pore diffusion control, a modified Sherwood Number and a porous solid reaction modulus. The definitions of these terms will be described in detail in the subsequent section.

This equation appropriately represents the physical processes involved in the reaction in a porous solid as it takes into account the process of gas diffusing into the interior of the porous solid. The relation was initially formulated with the assumption that the porous solid is constituted by small nonporous grains of a uniform size that can react according to a chemical reaction controlled shrinking-core scheme.[39] In subsequent papers, it has been demonstrated that eqs 1 and 2 are a reasonable approximation also for other types of porous solids.[41] Furthermore, these equations are exact for an isothermal reaction of a nonporous solid described by the shrinking-core model.[41] The relationship for the porous solid reaction modulus $\tilde{\sigma}^2$ given in eq 2 enables to identify the important controlling regimes. If $\tilde{\sigma}^2$ is smaller than 0.1, the system can be considered to be controlled by chemical reaction, whereas if the value of the parameter $\tilde{\sigma}^2$ is larger than 10, the system is controlled by the diffusion through the product layer and external mass transfer. Value of $\tilde{\sigma}^2$ close to one suggests that both chemical reaction and mass transfer are controlling. The utility and the advantages of the Law of Additive Reaction Times and of the porous solid reaction modulus, $\tilde{\sigma}^2$ have been verified for many systems with different forms of the conversion function, $g_{F_g}(X)$. The law has been demonstrated to provide approximate solution for many reactions of industrial interest, e.g. regeneration of coked catalyst pellets,[44] hydrogen reduction of porous nickel oxide pellets,[45] and simultaneous fluid−solid reactions.[46] In view of the above discussion, the Law of Additive Reaction Times offers a significant potential for the analysis and design of reactors in CLC systems as it offers a simple closed form solution that can assist in the design and optimization of reactors. In this paper, the copper oxidation reaction in the air reactor of a CLC system has been analyzed by the application of the Law of Additive Reaction Times.

In previous studies reported in the literature[14,17] on the kinetics of copper oxidation reaction occurring in the air reactor of a CLC system, the shrinking core model has been used which does not take into account the process of gas diffusing into the interior of the porous solids. These models assume that the reaction occurs at a sharp reaction interface between the unreacted and completely reacted zones which advances toward the center as the reaction proceeds. The shrinking core model is appropriate only when the pore diffusion is rate controlling, in which case eq 2 becomes identical to the relationship given by the shrinking core model.[40] The other extreme of this case is where pore diffusion is very fast under this condition, the reaction takes place over the entire solid at the same rate and the rate does not depend on the overall size of the solid. The shrinking core model always contains rate dependence on size for solids (spherical, cylindrical or flat plate shaped) even when pore diffusion is very fast.

2. APPLICATION OF THE LAW OF ADDITIVE REACTION TIMES FOR THE COPPER OXIDATION REACTION

The reaction considered in this work is $O_2(g) + 2Cu(s) \rightarrow 2CuO(s)$. For the general form of the first-order reaction $A(g) + bB(s) \rightarrow cC(g) + dD(s)$, an approximate solution of the form has been determined for grains and particles characterized by a shape factor.[40]

The dimensionless time is defined as

$$t_g^* = \frac{bk_g}{\tilde{\rho}_S}\left(\frac{A_g}{F_g V_g}\right)\left[C_{A0} - \frac{C_{C0}}{K_E}\right]t \quad (3)$$

The concentration of A, C_{A0} is evaluated using the ideal gas law. As there is no C, $C_{C0} = 0$.

The conversion function for a porous solid made up of grains under chemical reaction control is defined as[39]

$$g_{F_g}(X) = 1 - (1 - X)^{(1/F_g)} \quad (4)$$

The conversion function for pore diffusion control is defined as[43]

$$p_{F_p}(X) = 1 - \frac{F_p(1 - X)^{2/F_p} - 2(1 - X)}{F_p - 2} \quad (5)$$

The porous solid reaction modulus[41] for an isothermal first order reaction with respect to gaseous reactant A is defined as

$$\tilde{\sigma}^2 \equiv \left\{\frac{a_s k_g F_p}{2D_e}\right\}\left(\frac{A_g}{F_g V_g}\right)\left(\frac{V_p}{A_p}\right)^2\left(1 + \frac{1}{K_E}\right) \quad (6)$$

The effective diffusivity D_e has been evaluated using the approximation of Wakao and Smith[47] where

$$D_e = \varepsilon^2/\left[\frac{1}{D_K} + \frac{1}{D_M}\right] \quad (7)$$

The molecular diffusivity of O_2 in N_2, $D_{O_2-N_2}$ in cm^2/s has been determined using Fuller's Correlation[48]

$$D_M = D_{O_2-N_2} = \frac{0.00143T^{1.75}}{PM_{O_2-N_2}^{1/2}\left[(\Sigma_v)_{O_2}^{1/3} + (\Sigma_v)_{N_2}^{1/3}\right]^2} \quad (8)$$

The Knudsen Diffusivity, D_K has been determined using the relationship[49]

$$D_K = \frac{8\varepsilon}{3S\rho_p}\sqrt{\frac{2R_gT}{\pi M_{O_2}}} \quad (9)$$

The modified Sherwood number,[40] N_{Sh}^* has been used in the correlation, defined as follows, is used to account for the effect of

external mass transfer.

$$N_{Sh}^{*} = N_{Sh}\left(\frac{D_M}{D_e}\right) \tag{10}$$

The Sherwood Number N_{Sh} has been evaluated using the La Nauze and Jung[50] correlation for fluidized beds.

$$N_{Sh} = 2\varepsilon_{mf} + 0.69\left(\frac{Re_p}{\varepsilon_{mf}}\right)^{1/2} Sc^{1/3} \tag{11}$$

The viscosity of air in centipoises has been calculated using the correlation reported in the literature[51]

$$\mu = (4.38 \times 10^{-2})(1.01 \times 10^{-3}T - 0.093)^{5/9} \tag{12}$$

The value of the equilibrium constant K_E of the reaction $O_2(g) + 2Cu(s) \rightarrow 2CuO(s)$ is evaluated using the thermodynamic data given in Pankrantz.[52]

3. ANALYSIS OF EXPERIMENTAL DATA OF GARCÍA-LABIANO ET AL.[4] USING THE LAW OF ADDITIVE REACTION TIMES FOR COPPER OXIDATION

The experiments in the study of García-Labiano et al.[4] were conducted using particles with 10% CuO active content supported on alumina having a size of 0.8−1.2 mm which were crushed and sieved to obtain the desired particle size of 0.1−0.3 mm with a CuO layer thickness of 4.0×10^{-10} m which is equivalent to a Cu layer thickness of 2.3×10^{-10} m. The experiments were conducted at higher partial pressures of O_2 (0.21 atm), which makes the distinction of the Cu_2O phase and CuO phase difficult. This provides a justification to consider the oxidation of Cu to be a global one-step reaction. The following assumptions have been taken into account to analyze the data of García-Labiano et al.[4]

1. The Cu grains are considered to be flat plates with a shape factor $F_g = 1$ reacting only on one side

$$\left(\frac{F_g V_g}{A_g}\right) = L_g \tag{13}$$

2. The particle is considered to be spherical in shape with a shape factor $F_p = 3$

$$\left(\frac{V_p}{A_p}\right) = \frac{\frac{4}{3}\pi r_p^3}{4\pi r_p^2} = \frac{r_p}{3} \tag{14}$$

3. The conversion function for chemical reaction for a flat grain is

$$g_{F_g}(X) = X \tag{15}$$

4. The conversion function for pore diffusion control for a spherical particle is

$$p_{F_p}(X) = 1 - 3(1 - X)^{2/3} + 2(1 - X) \tag{16}$$

Table 1. Data Used for Analyzing Experiment on Cu Oxidation by García-Labiano et al.[4]

parameter	magnitude	source
L_g	2.3×10^{-10} m	García-Labiano et al.[4]
r_p	0.1 mm (Diameter has been evaluated by calculating the average of 0.1 mm and 0.3 mm)	García-Labiano et al.[4]
ε	0.57	García-Labiano et al.[4]
$\bar{\rho}_S$	140252 mol/m^3	García-Labiano et al.[4]
k_g	$4.7 \times 10^{-6} \exp(-15000/R_gT)$ m/s	García-Labiano et al.[4]
S	41.3 m^2/g	García-Labiano et al.[4]
ρ_p	1800 kg/m^3	García-Labiano et al.[4]
u	0.1 m/s	de Diego et al.[8]
u/u_{mf}	6 (suggested value 5−7)	de Diego et al.[8]
ϕ_p	1 (particles are spherical)	

For the reaction, $O_2(g) + 2Cu(s) \rightarrow 2CuO(s)$ applying the aforementioned considerations, eq 2 can be written as

$$\frac{2k_g}{\bar{\rho}_S}\left(\frac{1}{L_g}\right)C_{A0}t \cong X + \left\{\left\{\frac{3\alpha_S k_g}{2D_e}\right\}\left(\frac{1}{L_g}\right)\left(1 + \frac{1}{K_E}\right)\left(\frac{r_p}{3}\right)^2\right\} \times \left[\{1 - 3(1 - X)^{2/3} + 2(1 - X)\} + \frac{4X}{N_{Sh}\left(\frac{D_M}{D_e}\right)}\right] \tag{17}$$

Rearranging relation 17

$$t \cong \left[\left(\frac{\bar{\rho}_S L_g}{2k_g C_{A0}}\right)X\right] + \left[\left\{\left(\frac{\alpha_S \bar{\rho}_S r_p^2}{12C_{A0}D_e}\right)\left(1 + \frac{1}{K_E}\right)\right\} \times \{1 - 3(1 - X)^{2/3} + 2(1 - X)\}\right] + \left[\left\{\left(\frac{\alpha_S \bar{\rho}_S r_p^2}{3C_{A0}D_M N_{Sh}}\right)\left(1 + \frac{1}{K_E}\right)\right\}X\right] \tag{18}$$

Equation 18 equates the time required to achieve a certain conversion of copper to the sum of time required to attain the same conversion under chemical reaction control (conditions of rapid pore diffusion) and the time required to attain the same conversion under reaction rate control by pore diffusion and external mass transfer.

The volume fraction α_S for this case is calculated by considering the mass percentages of Cu and Al_2O_3, their respective densities and the reported value of porosity. It was calculated to be 0.01685.

The Archimedes number, Ar, in the fluidized bed calculation has been evaluated by the relation[53]

$$Ar = \frac{d_p^3 \rho_g(\rho_p - \rho_g)g}{\mu^2} \tag{19}$$

The voidage at the minimum fluidization was evaluated using Broadhurst and Becker's Correlation[54]

$$\varepsilon_{mb} \cong \varepsilon_{mf} = \frac{0.586}{\phi_P^{0.72} Ar^{0.029}}\left(\frac{\rho_g}{\rho_p}\right)^{0.021} \tag{20}$$

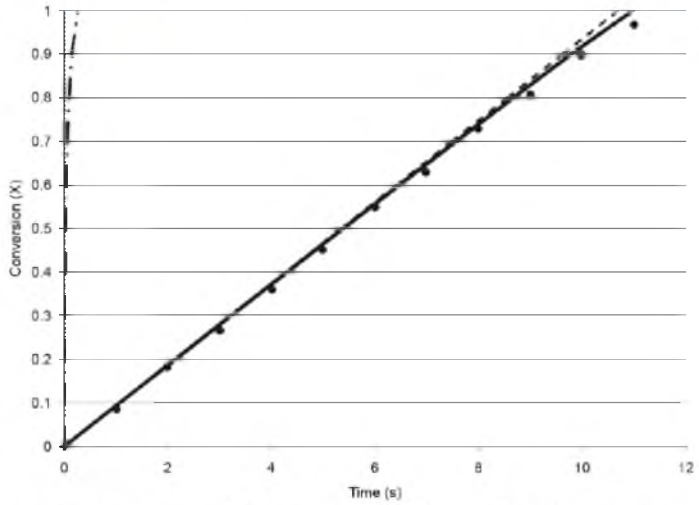

Figure 1. Conversion vs time for the oxidation reaction $2Cu(s) + O_2(g) \rightarrow 2CuO(s)$ at 773 K. The experiments were carried with a constant O_2 concentration of 21% [··· conversion for external mass transfer control, — ·· — conversion for pore diffusion control, - - - conversion for chemical reaction control, ● experimental data points (García-Labiano et al.[4]), — conversion predicted by expression 18].

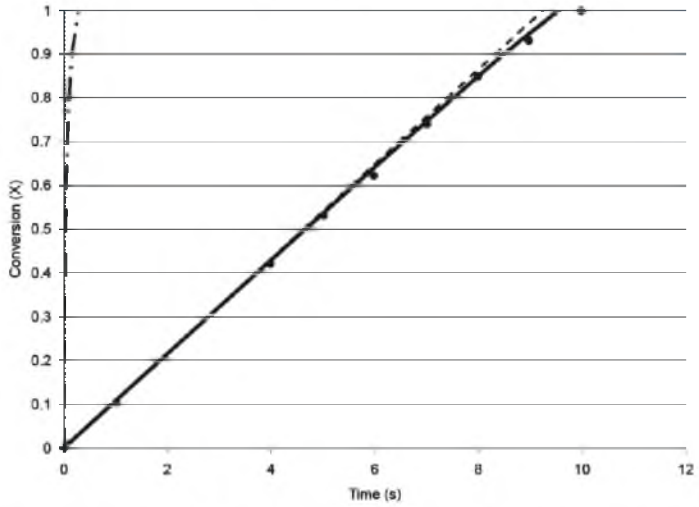

Figure 2. Conversion vs Time for the oxidation reaction $2Cu(s) + O_2(g) \rightarrow 2CuO(s)$ at 873 K. The experiments were carried with a constant O_2 concentration of 21%. [··· conversion for external mass transfer control, — ·· — conversion for pore diffusion control, - - - conversion for chemical reaction control, ● experimental data points (García-Labiano et al.[4]), — conversion predicted by expression 18].

Table 1 summarizes the parameters used to reanalyze García-Labiano's data using relation 18.

Figures 1−4 present the comparison of experimental data by García-Labiano et al.[4] at different temperatures with the results of applying the Law of Additive Reaction Times. Examining these figures reveal the following important conclusions:

(i) The Law of Additive Reaction Times predicts that the oxidation reaction in this experimental work is primarily controlled by chemical reaction. The prediction is in line with the initial assumption of García-Labiano et al.[4] of modeling the experiment neglecting the effects of external and internal mass transfer.

(ii) For the temperatures analyzed in this study, 773, 873, 923, and 1073 K, the prediction by the Law of Additive Reaction Times by eq 18 is consistent with the experimental data.

An important insight which could be obtained by the application of the Law of Additive Reaction Times is the determination of particle size where the effects of external and internal mass transfer will play a significant role in typical operating conditions for a CLC system. After validating the application of the Law of Additive Reaction Times with the experimental data of García-Labiano et al.,[4] the porous solid reaction modulus $\tilde{\sigma}^2$ is determined for different diameters at different temperatures of 773, 873, 923,

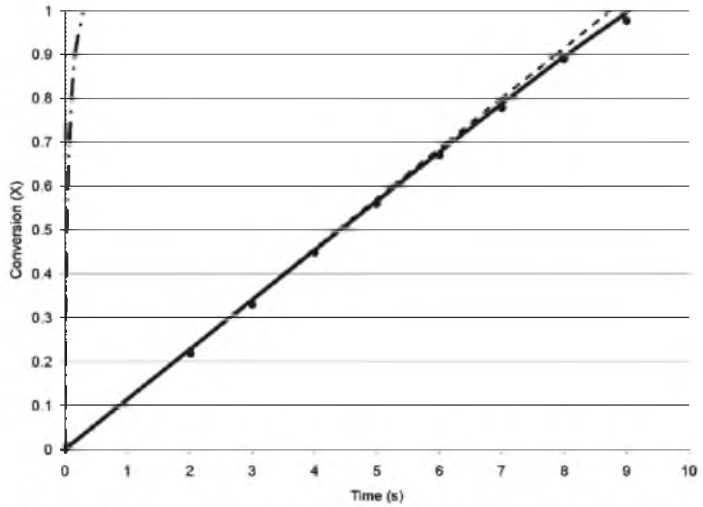

Figure 3. Conversion vs time for the oxidation reaction $2Cu(s) + O_2(g) \rightarrow 2CuO(s)$ at 923 K. The experiments were carried with a constant O_2 concentration of 21%. [··· conversion for external mass transfer control, — ·· — conversion for pore diffusion control, - - - conversion for chemical reaction control, ● experimental data points (García-Labiano et al.[4]), — conversion predicted by expression 18].

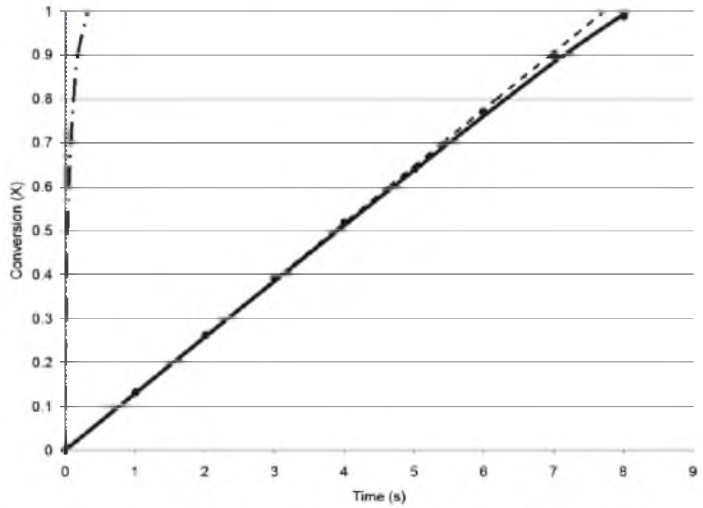

Figure 4. Conversion vs time for the oxidation reaction $2Cu(s) + O_2(g) \rightarrow 2CuO(s)$ at 1073 K. The experiments were carried with a constant O_2 concentration of 21% [··· conversion for external mass transfer control, — ·· — conversion for pore diffusion control, - - - conversion for chemical reaction control, ● experimental data points (García-Labiano et al.[4]), — conversion predicted by expression 18].

and 1023 K. The results are presented in Figure 5. It can be observed that the particles of the size 0.1−0.3 mm used in the study by García-Labiano et al.[4] are in the chemically controlled regimes as the magnitude of the porous solid reaction modulus $\hat{\sigma}^2$ is smaller than 0.1. The Law of Additive Reaction Times predicts that the effects of the external and internal mass transfer will become significant and are comparable to the effect of chemical reaction control in the experiment of García-Labiano et al.[4] when the value of the porous solid reaction modulus $\hat{\sigma}^2$ is unity. From Figure 5, the law predicts that for the particles used by García-Labiano et al.[4] sized between 0.8 and 1 mm, external and/or internal mass transfer effects become significant and should be duly considered for in the analysis. The size of the particles at which internal and/or external mass transfer effects become significant depends on the metal−metal oxide system, porosity, internal structure of the particle and the process conditions. As demonstrated in the current study on Cu oxidation, the Law of Additive Reaction Times helps in the analysis of these parameters. The prediction offered by this law is consistent with the observations on the effect of particle size made with the help of the detailed particle reaction model of García-Labiano et al.,[31] who reported that the reaction rate was independent of particle size under 0.2 mm. The application of the Law of Additive Reaction Times offers an approximate solution which

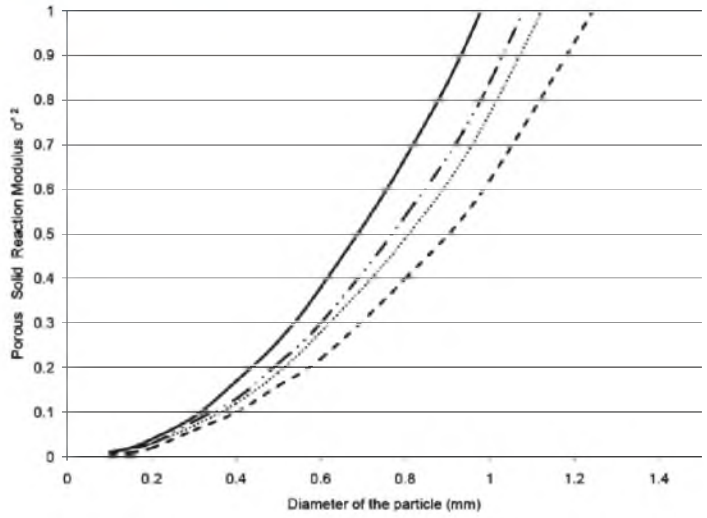

Figure 5. Porous Solid Reaction Modulus vs Diameter of particle at different temperatures for the oxidation reaction $2Cu(s) + O_2(g) \rightarrow 2CuO(s)$. The experiments were carried with a constant O_2 concentration of 21%. [- - - 773, ··· 823, — ·· — 923, and — 1073 K].

is valuable in providing quantitative basis for design and optimization and obviates the need of a numerical solution.

4. ANALYSIS OF EXPERIMENTAL DATA OF CHUANG ET AL.[17] USING THE LAW OF ADDITIVE REACTION TIMES FOR COPPER OXIDATION

To illustrate the utility of the Law of Additive Reaction Times for the case where internal and external mass transfer effects are important, one of the sets of experimental data for the copper oxidation reaction by Chuang et al.[17] has been considered. The experiment was conducted using particles with 82.5% CuO active content supported on alumina particles having sizes of 355−500 and 850−1000 μm. The experiment analyzed in this study for which the conversion vs time data for Cu oxidation was available was conducted at 700 °C and at an O_2 concentration of 1.3% in an O_2-N_2 mixture. The experiment analyzed in this study was carried out with an oxygen carrier having a particle size range of 850−1000 μm. In their study, the formation of Cu_2O was also considered in the formulation of mathematical relationships. To analyze their result by the Law of Additive Reaction Times, the following considerations are taken into account.

1. The Cu grains are considered to be spherical with a shape factor $F_g = 3$. It turns out that the overall reaction is controlled by pore diffusion and external mass transfer as will be demonstrated subsequently. Therefore the actual shape of the grains does not affect the rate analysis of this particular system. For the same reason, an accurate value of r_g is also unnecessary in this case.

$$\left(\frac{F_g V_g}{A_g}\right) = r_g \tag{21}$$

2. The particle is considered to be spherical in shape with a shape factor $F_p = 3$

$$\left(\frac{V_p}{A_p}\right) = \frac{\frac{4}{3}\pi r_p^3}{4\pi r_p^2} = \frac{r_p}{3} \tag{22}$$

3. The conversion function for chemical reaction for a spherical grain is

$$g_{F_g}(X) = 1 - (1 - X)^{(1/3)} \tag{23}$$

4. The conversion function for pore diffusion control for a spherical particle is

$$p_{F_p}(X) = 1 - 3(1 - X)^{2/3} + 2(1 - X) \tag{24}$$

Similarly applying the aforementioned considerations as in the previous case, eq 2 can be written as

$$\frac{2k_g}{\tilde{\rho}_S}\left(\frac{1}{r_g}\right) C_{A0} t \cong [1 - (1 - X)^{(1/3)}] + \left\{\left\{\frac{3\alpha_S k_g}{2D_e}\right\}\left(\frac{1}{r_g}\right)\left(1 + \frac{1}{K_E}\right)\left(\frac{r_p}{3}\right)^2\right\} \times \left[\{1 - 3(1 - X)^{2/3} + 2(1 - X)\} + \frac{4X}{N_{Sh}\left(\frac{D_M}{D_e}\right)}\right] \tag{25}$$

Rearranging eq 25

$$t \cong \left[\left(\frac{\tilde{\rho}_S r_g}{2k_g C_{A0}}\right)\{1 - (1 - X)^{(1/3)}\}\right] + \left[\left\{\left(\frac{\alpha_S \tilde{\rho}_S r_p^2}{12 C_{A0} D_e}\right)\left(1 + \frac{1}{K_E}\right)\right\}\{1 - 3(1 - X)^{2/3} + 2(1 - X)\}\right] + \left[\left(\frac{\alpha_S \tilde{\rho}_S r_p^2}{3 C_{A0} D_M N_{Sh}}\right)\left(1 + \frac{1}{K_E}\right)X\right] \tag{26}$$

As discussed by Chuang et al.,[17] the results of the experiment on Cu oxidation conducted at 700 °C and at an O_2 concentration of 1.3% in an O_2-N_2 mixture with a Cu based oxygen carrier with

particle sizes of 850−1000 μm indicate that the reaction is controlled by mass transfer. Hence in the light of their observation, the first term representing the contribution to the time of reaction by rapid pore diffusion in eq 26 can be neglected.

$$t \cong \left[\left\{\left(\frac{\alpha_S \tilde{\rho}_S r_p^2}{12 C_{A0} D_e}\right)\left(1+\frac{1}{K_E}\right)\right\}\{1-3(1-X)^{2/3}+2(1-X)\}\right] + \left[\left(\frac{\alpha_S \tilde{\rho}_S r_p^2}{3 C_{A0} D_M N_{Sh}}\right)\left(1+\frac{1}{K_E}\right)X\right] \quad (27)$$

The volume fraction α_S for this case is calculated by considering the mass percentages of Cu and Al_2O_3, their respective densities and the reported value of porosity. It was calculated to be 0.1442.

Table 2 summarizes the parameters that were used to reanalyze one of the sets of experimental data of Chuang et al.[17] using eq 27. Figure 6 represents the comparison of the experimental data with the predictions made by the Law of Additive Reaction Times. On observing Figure 6, it is evident that the oxidation reaction in this experiment is controlled by a combination of internal and external mass transfer. The observation made by the law is consistent with one of the conclusions drawn by Chuang et al.[17] that the oxidation reaction in this experiment was controlled by external mass transfer. As per the law the contributions of the internal mass transfer and external mass transfer process were of comparable magnitude in the oxidation reaction. The two terms of the right-hand side of eq 27 represent the contribution to time required to reach certain conversion by internal mass transfer and external mass transfer. It can be observed in Figure 6 that the reactivity of the solid is influenced significantly by internal mass transfer (pore diffusion) and external mass transfer. An attempt was made to calculate the magnitude of porous solid reaction modulus $\hat{\sigma}^2$ for Chuang et al.'s experimental data set[17] using the kinetic rate constant k_g and r_g obtained by García-Labiano et al.[4] The results indicate that the magnitude of $\hat{\sigma}^2$ was 0.57, indicating comparable contributions by chemical reaction and mass transfer. For a reaction dominated by mass transfer like this system, as shown in Figure 6, the value of $\hat{\sigma}^2$ should be at least 10. A possible explanation for a lower magnitude of $\hat{\sigma}^2$ determined for this study using García-Labiano et al.[4] experimental kinetic constants may be attributed to the difference in particle morphology arising from the different preparation methods for oxygen carrier particles, which affects the intrinsic reactivity of copper.

Table 2. Data Used for Analyzing Experiment on Cu Oxidation by Chuang et al.[17]

parameter	magnitude	source
r_g	2.3×10^{-10} m (assumed by considering that the thickness of Cu grain is equal to the radius of the grain)	García-Labiano et al.[4]
r_p	0.4625 mm (diameter has been evaluated by calculating the average of 0.85 mm and 1 mm)	Chuang et al.[17]
ε	0.77	Chuang et al.[17]
$\tilde{\rho}_S$	140252 mol/m^3	García-Labiano et al.[4]
S	6.3 m^2/g	Chuang et al.[17]
ρ_p	1820 kg/m^3	Chuang et al.[17]
u	0.343 m/s	Chuang et al.[17]
u/u_{mf}	6 (suggested value 2.5−7.8)	Chuang et al.[17]
ϕ_p	1 (particles are spherical)	

5. DISCUSSION

An important requirement in using the Law of Additive Reaction Times to analyze experimental data is to have well-characterized structural information about the particle in terms of porosity, surface area and particle structure. The analysis in this paper is based on the premise that the particle does not undergo any structural changes. CLC applications involve the use of metal oxides at elevated temperatures at which structural changes due to sintering may occur. In a recent paper, an approximate

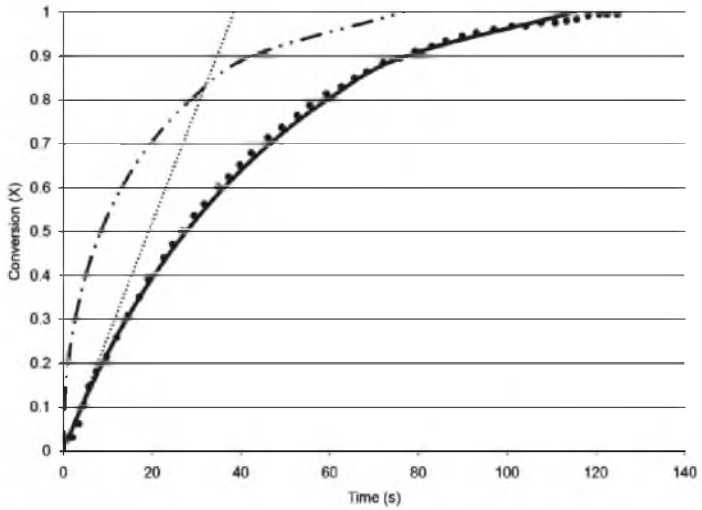

Figure 6. Conversion vs time for the oxidation reaction $2Cu(s) + O_2(g) \rightarrow 2CuO(s)$ at 973 K [· · · conversion for external mass transfer control, – · · – conversion for pore diffusion control, ● experimental data points (Chuang et al.[17]), — conversion predicted by expression 27].

solution based on the Law of Additive Reaction Times that takes into consideration changing porosity and effective diffusivity has been developed.[55]

As discussed by Fan and Li,[56] the development of the CLC technology is highly dependent on the understanding of the interrelationships between reaction and process engineering factors. The Law of Additive Reaction Times presents a quantitative basis to enhance the understanding of these factors by providing a mathematical relationship that takes into account the thermodynamic properties of metal oxides, rates of reduction and oxidation reactions, and the structure of the oxygen carrier. The analysis will provide deeper insights to the effect of reactor types, allow scale-up designs and facilitate analyses on overall process efficiency and economics. The current study on the analysis of copper oxidation using the Law of Additive Reaction Times provides a simplified approach which will help in interpreting conversion vs time data for a gas−solid reaction in an air reactor. It is expected to help in the design and optimization of the reactor configuration, as it provides a methodology to evaluate the magnitude of the controlling effects using the porous solid reaction modulus.

6. CONCLUSIONS

In this study the utility of the Law of Additive Reaction Times in analyzing data from experiments on Cu oxidation in Chemical Looping Combustion has been demonstrated. For two reported experimental cases on Cu oxidation controlled by chemical reaction or pore diffusion and mass transfer, the law has been used to reanalyze experimental data. As determined in the study, the porous solid reaction modulus can be utilized to identify the regime in which the reaction is controlled by chemical reaction (rapid intergrain pore diffusion), pore diffusion, external mass transfer, or a combination thereof. The identification of these regimes will be valuable in designing and optimizing gas−solid reactor configurations used in the Chemical Looping Combustion (CLC) technology.

AUTHOR INFORMATION

Corresponding Author

*Address: Department of Chemical Engineering, University of Utah, 50 South Central Campus Drive, Room 3290 MEB, Salt Lake City, UT 84112-9203. E-mail: asad.sahir@utah.edu. Tel.: +1-801-581-6915. Fax: +1-801-585-9291.

ACKNOWLEDGMENT

This material is based upon work supported by the U.S. Department of Energy under Award Number DE-NT0005015.

NOMENCLATURE

A_g = external surface area of an individual grain, m^2
A_P = external surface area of the particle, m^2
Ar = Archimedes Number (Defined in eq 19)
C_{A0} = concentration of the gaseous species A in the general form $A(g) + bB(s) \rightarrow cC(g) + dD(s)$, mol/m^3
C_{C0} = concentration of the gaseous species C in the general form $A(g) + bB(s) \rightarrow cC(g) + dD(s)$, mol/m^3
d_p = diameter of particle, m
D_e = effective diffusivity, m^2/s
D_K = Knudsen diffusivity, m^2/s
D_M = molecular diffusivity, m^2/s
F_g = shape factor for the grain (1, 2, or 3 for flat plates, long cylinders or spheres respectively)
F_p = shape factor for the particle (1, 2, or 3 for flat plates, long cylinders or spheres respectively)
g = gravitational constant, m/s^2
$g_{F_g}(X)$ = conversion function for chemical reaction control (defined in eq 4)
k_g = reaction rate constant for grain, m/s
K_E = equilibrium constant
L_g = thickness of grain, m
M = molecular mass
N_{Sh} = Sherwood number
N^*_{Sh} = modified Sherwood number (defined in eq 10)
$p_{F_p}(X)$ = conversion function for pore-diffusion control (defined in eq 5)
P = pressure (bar)
r_g = radius of a grain, m
r_p = radius of a particle, m
R_g = gas constant, J/mol K
Re_p = particle Reynolds number
S = specific surface area, m^2/g
Sc = Schmidt number
t = time, s
t^*_g = dimensionless time (defined in eq 3)
T = temperature, K
u = superficial velocity of gas through the bed, m/s
u_{mf} = minimum fluidization velocity, m/s
V_g = volume of a grain, m^3
V_P = volume of a particle, m^3
X = conversion

Greek Symbols

α_S = fraction of particle volume initially occupied by solid reactant
ε = porosity
ε_{mb} = bed voidage at minimum fluidization
ε_{mf} = bed voidage at minimum bubbling point
ϕ^2 = porous solid reaction modulus (defined in eq 6)
ρ_g = density of gas (kg/m^3)
ρ_p = density of particle (kg/m^3)
$\tilde{\rho}_S$ = molar density of solid reactant (mol/m^3)
μ = viscosity (kg/m s)
ϕ_p = sphericity
(Σ_v) = diffusion volume of a species, cm^3

REFERENCES

(1) Lyngfelt, A.; Leckner, B.; Mattisson, T. A Fluidized-Bed Combustion Process with Inherent CO_2 Separation: Application of Chemical-Looping Combustion. *Chem. Eng. Sci.* **2001**, *56*, 3101–3113.

(2) Fan, L. S. *Chemical Looping Systems for Fossil Energy Conversions*; Wiley-AIChE: Hoboken, NJ, 2010.

(3) Mattisson, T.; Järdnäs, A; Lyngfelt, A. Reactivity of Some Metal Oxides Supported on Alumina with Alternating Methane and Oxygen—Application for Chemical-Looping Combustion. *Energy Fuels* **2003**, *17* (3), 643–651.

(4) García-Labiano, F.; de Diego, L. F.; Adánez, J.; Abad, M.; Gayan, P. Reduction and Oxidation Kinetics of a Copper-Based Oxygen Carrier Prepared by Impregnation for Chemical-Looping Combustion. *Ind. Eng. Chem. Res.* **2004**, *43* (26), 8168–8177.

(5) Cho, P.; Mattisson, T.; Lyngfelt, A. Comparison of Iron-, Nickel-, Copper-, and Manganese-Based Oxygen Carriers for Chemical-Looping Combustion. *Fuel* **2004**, *83* (9), 1215–1225.

(6) De Diego, L. F.; García-Labiano, F.; Adánez, J.; Gayan, P.; Abad, A.; Corbella, B. M.; Palacios, J. M. Development of Cu-Based Oxygen Carriers for Chemical-Looping Combustion. *Fuel* **2004**, *83* (13), 1749–1757.

(7) Corbella, B. M.; De Diego, L. F.; García, F.; Adánez, J.; Palacios, J. M. The Performance in a Fixed Bed Reactor of Copper-Based Oxides on Titania as Oxygen Carriers for Chemical Looping Combustion of Methane. *Energy Fuels* **2005**, *19* (2), 433–441.

(8) De Diego, L. F.; Gayan, P.; García-Labiano, F.; Celaya, J.; Abad, A.; Adánez, J. Impregnated CuO/Al_2O_3 Oxygen Carriersfor Chemical-Looping Combustion: Avoiding Fluidized Bed Agglomeration. *Energy Fuels* **2005**, *19* (5), 1850–1856.

(9) Adánez, J.; Gayan, P.; Celaya, J.; de Diego, L. F.; García-Labiano, F.; Abad, A. Chemical Looping Combustion in a 10 $kW_{(th)}$ Prototype Using a CuO/Al_2O_3 Oxygen Carrier: Effect of Operating Conditions on Methane Combustion. *Ind. Eng. Chem. Res.* **2006**, *45* (17), 6075–6080.

(10) Corbella, B. M.; De Diego, L. F.; García-Labiano, F.; Adánez, J.; Palacios, J. M. Characterization and Performance in a Multicycle Test in a Fixed-Bed Reactor of Silica-Supported Copper Oxide as Oxygen Carrier for Chemical-Looping Combustion of Methane. *Energy Fuels* **2006**, *20* (1), 148–154.

(11) Cao, Y.; Casenas, B.; Pan, W. Investigation of Chemical Looping Combustion by Solid Fuels. 2. Redox Reaction Kinetics and Product Characterization with Coal, Biomass, and Solid Waste as Solid Fuels and CuO as an Oxygen Carrier. *Energy Fuels* **2006**, *20* (5), 1845–1854.

(12) De Diego, L. F.; García-Labiano, F.; Gayan, P.; Celaya, J.; Palacios, J. M.; Adanez, J. Operation of a 10 kW_{th} Chemical-Looping Combustor during 200 h with a $CuO-Al_2O_3$ Oxygen Carrier. *Fuel* **2007**, *86* (7–8), 1036–1045.

(13) Chuang, S. Y.; Dennis, J. S.; Hayhurst, A. N.; Scott, S. A. Development and Performance of Cu-Based Oxygen Carriers for Chemical-Looping Combustion. *Combust. Flame* **2008**, *154* (1–2), 109–121.

(14) Tian, H.; Chaudhari, K.; Simonyi, T.; Poston, J.; Tengfei, L.; Sanders, T.; Veser, G.; Siriwardane, R. Chemical-Looping Combustion of Coal-Derived Synthesis Gas over Copper Oxide Oxygen Carriers. *Energy Fuels* **2008**, *22* (6), 3744–3755.

(15) Forero, C. F.; Gayan, P.; De Diego, L. F.; Abad, A.; García-Labiano, F.; Adánez, J. Syngas Combustion in a 500 W_{th} Chemical-Looping Combustion System Using an Impregnated Cu-Based Oxygen Carrier. *Fuel Process. Technol.* **2009**, *90* (12), 1471–1479.

(16) Siriwardane, R.; Tian, H.; Richards, G; Simonyi, T.; Poston, J. Chemical-Looping Combustion of Coal with Metal Oxide Oxygen Carriers. *Energy Fuels* **2009**, *23* (8), 3885–3892.

(17) Chuang, S. Y.; Dennis, J. S.; Hayhurst, A. N.; Scott, S. A. Kinetics of the Oxidation of a Co-precipitated Mixture of Cu and Al_2O_3 by O_2 for Chemical-Looping Combustion. *Energy Fuels* **2010**, *24*, 3917–3927.

(18) Chuang, S. Y.; et al. Kinetics of the Chemical Looping Oxidation of H_2 by a Co-precipitated Mixture of CuO and Al_2O_3. *Chem. Eng. Res. Des.* **2011**, *89* (9), 1511–1523.

(19) Dennis, J. S.; Scott, S. A. In Situ Gasification of a Lignite Coal and CO_2 Separation Using Chemical Looping with a Cu-Based Oxygen Carrier. *Fuel* **2010**, *89* (7), 1623–1640.

(20) Dennis, J. S.; Müller, C. R.; Scott, S. A. In Situ Gasification and CO_2 Separation Using Chemical Looping with a Cu-Based Oxygen Carrier: Performance with Bituminous Coals. *Fuel* **2010**, *89* (9), 2353–2364.

(21) Noorman, S.; Gallucci, F.; van SintAnnaland, M.; Kuipers, H. J. A. M. Experimental Investigation of a CuO/Al_2O_3 Oxygen Carrier for Chemical-Looping Combustion. *Ind. Eng. Chem. Res.* **2010**, *49* (20), 9720–9728.

(22) Goldstein, E. A.; Mitchell, R. E. Chemical Kinetics of Copper Oxide Reduction with Carbon Monoxide. *Proc. Combust. Inst.* **2011**, *33* (2), 2803–2810.

(23) Cao, Y.; Li, B.; Zhao, H. Y.; Lin, C.; Sit, S. P.; Pan, W. Investigation of Asphalt (Bitumen)-Fuelled Chemical Looping Combustion Using Durable Copper-Based Oxygen Carrier. *Energy Proced.* **2011**, *4*, 457–464.

(24) Gayan, P.; Forero, C. R.; Abad, A.; De Diego, L. F.; García-Labiano, F.; Adánez, J. Effect of Support on the Behavior of Cu-Based Oxygen Carriers during Long-Term CLC Operation at Temperatures above 1073 K. *Energy Fuels* **2011**, *25* (3), 1316–1326.

(25) Forero, C. R.; et al. High Temperature Behavior of a CuO/Al_2O_3 Oxygen Carrier for Chemical-Looping Combustion. *Int. J. Greenhouse Gas Control* **2011**, *5* (4), 659–667.

(26) Abad, A.; Adánez, J.; García-Labiano, F.; de Diego, L. F.; Gayan, P.; Celaya, J. Mapping of the Range of Operational Conditions for Cu-, Fe-, and Ni-Based Oxygen Carriers in Chemical-Looping Combustion. *Chem. Eng. Sci.* **2007**, *62* (1–2), 533–549.

(27) García-Labiano, F.; Adánez, J.; de Diego, L. F.; Gayan, P.; Abad, A. Effect of Pressure on the Behavior of Copper-, Iron-, and Nickel-Based Oxygen Carriers for Chemical-Looping Combustion. *Energy Fuels* **2006**, *20* (1), 26–33.

(28) García-Labiano, F.; Gayán, P.; Adánez, J.; de Diego, L. F.; Forero, C. R. Solid Waste Management of a Chemical-Looping Combustion Plant Using Cu-Based Oxygen Carriers. *Environ. Sci. Technol.* **2007**, *41* (16), 5882–5887.

(29) Forero, C. R.; Gayán, P.; García-Labiano, F.; de Diego, L. F.; Abad, A.; Adánez, J. Effect of Gas Composition in Chemical-Looping Combustion with Copper-Based Oxygen Carriers: Fate of Sulphur. *Int. J. Greenhouse Gas Control* **2010**, *4*, 762–770.

(30) Gayán, P.; Forero, C. R.; de Diego, L. F.; Abad, A.; García-Labiano, F.; Adánez, J. Effect of Gas Composition in Chemical-Looping Combustion with Copper-Based Oxygen Carriers: Fate of Light Hydrocarbons. *Int. J. Greenhouse Gas Control* **2010**, *4*, 13–22.

(31) García-Labiano, F.; de Diego, L. F.; Adánez, J.; Abad, A.; Gayán, P. Temperature Variations in the Oxygen Carrier Particles during Their Reduction and Oxidation in a Chemical-Looping Combustion System. *Chem. Eng. Sci.* **2005**, *60*, 851–862.

(32) Noorman, S.; Gallucci, F.; van SintAnnaland, M.; Kuipers, J. A. M. A Theoretical Investigation of CLC in Packed Beds. Part 1: Particle Model. *Chem. Eng. J.* **2011**, *167* (1), 297–307.

(33) Abad, A.; Adánez, J.; García-Labiano, F.; de Diego, L. F.; Gayán, P. Modeling of the Chemical-Looping Combustion of Methane Using a Cu-Based Oxygen-Carrier. *Combust. Flame* **2010**, *157* (3), 602–615.

(34) Noorman, S.; Gallucci, F.; van SintAnnaland, M.; Kuipers, J. A. M. A Theoretical Investigation of CLC in Packed Beds. Part 2: Reactor Model. *Chem. Eng. J.* **2011**, *167* (1), 369–376.

(35) Mattisson, T.; Lyngfelt, A.; Leion, H. Chemical-Looping with Oxygen Uncoupling for Combustion of Solid Fuels. *Int. J. Greenhouse Gas Control* **2009**, *3*, 11–19.

(36) Mattisson, T.; Leion, H.; Lyngfelt, A. Chemical-Looping with Oxygen Uncoupling Using CuO/ZrO_2 with Petroleum Coke. *Fuel* **2009**, *88* (4), 683–690.

(37) Eyring, E. M.; Konya, G.; Lighty, J. S.; Sahir, A. H.; Sarofim, A. F.; Whitty, K. J. Chemical Looping with Copper Oxide as Carrier and Coal as Fuel. *Oil Gas Sci. Technol. - Rev. IFP* **2011**, *66* (2), 209–221.

(38) Son, S. R.; Go, K. S.; Kim, S. D. Thermogravimetric Analysis of Copper Oxide for Chemical-Looping Hydrogen Generation. *Ind. Eng. Chem. Res.* **2009**, *48* (1), 380–387.

(39) Sohn, H. Y.; Szekely, J. A Structural Model for Gas-Solid Reactions with a Moving Boundary—III: A General Dimensionless Representation of the Irreversible Reaction between a Porous Solid and a Reactant Gas. *Chem. Eng. Sci.* **1972**, *27*, 763–778.

(40) Szekely, J., Evans, J. W., Sohn, H. Y. *Gas Solid Reactions*; Academic Press: New York, 1976.

(41) Sohn, H. Y. The Law of Additive Reaction Times in Fluid-Solid Reactions. *Metall. Trans. B* **1978**, *9B*, 89–96.

(42) Sohn, H. Y. The Effects of Reactant Starvation and Mass Transfer in the Rate Measurement of Fluid-Solid Reactions with Small Equilibrium Constants. *Chem. Eng. Sci.* **2004**, *59*, 4361–4368.

(43) Sohn, H. Y.; Sohn, H. J. The Effect of Bulk Flow Due to Volume Change in the Gas Phase on Gas–Solid Reactions: Initially Nonporous Solids. *Ind. Eng. Chem. Process Des. Dev.* **1980**, *19*, 237–42.

(44) Sohn, H. Y.; Wall, D. R. Application of the Law of Additive Reaction Times of the Regeneration of Coked Catalyst Pellets. *Chem. Eng. Sci.* **1989**, *44*, 442–444.

(45) Sohn, H. Y.; Kim, D. The Law of Additive Reaction Times Applied to the Hydrogen Reduction of Porous Nickel-Oxide Pellets. *Metall. Trans. B* **1984**, *15*, 403–406.

(46) Sohn, H. Y.; Braun, R. L. Simultaneous Fluid-Solid Reactions in Porous Solids: Reactions between One Solid and Two Fluid Reactants. *Chem. Eng. Sci.* **1980**, *35* (7), 1625–1635.

(47) Wakao, N.; Smith, J. M. Diffusion in Catalyst Pellets. *Chem. Eng. Sci.* **1962**, *17* (11), 825–834.

(48) Poling, B. E.; Prausnitz, J. M.; O'Connell, J. P. *The Properties of Gases and Liquids*; Mc-Graw Hill: New York, 2001.

(49) Petersen, E. E. *Chemical Reaction Analysis*; Prentice Hall: NJ, 1965.

(50) La Nauze, R. D.; Jung., K. Fundamentals of Coal Combustion in Fluidized Beds. *Chem. Eng. Res. Des.* **1985**, *63*, 3–33.

(51) Lo, H. Y.; Carroll, D. L.; Stiel, L. I. Viscosity of Gaseous Air at Moderate and High Pressures. *J. Chem. Eng. Data* **1966**, *11* (4), 540–544.

(52) Pankrantz, L. B. *Thermodynamic Properties of Elements and Oxides-Bulletin 672*; U.S. Department of the Interior, Bureau of Mines, 1982.

(53) Kunii, D.; Levenspiel, O., *Fluidization Engineering*; Butterworth Heinemann, 1991.

(54) Broadhurst, T. E.; Becker, H. A. Onset of Fluidization and Slugging in Beds of Uniform Particles. *AIChE J.* **1975**, *21* (2), 238–247.

(55) Sohn, H. Y.; Perez-Fontes, S. E. Application of the Law of Additive Reaction Times to Fluid−Solid Reactions in Porous Pellets with Changing Effective Diffusivity. *Metall. Trans. B* **2010**, 1261–1267.

(56) Fan, L. S.; Li, F. Chemical Looping Technology and Its Fossil Energy Conversion Applications. *Ind. Eng. Chem. Res.* **2010**, *49*, 10200–10211.

CHAPTER 3

RATE ANALYSIS OF CHEMICAL-LOOPING WITH OXYGEN UNCOUPLING (CLOU) FOR SOLID FUELS

Asad H. Sahir, JoAnn S. Lighty
Department of Chemical Engineering
The University of Utah
Salt Lake City, Utah, 84112-9203

Hong Yong Sohn
Department of Metallurgical Engineering
The University of Utah
Salt Lake City, Utah, 84112

Henrik Leion
Department of Environmental Inorganic Chemistry
Chalmers University of Technology
S-412 96 Göteborg, Sweden

energy&fuels

Article

pubs.acs.org/EF

Rate Analysis of Chemical-Looping with Oxygen Uncoupling (CLOU) for Solid Fuels

Asad H. Sahir,*[†] Hong Yong Sohn,[‡] Henrik Leion,[§] and JoAnn S. Lighty[†]

[†]Department of Chemical Engineering, University of Utah, Salt Lake City, Utah 84112-9203

[‡]Department of Metallurgical Engineering, University of Utah, Salt Lake City, Utah 84112

[§]Department of Environmental Inorganic Chemistry, Chalmers University of Technology, S-41296 Göteborg, Sweden

ABSTRACT: Chemical-looping with oxygen uncoupling (CLOU) offers a promise to reduce energy penalty by facilitating the capture of CO_2 emitted from power plants. It has a potential to lower the oxygen carrier inventory of the fuel reactor in contrast to chemical-looping combustion (CLC). The primary mechanism in CLOU for the combustion of solid fuels is their reaction with gaseous oxygen released by the decomposition of a metal oxide, which differs from CLC of solid fuels where the solid fuel has to be gasified first. The slower gasification reaction in CLC is subsequently followed by combustion of the fuel with a circulating oxygen carrier. The present study is concerned with the rate analysis from reported batch fluidized bed CLOU experimental data of Mexican petcoke particles by a CuO/ZrO_2 oxygen carrier. The methodology to determine the kinetic parameters for CuO decomposition and solid fuel oxidation during the fuel reactor stage and for Cu_2O oxidation in the air reactor stage have been discussed. The results of the study are expected to help in the development of a process model for CLOU, furthering the development of a pilot scale process.

1. INTRODUCTION

Technologies based on the concept of chemical-looping combustion (CLC) have attracted significant attention in the past decade due to its potential to reduce energy penalty and the cost associated with CO_2 capture from coal fired power plants.[1−3] A chemical-looping combustion system typically involves two interconnected fluidized bed reactors with a metal oxide circulating between them. One of the reactors serves as a fuel reactor, in which the fuel is combusted with the help of oxygen supplied by the circulating metal oxide. The metal oxide after being reduced is regenerated by reaction with atmospheric oxygen in the air reactor. As a variant of chemical-looping combustion (CLC), chemical-looping with oxygen uncoupling (CLOU), provides a possibility to obtain lower fuel reactor volumes, especially for the case of combustion of solid fuels.[4] In CLC, it is necessary to first gasify the carbonaceous solid fuel to form syngas, which is subsequently oxidized by direct reaction with a circulating oxygen carrier. The solid carbonaceous fuel in CLOU burns directly by oxygen gas released by the decomposition of the circulating metal oxide (e.g., CuO), which has a faster rate than gasification reactions associated with the CLC process.

A 45−60 fold increase in reaction rate has been reported of the carbon residue in petcoke when reacted with a CuO based oxygen carrier in CLOU experiments, compared to the CLC process with an iron based oxygen carrier in the temperature range 950−985 °C.[5,6] A preliminary process scheme for CLOU representing the material and energy balances and process modeling relationships has been discussed by Eyring et al.[7] Based on the promise offered by CLOU, further studies have been conducted to identify suitable supports for CuO.[8,9] CuO has been identified as one of the candidate metals for a CLOU process owing to its high reactivity and oxygen transport capacity.[8] In a recent study, the CLOU combustion of a bituminous Colombian coal was demonstrated in a continuously operated 1.5 kW_{th} unit using 60 wt % CuO supported on $MgAl_2O_4$.[10] A lower solid inventory of 142 kg CuO/MW_{th} in CLOU[10] compares to CLC where inventories of 1200 kg Fe_2O_3/MW_{th} for combustion of petcoke with a 60% Fe_2O_3 /40% $MgAl_2O_4$ oxygen carrier have been estimated.[11] The motivation behind the current study is to develop a methodology to conduct a rate analysis for a CLOU process for solid carbonaceous fuels using reported literature data for combustion of Mexican petcoke using CuO supported on ZrO_2 as the oxygen carrier.[4,5] It is hoped that the result of this study will facilitate the development of a pilot scale process for CLOU.

2. ANALYSIS OF THE CLOU EXPERIMENTS FOR COMBUSTION OF MEXICAN PETCOKE[4,5]

The reported CLOU experimental data on Mexican petcoke and CuO/ZrO_2 oxygen carrier particles have been used for analysis in this paper.[4,5] The Mexican petcoke had particle sizes between 180 and 250 μm, and the oxygen carrier size was in the 125−180 μm range. 40% CuO was loaded on a ZrO_2 support, which was prepared by freeze-granulation. Previous studies[4,5] have reported a crushing strength of 0.8 N and good performance of the oxygen carrier. The oxygen and carbon dioxide concentration profiles with respect to time were obtained for the CLOU combustion of 0.1 g of Mexican petroleum coke, whose ultimate analysis showed 88.8 mass % carbon, 3.1 mass % hydrogen, 1.0 mass % nitrogen, 6.6 mass % sulfur, and 0.5 mass % oxygen (dry, ash-free basis). This was done in a batch fluidized bed consisting of 15 g of the oxygen carrier. The analysis has been performed for three experimental data sets obtained at 900, 950, and 985 °C.

Received: March 14, 2012
Revised: May 23, 2012
Published: May 24, 2012

The CuO decomposition reaction was studied in the experiment while the CuO/ZrO_2 particles were kept fluidized by pure N_2 which was introduced at the bottom of the reactor through a porous quartz plate. The experiments were conducted in a cylindrical-shaped batch fluidized bed constructed of quartz of a total length of 870 mm and a diameter of 22 mm. The effluent gases were cooled and analyzed for CO, CO_2, CH_4, and O_2 at the reactor exhaust (See refs 4 and 5 for details). At this stage, the decomposition of CuO occurred, accompanied by the release of gaseous O_2, which is characterized by the reaction: $4CuO(s) \rightarrow 2Cu_2O(s) + O_2(g)$. The kinetics of the CuO decomposition reaction can be obtained by analyzing the rate of oxygen release of this stage. The product of the oxygen concentration and the fluidizing gas flow rate provides a measure of the oxygen generation after the switch to the nitrogen flow and before the introduction of the petcoke particles. In this study, the corrections to the gaseous concentrations due to axial dispersion have not been included (dispersion number < 0.02).

At a particular instant in the experiment, petcoke particles were introduced in the top of the reactor where they react with the gaseous oxygen released from the CuO decomposition reaction to form CO_2. As the fuel was dropped into the reactor, volatiles were immediately released as evidenced by trace amounts of CO and CH_4. These volatiles escaped the reactor before they could react with the active oxygen carrier bed located at the bottom of the reactor, as a result of the upward flowing fluidizing gas. Figure 1 represents the effluent gaseous concentration data for CO_2,

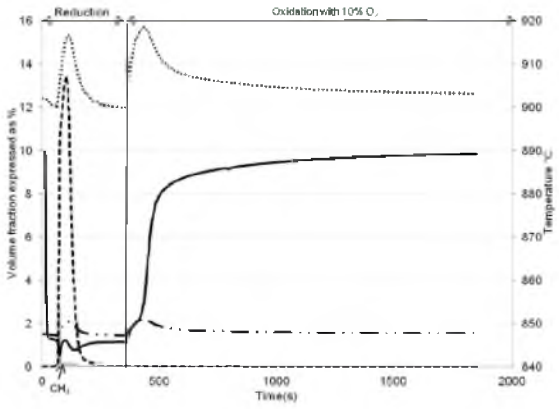

Figure 1. Effluent gas concentrations: — O_2, – •• – equilibrium O_2 (determined by correlating from temperature measurements), - - - CO_2, •••• temperature, CH_4 has been represented by a light gray trace. Experiments were conducted at 900 °C[4,5].

CH_4, and O_2 at 900 °C. As can be seen from Figure 1, the effluent concentration of O_2 is less than the prevailing equilibrium concentration of O_2 resulting from the CuO decomposition. The CuO amount can be calculated at any time from the initial amount of CuO minus the cumulative loss of O_2 in the effluent O_2 and CO_2. The conversion of CuO with respect to time under the presence of a carbonaceous fuel can thus be determined. The formation of Cu_2O can also be calculated by taking into account the stoichiometry of the chemical reaction $4CuO(s) \rightarrow 2Cu_2O(s) + O_2(g)$. The conversion of carbon in the decomposition phase is obtained by a material balance on carbon, taking into account the amount of carbon present in the Mexican petcoke introduced in the reactor and the effluent CO_2, CO, and CH_4 concentration profiles. Carbon mass balances were within 81 to 92%. For this study, carbon mass normalized to one based on measuring the total amount of carbon exiting as gaseous combustion product was considered. The difference in carbon mass balance could be explained by carbon particle loss. The aforementioned CuO decomposition and the subsequent addition of petcoke particles simulate the fuel reactor stage in the batch fluidized experimental set up.

Figure 2 represents the conversion of CuO with time at temperatures of 900, 950, and 985 °C. The figure includes the

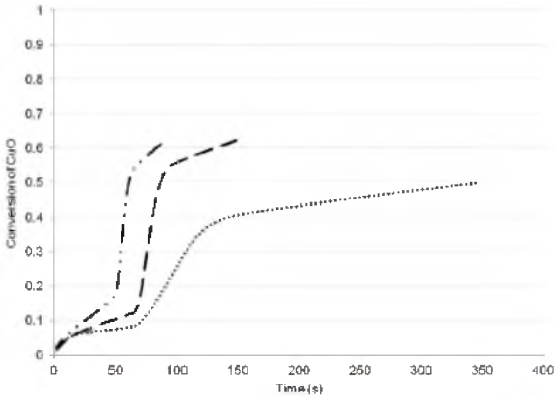

Figure 2. Conversion of CuO vs time [•••• 900 °C, - - - 950 °C, – •• – 985 °C].

time periods when CuO is introduced in N_2, represented by an initial slope of a lower magnitude and the phase where petcoke particles are introduced in the reactor represented by a slope of higher magnitude. The difference in the magnitudes of slopes occurs as the rate of CuO decomposition reaction is enhanced due to the removal of O_2 by the petcoke particles to form CO_2. After the fuel particles are burnt, the slope of conversion of CuO vs time again decreases. From Figure 2, it can be seen that the rate of CuO decomposition increases with temperature. The time taken to attain 40% conversion of CuO particles varied from 142 s at 900 °C to 56 s at 985 °C. The area under the CO_2, CO, and CH_4 peaks provide information regarding the consumption of carbon with respect to time. Figure 3 represents the conversion of Mexican petcoke fuel for the temperatures analyzed in the study. As expected, the rate of conversion of fuel increases with temperature. It can be seen that the time taken to attain 95% conversion varied from 78 s at 900 °C to 15 s at 985 °C.

To simulate the air reactor in the batch fluidized bed experimental setup, reduced oxygen carrier particles were fluidized in a 10% oxygen in nitrogen gaseous mixture (for experiments conducted at 900 and 950 °C). The rate of oxygen consumption is given by the fluidizing gas flow rate times the difference between the inlet oxygen concentration of 10% and the measured effluent oxygen concentration. The concentration of the unreacted Cu_2O at any time is calculated by means of a material balance. Figure 4 represents conversion of Cu_2O with time at 900 and 950 °C. In this study, the Cu_2O oxidation data at 985 °C were not considered since these data were at 21% inlet O_2 concentration versus 10% O_2. From this figure, it can be inferred that the Cu_2O oxidation process occurs at a faster rate at a lower temperature of 900 °C than at 950 °C. 60% of the Cu_2O formed in the reduction phase was regenerated in 112 s at 900 °C, as

dx.doi.org/10.1021/ef300452p | Energy Fuels 2012, 26, 4395–4404

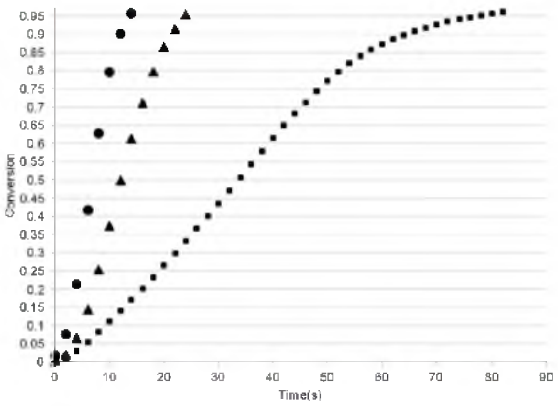

Figure 3. Conversion of Mexican petcoke vs time, from experimental data [■ 900 °C, ▲950 °C, ●985 °C].

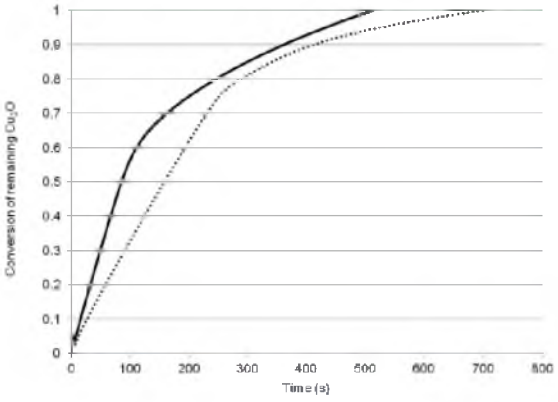

Figure 4. Conversion of remaining Cu_2O at 10% oxidation from experimental data [– 900 °C, ●●●● 950 °C].

compared to 194 s at 950 °C. The decrease in oxidation rate with increase in temperature has been attributed to the oxidation rate being controlled by the diffusion of oxygen through the CuO layer engulfing the Cu_2O. As bulk diffusion through the CuO is slow, the rate is controlled by the diffusion through grain boundaries in the CuO. With an increase in temperature, the grains grow rapidly and cause a reduction in the rate of oxidation.[12,13] This refers to the reaction of individual Cu_2O grains. The particle as a whole still retains porosity formed by the matrix material. The reduction in the rate of Cu_2O oxidation with temperature in the temperature range 850–950 °C has also been observed in other experimental studies.[7]

3. METHODOLOGY TO OBTAIN KINETIC INFORMATION FROM CONVERSION VERSUS TIME DATA IN A CLOU EXPERIMENT

The process of CuO decomposition in the fuel reactor has been analyzed using a first order rate expression, and the process of Cu_2O oxidation in the air reactor has been analyzed using the Law of Additive Reaction Times,[14–16] a method developed to analyze gas solid reactions for porous solids.

When petcoke particles are introduced in the fluidized bed, an increase in temperature, ranging between 10 to 15 °C for the experiments conducted in the temperature range 900–985 °C, occurs as a result of fuel combustion.[4,5] An average of the temperature measurements, T_{avg} for each experimental data set in the time period where CuO decomposition and fuel combustion occur simultaneously was used in the rate equations for CuO decomposition and char oxidation.

3.1. Determination of Apparent Rate Constants for CuO Decomposition. The conversion vs time data for CuO decomposition was analyzed by using a simplified picture of a fluidized bed reactor, in which the solid particles are fully mixed and the gas is in a plug flow. As seen in Figure 2, there are two distinct slopes, one of a lower magnitude, which represents the evolution of O_2 when the fuel particles are not introduced. The slope of higher magnitude is for the conversion of CuO vs time during the consumption of O_2 by fuel particles. The CuO decomposition has been analyzed by the following general form of the rate equation. The effect of intrapartide diffusion and external mass transfer for CuO decomposition was investigated, and it was found that they do not have an effect on the reaction rate.

$$\frac{dX_{CuO}}{dt} = k_{CuO} f_1(p_{O_2}) f_2(X_{CuO}) \tag{1}$$

The rate of CuO decomposition has been analyzed by taking into account the effect of the oxygen concentration by a function $f_1(p_{O_2})$, incorporating the equilibrium limitation for the decomposition reaction, and a conversion function $f_2(X_{CuO})$, which considers the reaction mechanism and geometrical change in solid as the reaction proceeds. Assuming a first-order dependence on p_{O_2},

$$f_1(p_{O_2}) = p_{O_2,e} - p_{O_2} \tag{2}$$

The equilibrium relationship for the reaction $4CuO(s) \rightarrow 2Cu_2O(s) + O_2(g)$ (assuming pure solid phases) can be expressed as

$$K_E = \frac{a_{Cu_2O}^2 a_{O_2}}{a_{CuO}^4} = p_{O_2,e} = e^{(-\Delta G^\circ/RT)} \tag{3}$$

Substituting $\Delta G^\circ = \Delta H^\circ - T\Delta S^\circ$ in eq 3 yields

$$p_{O_2,e} = e^{(-\Delta H^\circ/RT)} e^{(-\Delta S^\circ/R)} \sim e^{(-\Delta H^\circ/RT)} \tag{4}$$

Equation 4 denotes a strong temperature dependence of partial pressure of oxygen at equilibrium conditions on the standard enthalpy of reaction and a weak dependence on the standard entropy of the reaction.

The rate constant k_{CuO} also has an Arrhenius temperature dependence

$$k_{CuO} = k_{0,CuO} e^{(-E/RT)} \tag{5}$$

Therefore, the temperature dependence for the CuO decomposition reaction primarily depends on two terms: the energy required to overcome the thermodynamic barrier for the CuO decomposition reaction, represented by $(-\Delta H^\circ)$ and the activation energy (E) to overcome the kinetic barrier. A detailed description of the influence of chemical equilibrium and the consequent falsification of activation energy has been discussed by Sohn.[17] The procedure for analyzing the kinetics of the CuO decomposition, incorporating the individual contributions of kinetic and thermodynamic terms, has previously been used in the detailed analysis of dehydrogenation kinetics of the Mg–Ti–H hydrogen storage system.[18]

dx.doi.org/10.1021/ef300452p | Energy Fuels 2012, 26, 4395–4404

Taking into consideration the variation of p_{O_2} along the bed height, the arithmetic mean of the O_2 partial pressure driving forces at the inlet and outlet was used for $f_1(p_{O_2})$.

$$(p_{O_2,e} - p_{O_2})_{avg} = \frac{(p_{O_2,e} - p_{O_2,in}) + (p_{O_2,e} - p_{O_2,out})}{2} \quad (6)$$

While the log mean of the driving force is the appropriate average for a first order process, in this case, the experimental values of exit p_{O_2} is sometimes very close to $p_{O_2,e}$, causing the log mean to be unreliable or undefined. Thus, the arithmetic mean was used in this work as an approximate alternative. As the partial pressure of oxygen at the inlet is zero for the fuel reactor stage of the experiment, eq 6 simplifies to

$$f_1(p_{O_2,e}) = (p_{O_2,e} - p_{O_2})_{avg} = \frac{(2p_{O_2,e} - p_{O_2,out})}{2} \quad (7)$$

The equilibrium partial pressure $p_{O_2,e}$[19] has been determined by correlating the measurements of the temperature of the bed. The outlet partial pressure $p_{O_2,out}$ was obtained from the oxygen outlet concentration experimental data.

The following first-order conversion function for $f_2(X_{CuO})$ was found to yield a satisfactory representation of the experimental data:

$$f_2(X_{CuO}) = (1 - X_{CuO}) \quad (8)$$

The substitution of $f_1(p_{O_2})$ and $f_2(X_{CuO})$ in eq 1 yields

$$\frac{dX_{CuO}}{dt} = k_{CuO}(p_{O_2,e} - p_{O_2})_{avg}(1 - X_{CuO}) \quad (9)$$

The different slopes in Figure 2 represent the effect of the oxygen concentration driving force $(p_{O_2,e} - p_{O_2})_{avg}$. In the absence of fuel particles, $p_{O_2,out}$ approaches $p_{O_2,e}$, and thus, the driving force is reduced substantially. Hence, kinetic analysis of the regime where no fuel particles have been introduced in the reactor may result in a certain degree of error in the determination of underlying controlling factor (chemical reaction or mass transfer) and, consequently, the relevant kinetic parameters. When both fuel combustion and CuO decomposition occur, in this case from 66 to 90 s at 950 °C in Figure 2, the slope of the curve, obtained by a plot between $-\ln(1 - X_{CuO})/(p_{O_2,e} - p_{O_2})_{avg}$ vs time yields the rate constant k_{CuO}. The rate constant for CuO decomposition k_{CuO} was calculated on the basis of these measurements. A plot of k_{CuO} versus $1/T_{avg}$, according to the Arrhenius relation, is shown in Figure 5. The fit yields the following equation for the reaction rate constant:

$$k_{CuO} = 3e^{(-2350/T)} \quad (10)$$

The activation energy from the first order rate constant k_{CuO} of the data for CuO/ZrO_2 particles was calculated to be 20 kJ/mol. The largest error is likely to be in the outlet oxygen concentration, since this has been assumed as the local oxygen concentration prevailing in the reactor. This was further investigated mathematically by lowering the experimental outlet oxygen concentration by 50% and determining k_{CuO}. This resulted in approximately 25% difference in the activation energy. Therefore, 20 kJ/mol ±5 kJ/mol is likely to be the range of activation energy of CuO determined. This energy represents the energy required to overcome the kinetic barrier. To consider the

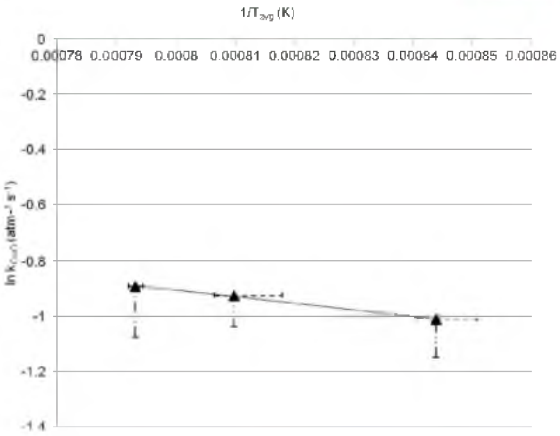

Figure 5. Logarithm of rate constant of CuO decomposition ($\ln k_{CuO}$) vs $1/T_{avg}$ [▲ experimental data, — equation fit, - - error bar representing the temperature measurement range, — •• — error bar representing the scenario if the outlet partial pressure of O_2 is reduced by half.

effect of the thermodynamic barrier under the condition where the oxygen concentration driving force is significant as a result of the introduction of fuel particles ($p_{O_2,out} \ll p_{O_2,e}$) or

$$f_1(p_{O_2}) \approx p_{O_2,e} \quad (11)$$

Substituting eqs 4, 5, and 11 into eq 1 yields:

$$\frac{dX_{CuO}}{dt} = k_{0,CuO}e^{[-(E+\Delta H^0)/RT]}f_2(X_{CuO}) \quad (12)$$

The standard enthalpy of reaction at 1200 K (927 °C) for the reaction $4CuO(s) \rightarrow 2Cu_2O(s) + O_2(g)$ is 261 kJ/mol.[19] The sum of the standard enthalpy of reaction and the activation energy obtained for CuO supported on ZrO_2 particles in the size range 125−180 μm by analyzing batch fluidized bed data is 281 kJ/mol. The value is close to the reported activation energy values of 322 kJ/mol for pure unsupported CuO particles of the sizes of 10 μm[20] and 327 kJ/mol for pure unsupported CuO particles in the size range of 1−10 μm[7] obtained from thermogravimetric analysis (TGA) experiments on CuO decomposition. The experimental data obtained by TGA[7,20] was modeled by a first order CuO decomposition model and does not consider the separation of effects of chemical kinetics and partial pressure (thermodynamics). The above rate analysis, although it contains certain simplifying assumptions, is in excellent agreement with other independent measurements. It also indicates that the kinetic barrier is much smaller than the thermodynamic barrier for CuO decomposition, that is, approximately 20 kJ/mol as compared with 260 kJ/mol.

A comparison was made between the experimental data of CuO decomposition vs time and the rate equation represented by

$$\frac{dX_{CuO}}{dt} = k_{CuO}\overline{(p_{O_2,e} - p_{O_2})_{avg}}(1 - X_{CuO}) \quad (13)$$

where k_{CuO} is provided by eq 10 and $\overline{(p_{O_2,e} - p_{O_2})_{avg}}$ is the average of all the experimental measurements of $(p_{O_2,e} - p_{O_2})_{avg}$ obtained in the time period when CuO decomposition and fuel combustion occur simultaneously. For each temperature condition, the variable driving force $(p_{O_2,e} - p_{O_2})_{avg}$ during the

dx.doi.org/10.1021/ef300452n | Energy Fuels 2012, 26, 4395−4404

course of the experiment is represented by $\overline{(p_{O_2,e} - p_{O_2})_{avg}}$ to facilitate a comparison, which is presented in Figure 6. It can be

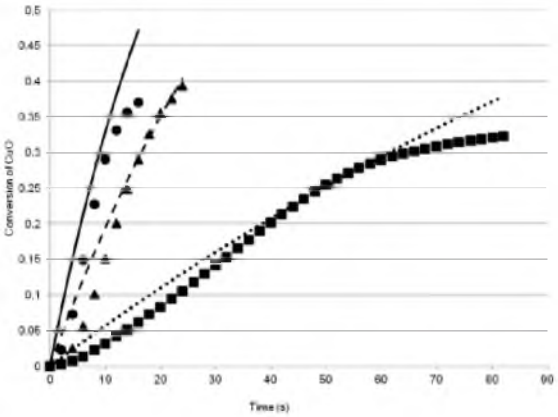

Figure 6. Comparison of experimental data and prediction from rate equation of CuO decomposition with time [■ experimental data 900 °C; ●●●● prediction 900 °C; ▲ experimental data 950 °C; – – – predictions 950 °C; ● experimental data 985 °C; – prediction 985 °C].

observed from the figure that eq 13 reasonably predicts the experimental data for CuO decomposition. Table 1 lists the values of parameters that were used to analyze the experimental data for CuO decomposition.

Table 1. Data Used for Developing the Rate Equation for CuO Decomposition[4,5]

param.	value (atm)
$\overline{(p_{O_2,e} - p_{O_2})_{avg}}$ for experiments at 900 °C (T_{avg} = 912 °C)	0.014
$\overline{(p_{O_2,e} - p_{O_2})_{avg}}$ for experiments at 950 °C (T_{avg} = 962 °C)	0.052
$\overline{(p_{O_2,e} - p_{O_2})_{avg}}$ for experiments at 985 °C (T_{avg} = 987 °C)	0.085

3.2. Determination of Reaction Rate Constants for Cu_2O Oxidation Reaction. To analyze the Cu_2O oxidation process in the air reactor phase of the batch fluidized bed experiment, a closed-form equation for the relationship between the conversion of solid reactant and time, known as the Law of Additive Reaction Times,[14] was utilized. Conceptually, the law states that

$$\begin{bmatrix}\text{Time required}\\ \text{to attain a certain}\\ \text{conversion}\end{bmatrix} \cong \begin{bmatrix}\text{Time required}\\ \text{to attain the same}\\ \text{conversion under the}\\ \text{conditions of rapid}\\ \text{pore diffusion}\end{bmatrix} + \begin{bmatrix}\text{Time required}\\ \text{to attain the same}\\ \text{conversion under the}\\ \text{rate control by}\\ \text{pore diffusion and}\\ \text{external mass transfer}\end{bmatrix} \quad (14)$$

Mathematically, eq 14 is expressed as

$$t_g^* \cong g_{F_g}(X) + \tilde{\sigma}^2\left(p_{F_p}(X) + \frac{4X}{N_{Sh}^*}\right) \quad (15)$$

Equation 15 is a dimensionless relationship between conversion and time expressed in terms of a conversion function for chemical reaction control, a conversion function for pore diffusion control, a modified Sherwood number, and a porous solid reaction modulus. The law is applicable for isothermal reactions in which the effective diffusivity of the solid remains constant during the reaction.[21] In a recent paper, it was shown that Cu oxidation reaction in an air reactor can be analyzed using the Law of Additive Reaction Times for a CLC System.[22]

For the general form of the first-order reaction A(g) + bB(s) → cC(g) + dD(s), an approximate solution of the form has been determined for grains and pellets characterized by a shape factor.

The dimensionless time, t_g^* is defined as[16]

$$t_g^* = \frac{bk_g}{\tilde{\rho}_S}\left(\frac{A_g}{F_g V_g}\right)\left[C_{A0} - \frac{C_{C0}}{K_E}\right]t \quad (16)$$

The conversion function for a porous solid made up of grains under chemical reaction control, $g_{F_g}(X)$, can be expressed as[15]

$$g_{F_g}(X) = 1 - (1 - X)^{1/F_g} \quad (17)$$

The conversion function for pore diffusion control $p_{F_p}(X)$ is represented by[23]

$$p_{F_p}(X) = 1 - \frac{F_p(1 - X)^{2/F_p} - 2(1 - X)}{F_p - 2} \quad (18)$$

The porous solid reaction modulus,[14] $\tilde{\sigma}^2$, for an isothermal first order reaction with respect to gaseous reactant A is defined as

$$\tilde{\sigma}^2 \equiv \left\{\frac{a_S k_g F_p}{2D_e}\right\}\left(\frac{A_g}{F_g V_g}\right)\left(\frac{V_p}{A_p}\right)^2 \quad (19)$$

The modified Sherwood number,[16] N_{Sh}^*, defined as follows, is used to account for the effect of external mass transfer.

$$N_{Sh}^* = N_{Sh}\left(\frac{D_M}{D_e}\right) \quad (20)$$

The relationships used to determine the values of molecular diffusivity, D_M, effective diffusivity, D_e, and Sherwood number, N_{Sh}, for the case of Cu_2O oxidation are similar to that applied to Cu oxidation, which has been reported previously.[22] For the current analysis of Cu_2O apparent rate constants was determined since the diffusion through the CuO product layer around each individual grain changes with conversion as previously discussed.[12,13]

To analyze the Cu_2O oxidation reaction, the analysis using the Law of Additive Reaction Times has been performed using the following considerations. Since structural data for grain dimensions was not available, an apparent rate constant for Cu_2O oxidation, $k_{Cu_2O,app}$ is determined by

$$k_{Cu_2O,app} = \frac{k_g}{r_g} \quad (21)$$

The dimensionless time, t_g^*, in this case is defined as

dx.doi.org/10.1021/ef300452p | Energy Fuels 2012, 26, 4395–4404

$$t_g^* = \frac{bk_{Cu_2O,app}}{\tilde{\rho}_{S,Cu_2O}}\left[\frac{P_{O_2}}{RT} - \frac{P_{O_2,e}}{RT}\right]_{avg} t \quad (22)$$

where

$$\left[\frac{P_{O_2}}{RT} - \frac{P_{O_2,e}}{RT}\right]_{avg} = \left[\left[\frac{P_{O_2,in}}{RT_{avg}} - \frac{P_{O_2,e}}{RT_{avg}}\right] + \left[\frac{P_{O_2,out}}{RT_{avg}} - \frac{P_{O_2,e}}{RT_{avg}}\right]\right]/2 \quad (23)$$

An average $\left[\frac{P_{O_2}}{RT} - \frac{P_{O_2,e}}{RT}\right]_{avg}$ of the arithmetic mean of the measurements of the driving force due to the variation in oxygen concentration driving force $\left[\frac{P_{O_2}}{RT} - \frac{P_{O_2,e}}{RT}\right]_{avg}$ was evaluated with the help of experimentally measured bed temperature, inlet O_2 concentration and measured exit O_2 concentration of 10% at 900 and 950 °C. To account for the exothermic reaction in the oxidation process, which causes a variation of 20 at 900 °C and 13 at 950 °C, an average temperature T_{avg} was used for the analysis. Table 2 lists the values of parameters that were used to analyze the experimental data for Cu_2O oxidation.

Table 2. Data Used for Developing the Rate Equation for Cu_2O Oxidation[4,5]

param.	value
r_p	76.5 μm[a]
ϵ	0.64
S	1.4 m^2/g
ρ_p	2140 kg/m^3
u	0.04 m/s (at NTP)
u/u_{mf}	27
$\tilde{\rho}_{S,Cu_2O}$	41931.6 mol/m^3
α_S	0.1425
$p_{O_2,in}$	0.1 atm
$\overline{(p_{O_2} - p_{O_2,e})_{avg}}$ for experiments at 900 °C (T_{avg} = 911 °C)	0.059 atm
$\overline{(p_{O_2} - p_{O_2,e})_{avg}}$ for experiments at 950 °C (T_{avg} = 959 °C)	0.021 atm

[a]Diameter was evaluated by taking the average of 125 and 180 μm.

The equilibrium partial pressure of oxygen was determined with the help of thermodynamic tables.[19]

The conversion function for chemical reaction for a spherical grain is

$$g_{F_g}(X) = 1 - (1 - X)^{1/3} \quad (24)$$

The choice of a spherical geometry for a grain was made after applying the conversion function for chemical reaction of various geometries and identifying a suitable fit to the experimental data.

The conversion function for gas diffusion through pores for a spherical particle is

$$p_{F_p}(X) = 1 - 3(1 - X)^{2/3} + 2(1 - X) \quad (25)$$

Applying the aforementioned considerations as in the previous case, eq 15 can be written for modeling the Cu_2O oxidation process as

$$t \cong \left[\left(\frac{RT_{avg}\alpha_g\tilde{\rho}_{s,Cu_2O}}{2k_{Cu_2O,app}\overline{(p_{O_2} - p_{O_2,e})_{avg}}}\right)\{1 - (1 - X)^{1/3}\}\right] + \left[\left(\frac{RT_{avg}\alpha_g\tilde{\rho}_{s,Cu_2O}r_p^2}{12D_e\overline{(p_{O_2} - p_{O_2,e})_{avg}}}\right)\{1 - 3(1 - X)^{2/3} + 2(1 - X)\}\right] + \left[\left(\frac{RT_{avg}\alpha_g\tilde{\rho}_{s,Cu_2O}r_p^2}{3D_MN_{Sh}\overline{(p_{O_2} - p_{O_2,e})_{avg}}}\right)X\right] \quad (26)$$

Equation 26 relates the time required to achieve a certain conversion of Cu_2O to the sum of time required to attain the same conversion under chemical reaction control plus the time required to attain the same conversion under reaction rate control by gas pore diffusion and external mass transfer effects. The first term on the right hand side of eq 26 incorporating the $g_{F_g}(X)$ function represents the rate of the reaction of individual grains. At higher temperatures, the apparent rate constant $k_{Cu_2O,app}$ contained in this term may contain the effect of solid state diffusion in CuO layer. At higher temperatures, due to sintering, a CuO layer over the Cu_2O grain may become less porous or very dense.[12,13] In such a case, the Cu_2O oxidation could proceed through the solid state diffusion of species. Using the parameters in Table 2, it was determined that the Cu_2O oxidation is not affected by gas pore diffusion and external mass transfer. As previously discussed, the rate of Cu_2O oxidation decreases at higher conversions,[7,12,13] with 80% of the conversion taking place at 246 s at 900 °C and 290 s at 950 °C. Hence, the term $\overline{(p_{O_2} - p_{O_2,e})_{avg}}$ mentioned in Table 2 and utilized in eq 26 has been evaluated for the experimental data up to 80% conversion in this analysis. As for any gas solid reaction, when the conversion vs time profile has a long tail, small differences in measured conversion over a long time interval become sensitive to error. Hence, inclusion of experimental data at higher conversions may not be representative of the driving force as described by eq 23. Figures 7 and 8 represent the comparison of

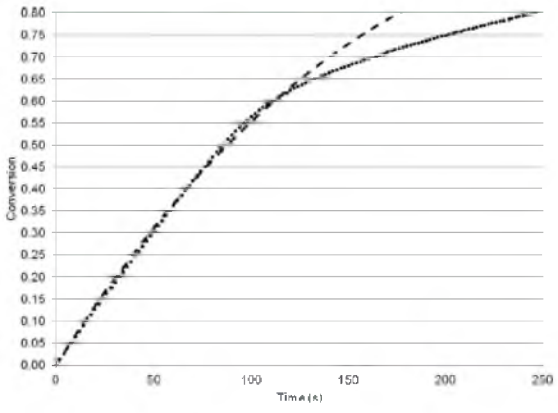

Figure 7. Comparison of experimental data for conversion of Cu_2O vs time at temperatures of 900 °C (oxidation with 10% O_2 in N_2) with the expression 26 derived by the Law of Additive Reaction Times for k_{app,Cu_2O} = 11.50 s^{-1} (● experimental data points; - - - conversion for chemical reaction control).

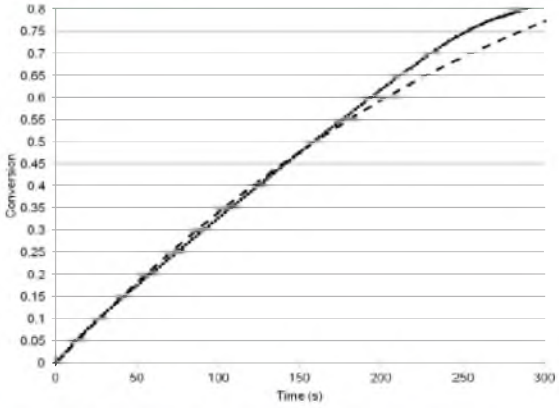

Figure 8. Comparison of experimental data for conversion of Cu_2O vs time at temperatures of 950 °C (oxidation with 10% O_2 in N_2) with the expression 26 derived by the Law of Additive Reaction Times for $k_{appCu_2O} = 18.6\ s^{-1}$ (● experimental data points; - - - conversion for chemical reaction control).

experimental Cu_2O conversion vs time data at 900 and 950 °C (both at 10% O_2 inlet concentration) with eq 26. The value of $k_{Cu_2O,app}$ calculated for the oxidation experiment at 900 °C is 11.5 s^{-1} and 950 °C is 18.6 s^{-1}. These apparent rate constants take into account the previously mentioned resistance to the O_2 diffusing through the nonporous and more dense CuO product layer around each grain of Cu_2O.[12,15] In the data analyzed, the gas pore diffusion through the particle from its outer surface to its interior and the external mass transfer were much faster than the reaction of each grain of Cu_2O distributed throughout the particle. Thus, the overall rate for Cu_2O oxidation is controlled by the reaction of each Cu_2O grain, which is slower as the temperature increases due to the reason explained previously.

3.3. Determination of Global Reaction Rate Constants for Char Oxidation Reaction. The global reaction rate constant was obtained by fitting the value of $k_{r,C}$ to the shrinking sphere equation with a half-order dependence on partial pressure of oxygen:[24]

$$\frac{dr_C}{dt} = -\frac{k_{r,C}}{\rho_C} p_{O_2,avg}^{1/2} \tag{27}$$

The value of $p_{O_2,avg}^{1/2}$ was calculated by the following relation, based on the fact that the arithmetic average is the correct average when the rate has a half-order dependence on the driving force[25]

$$p_{O_2,avg}^{1/2} = \frac{p_{O_2,in}^{1/2} + p_{O_2,out}^{1/2}}{2} = \frac{p_{O_2,out}^{1/2}}{2}, \ (\text{as } p_{O_2,in} = 0) \tag{28}$$

Equation 27 can be integrated within the limits of initial radius of the particle and 95% burnout. Figure 9 represents the logarithm of $k_{r,C}$ plotted versus the inverse of the average temperature, T_{avg} which yielded the activation energy and pre-exponential factor. The reaction rate constant $k_{r,C}$ was investigated in the same temperature range as CuO decomposition. Thus,

$$k_{r,C} = 930e^{(-15500/T)} \tag{29}$$

The activation energy for the Mexican petcoke was calculated to be 129 kJ/mol by eq 29. Hurt and Mitchell[24] studied a variety of U.S. coals in the size range 106−125 μm and in the temperature

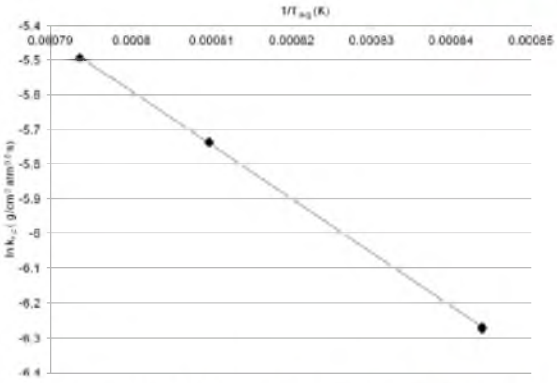

Figure 9. Logarithm of global reaction rate constant of Mexican petcoke oxidation (ln $k_{r,C}$) vs $1/T_{avg}$ [◆ experimental data; − equation fit].

range 1227−1427 °C. They found that Pocahontas coal char, having comparable carbon content and heating value as compared to the petcoke, had an activation energy of 126 kJ/mol. The ultimate analysis of Pocahontas coal analyzed by Hurt and Mitchell[24] and Mexican petcoke are compared in Table 3. The pre-exponential factors for the two solid fuels were 930 g/(cm^2 atm$^{0.5}$ s) for Mexican petcoke versus 114 g/(cm^2 atm$^{0.5}$ s) reported for Pocahontas coal char.

The experimental data was compared with the help of reaction rate constant for carbon oxidation provided by eq 29, substituted in the rate equation, eq 27. The partial pressure of oxygen was computed at the average of outlet pressures $\overline{p_{O_2,avg}}$ during the combustion period. The parameters used to compare the prediction made by the rate equation with the determined reaction rate constant for petcoke oxidation are listed in Table 4. The results of the comparison are represented in Figure 10, which indicates the adequacy of the relationship utilized to predict the conversion of solid fuel used in the experimental study.

4. DISCUSSION

The development of the CLOU process holds significant potential as a solid fuel combustion technology. In this study, rate analysis of the CLOU process was conducted for both the air and fuel reactors by interpreting experimental data on Mexican petcoke combustion with CuO supported on ZrO_2 particles. The analysis with petcoke represents a conservative estimation of the CuO decomposition reaction, since petcoke reacts slowly. For the temperatures studied, oxygen concentration in the exhaust gas was not zero. Since the partial pressure of O_2 around the CuO oxygen carrier creates a resistance for the O_2 release, a faster reacting fuel might consume more of the oxygen, enhancing the O_2 release and giving a faster overall reactivity for CuO decomposition.

The CuO decomposition reaction was investigated in the regime where fuel particles were introduced, which is characterized by the presence of a substantial oxygen concentration driving force. The rate equation for CuO decomposition took into account a first-order dependence on p_{O_2}, which incorporates the equilibrium limitation and a first order conversion function with respect to solid reactant. The apparent activation energy for CuO decomposition reaction was determined to be 280 kJ/mol, which accounts for the energy requirements to overcome the kinetic and thermodynamic

dx.doi.org/10.1021/ef300452p | Energy Fuels 2012, 26, 4395−4404

Table 3. Ultimate Analysis for Non-reactive Coals Used for Comparison[5,26]

coal	C (wt % d.a.f)	H (wt % d.a.f)	O (wt % d.a.f)	N (wt % d.a.f)	S (wt % d.a.f)	Cl (wt % d.a.f)	heating value (MJ/kg), as rec'd.
Mexican petcoke	88.8	3.1	0.5	1.0	6.6		30.9
Pocahontas	91.48	4.38	2.30	1.10	0.69	0.06	33.4

Table 4. Data Used for Developing the Rate Equation for Petcoke Oxidation

param.	value	source
d_C	215 μm[a]	Mattisson et al.[5]
ρ_C	1.02 g/cm^3	estimated by API Gravity[27]
$\overline{P_{O_2,avg}}$ experiments at 900 °C (T_{avg} = 912 °C)	0.0095 atm	estimated from the experimental data[4,5]
$\overline{P_{O_2,avg}}$ experiments at 950 °C (T_{avg} = 962 °C)	0.024 atm	estimated from the experimental data[4,5]
$\overline{P_{O_2,avg}}$ experiments at 985 °C (T_{avg} = 987 °C)	0.044 atm	estimated from the experimental data[4,5]

[a]Diameter has been evaluated by calculating the average of 180 and 250 μm.

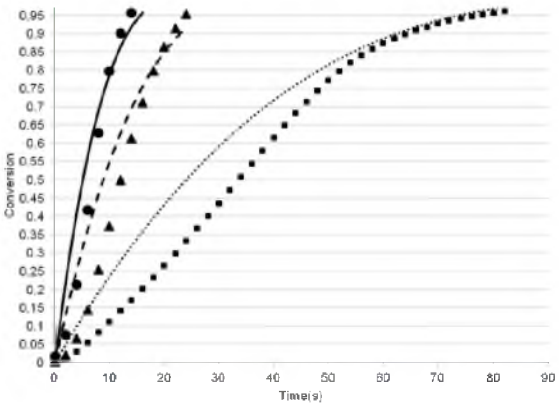

Figure 10. Comparison of experimental data and prediction by rate equation of Mexican petcoke particles with time [■ experimental data, 900 °C; ●●●● prediction, 900 °C; ▲ experimental data, 950 °C; – – – prediction, 950 °C; ● experimental data, 985 °C; – prediction, 985 °C].

barrier. The results obtained were consistent with the findings reported in literature;[7,20] however, the analysis indicates that the kinetic barrier is much smaller than the thermodynamic barrier in the investigated temperature range of 900−985 °C.

The Cu_2O oxidation process in the air reactor was investigated at 900 and 950 °C by applying the Law of Additive Reaction Times. The analysis of the experimental data indicated that internal and external mass transfer did not play a significant role in the oxidation process. It is important to mention that further study is warranted, since studies[12,13] suggest that at higher conversions of Cu_2O, reaction rates changes due to variability in diffusion of O_2 through the CuO product layer over Cu_2O grains.

The Mexican petcoke oxidation reaction was analyzed by the shrinking sphere model, incorporating a global reaction rate constant. The activation energy for petcoke oxidation was determined to be 129 kJ/mol, which compares well with the reported experimental data[24] obtained for pulverized coal char oxidation on particles of a similar size range and properties.

5. CONCLUSIONS

The results presented in this paper show an excellent agreement with independently obtained experimental data, thus indicating that the aforementioned rate analysis is satisfactory, although it contains simplifying assumptions. The rate analysis of the experimental data through the concepts discussed in this paper is expected to facilitate the pilot scale development of CLOU process for solid carbonaceous fuels. The apparent activation energy for CuO decomposition reaction was determined to be 280 kJ/mol. The energy requirements to overcome the thermodynamic barrier for CuO decomposition are substantially larger than the kinetic barrier. The activation energy for petcoke oxidation was estimated at 129 kJ/mol. The apparent rate constants for Cu_2O oxidation were also determined.

■ AUTHOR INFORMATION

Corresponding Author

*E-mail: asad.sahir@utah.edu. Tel.: +1-801-581-6915. Fax: +1-801-585-9291.

Notes

The authors declare no competing financial interest.

■ ACKNOWLEDGMENTS

This material is based upon work supported by the Department of Energy under Award No. DE-NT0005015. The views and opinions of authors expressed herein do not necessarily state or reflect those of the United States Government or any agency thereof. The authors acknowledge the work of the late Prof. Adel Sarofim (deceased Dec. 4, 2011). At the time of his death, he was closely involved in this work and made many important intellectual contributions.

■ NOMENCLATURE

a = activity coefficient
A_g = external surface area of an individual grain, m^2
A_p = external surface area of the particle, m^2
b = number of moles of solid B reacted per mole of fluid reactant A
C_{A0} = concentration of the gaseous species A in the general form A(g)+bB(s) → cC(g) + dD(s), mol/m^3
C_{C0} = concentration of the gaseous species C in the general form A(g)+bB(s) → cC(g) + dD(s), mol/m^3
d_C = diameter of the carbonaceous fuel particle, m
d_p = diameter of particle, m
D_e = effective diffusivity, m^2/s
D_M = molecular diffusivity, m^2/s
E = activation energy, kJ/mol
$f_1(p_{O_2})$ = dependence of rate on oxygen partial pressure
$f_1(X)$ = dependence of rate on fractional conversion
F_g = shape factor for the grain (1, 2, or 3 for flat plates, long cylinders or spheres respectively)
F_p = shape factor for the particle (1, 2, or 3 for flat plates, long cylinders or spheres respectively)
$g_{F_g}(X)$ = conversion function for chemical reaction control (defined in eq 17)
ΔG° = standard gibbs free energy of reaction, kJ/mol

ΔH° = standard enthalpy of reaction, kJ/mol
$k_{0,CuO}$ = pre-exponential factor, atm^{-1} s^{-1}
k_{CuO} = reaction rate constant of CuO decomposition, atm^{-1} s^{-1}
$k_{Cu_2O,app}$ = apparent reaction rate constant of Cu_2O oxidation, s^{-1}
k_g = reaction rate constant for grain, m/s
k_{gC} = reaction rate constant of coal char oxidation, g/$cm^2 atm^{0.5} s$
K_p = equilibrium constant
N_{Sh} = Sherwood number
N_{Sh}^* = modified Sherwood number (defined in eq 20)
$p_{O_2,in}$ = partial pressure of oxygen at inlet of reactor, atm
$p_{O_2,e}$ = partial pressure of oxygen in the equilibrium conditions of CuO decomposition, atm
$p_{O_2,out}$ = partial pressure of oxygen at the exit of reactor, atm
$p_{F_p}(X)$ = conversion function for pore-diffusion control (defined in eq 18)
r_C = radius of the carbonaceous fuel particle, m
r_g = radius of a grain, m
r_p = radius of the oxygen carrier particle, m
R = gas constant, J/(mol K)
S = specific surface area, m^2/g
ΔS° = standard entropy of reaction, kJ/(mol K)
t = time, s
t_g^* = dimensionless time (defined in eq 16)
u = superficial velocity, m/s
u/u_{mf} = ratio of superficial velocity to minimum fluidizing velocity
T = temperature, K
T_{avg} = average of the temperature, K
V_g = volume of a grain, m^3
V_p = volume of a particle, m^3
X_{CuO} = conversion of CuO

Greek Symbols

α_S = fraction of particle volume initially occupied by solid reactant
ε = porosity
$\hat{\sigma}^2$ = porous solid reaction modulus (defined in eq 19)
ρ_C = density of carbonaceous particle (g/cm^3)
ρ_p = density of particle (kg/m^3)
$\bar{\rho}_S$ = molar density of solid reactant (mol/m^3)
$\bar{\rho}_{S,Cu_2O}$ = molar density of Cu_2O (mol/m^3)

Abbreviations

CLOU = chemical looping with oxygen uncoupling
CLC = chemical looping combustion
d.a.f = dry ash free
kW_{th} = kilowatt thermal
MW_{th} = megawatt thermal

REFERENCES

(1) Adanez, J.; Abad, A.; Garcia-Labiano, F.; Gayan, P.; de Diego, L. F. Progress in Chemical-Looping Combustion and Reforming Technologies. *Prog. Energy Combust. Sci.* **2012**, *38* (2), 215−282.
(2) Fan, L. S., *Chemical Looping Systems for Fossil Energy Conversions*; Wiley-AIChE: Hoboken, NJ, 2010.
(3) Moghtaderi, B. Review of the Recent Chemical Looping Process Developments for Novel Energy and Fuel Applications. *Energy Fuels* **2011**, *26* (1), 15−40.
(4) Mattisson, T.; Lyngfelt, A.; Leion, H. Chemical-Looping with Oxygen Uncoupling for Combustion of Solid Fuels. *Int. J. Greenhouse Gas Control* **2009**, *3* (1), 11−19.
(5) Mattisson, T.; Leion, H.; Lyngfelt, A. Chemical-Looping with Oxygen Uncoupling Using CuO/ZrO_2 with Petroleum Coke. *Fuel* **2009**, *88* (4), 683−690.
(6) Leion, H.; Mattisson, T.; Lyngfelt, A. Using Chemical-Looping with Oxygen Uncoupling (CLOU) for Combustion of Six Different Solid Fuels. *Energy Procedia* **2009**, *1* (1), 447−453.
(7) Eyring, E. M.; Konya, G.; Lighty, J. S.; Sahir, A. H.; Sarofim, A. F.; Whitty, K. Chemical Looping with Copper Oxide as Carrier and Coal as Fuel. *Oil Gas Sci. Technol. Rev. IFP Energies nouvelles* **2011**, *66* (2), 209−221.
(8) Arjmand, M.; Azad, A.-M.; Leion, H.; Lyngfelt, A.; Mattisson, T. Prospects of Al_2O_3 and $MgAl_2O_4$-Supported CuO Oxygen Carriers in Chemical-Looping Combustion (CLC) and Chemical-Looping with Oxygen Uncoupling (CLOU). *Energy Fuels* **2011**, *25* (11), 5493−5502.
(9) Adanez-Rubio, I.; Gayan, P.; Garcia-Labiano, F.; De Diego, L. F.; Adanez, J.; Abad, A. Development of CuO-Based Oxygen-Carrier Materials Suitable for Chemical-Looping with Oxygen Uncoupling (CLOU) process. *Energy Proc.* **2011**, *4*, 417−424.
(10) Abad, A.; Adánez-Rubio, I.; Gayán, P.; García-Labiano, F.; de Diego, L. F.; Adánez, J. Demonstration of Chemical-Looping with Oxygen Uncoupling (CLOU) Process in a 1.5 kW_{th} Continuously Operating Unit Using a Cu-Based Oxygen Carrier. *Int. J. Greenhouse Gas Control* **2012**, *6*, 189−200.
(11) Leion, H.; Mattisson, T.; Lyngfelt, A. The Use of Petroleum Coke As Fuel in Chemical-Looping Combustion. *Fuel* **2007**, *86* (12−13), 1947−1958.
(12) Zhu, Y.; Mimura, K.; Isshiki, M. Oxidation Mechanism of Cu_2O to CuO at 600−1050°C. *Oxid. Met.* **2004**, *62* (3−4), 207−222.
(13) Prisedsky, V. V.; Vinogradov, V. M. Fragmentation of Diffusion Zone in High-Temperature Oxidation of Copper. *J. Solid State Chem.* **2004**, *177* (11), 4258−4268.
(14) Sohn, H. Y. The Law of Additive Reaction Times in Fluid−Solid Reactions. *Metall. Trans. B* **1978**, *9* (1), 89−96.
(15) Sohn, H. Y.; Szekely, J. A Structural Model for Gas-Solid Reactions with a Moving Boundary-III. A General Dimensionless Representation of the Irreversible Reaction between a Porous Solid and a Reactant Gas. *Chem. Eng. Sci.* **1972**, *27* (4), 763−778.
(16) Szekely, J.; Evans, J. W.; Sohn, H. Y. *Gas−Solid Reactions*; Academic Press: New York, 1976.
(17) Sohn, H. The Influence of Chemical Equilibrium on Fluid−Solid Reaction Rates and the Falsification of Activation Energy. *Metall. Mater. Trans. B* **2004**, *35* (1), 121−131.
(18) Sohn, H. Y.; Emami, S. Kinetics of Dehydrogenation of the Mg−Ti−H Hydrogen Storage System. *Int. J. Hydrogen Energy* **2011**, *36* (14), 8344−8350.
(19) Pankratz, L. B. *Thermodynamic Properties of Elements and Oxides—Bulletin 672*; U.S. Department of the Interior, Bureau of Mines: Washington, DC, 1982.
(20) Chadda, D.; Ford, J. D.; Fahim, M. A. Chemical Energy Storage by the Reaction Cycle CuO/Cu_2O. *Int. J. Energy Res.* **1989**, *13* (1), 63−73.
(21) Sohn, H. Y. The Effects of Reactant Starvation and Mass Transfer in the Rate Measurement of Fluid−Solid Reactions with Small Equilibrium Constants. *Chem. Eng. Sci.* **2004**, *59* (20), 4361−4368.
(22) Sahir, A. H.; Lighty, J. S.; Sohn, H. Y. Kinetics of Copper Oxidation in the Air Reactor of a Chemical Looping Combustion System Using the Law of Additive Reaction Times. *Ind. Eng. Chem. Res.* **2011**, *50* (23), 13330−13339.
(23) Sohn, H. Y.; Sohn, H. J. The Effect of Bulk Flow Due to Volume Change in the Gas Phase on Gas−Solid Reactions: Initially Nonporous Solids. *Ind. Eng. Chem. Process Des. Dev.* **1980**, *19* (2), 237−242.
(24) Hurt, R. H.; Mitchell, R. E. Unified High-Temperature Char Combustion Kinetics for a Suite of Coals of Various Rank. *Symp. (Int.) Combust.* **1992**, *24* (1), 1243−1250.
(25) Wang, H. Reduction Kinetics of Iron Ore Concentrate Particles Relevant to a Novel Green Ironmaking Process. Ph.D. Dissertation, University of Utah, Salt Lake City, UT, 2011. Wang, H.; Sohn, H. Y.

Complete Rate Expression for the Hydrogen Reduction of Iron Ore Concentrate Relevant to a Novel Ironmaking Process, *Metall. Mater. Trans. B* **2012**, submitted for publication.

(26) Smith, K. L.; Smoot, L. D.; Fletcher, T. H.; Pugmire, R. J. *The Structure and Reaction Processes of Coal*; Plenum Press: New York, 1994.

(27) Marín-Sánchez, J. E.; Rodríguez-Toral, M. A. An Estimation of Cogeneration Potential by Using Refinery Residuals in Mexico. *Energy Policy* **2007**, 35 (11), 5876−5891.

CHAPTER 4

DEVELOPMENT OF A FLUIDIZED BED MODEL OF THE FUEL REACTOR FOR A CHEMICAL-LOOPING WITH OXYGEN UNCOUPLING PROCESS

4.1. Background

This chapter is concerned with the modeling of the fuel reactor stage of a bench-scale fluidized-bed reactor for the CLOU process. The insights derived from the analysis shall assist in the fluidized-bed modeling for a 100-200 kW_{th} CLOU Process Development Unit (PDU) currently under construction at the University of Utah. The kinetic equations of CuO decomposition and petcoke oxidation occurring in the CLOU process discussed in Chapter 3 have been employed in this study.

The analysis is an attempt to validate the CLOU experimental data of Mattisson et al. in a bench-scale batch fluidized-bed reactor using Mexican petcoke as a fuel, and employing 40% CuO supported on ZrO_2 as oxygen carrier particles.[1] In their study in the fuel reactor stage of the CLOU experiment, the two reactions: decomposition of CuO ($4CuO(s) \rightarrow 2Cu_2O(s) + O_2(g)$) and petcoke oxidation (approximated as $C(s) + O_2(g) \rightarrow CO_2(g)$) occur simultaneously. The experimental data on O_2 and CO_2 concentration trends at temperatures of 885, 900, 935, 950, and 985°C have been validated with the model.

4.2. Assumptions, equations, semi-empirical correlations for design

4.2.1. Assumptions made for modeling

The stage in the batch fluidized-bed reactor experiment where the fuel particles are introduced in the reactor is modeled, i.e. the CuO decomposition reaction and carbon oxidation reaction are occurring simultaneously. The oxygen concentration changes with respect to time and height. The following assumptions have been made for modeling the experimental bench-scale CLOU batch fluidized-bed reactor of Mattisson et al.[1]:

- The solids are considered to be well-mixed in the reactor.

- The gases (oxygen and carbon dioxide) are present in the emulsion and the bubble phase and the process of interchange of gases occurs between the two phases.
- The solids are only in the emulsion phase and the CuO decomposition and petcoke oxidation reactions occur in it.

4.2.2. Material balance equations

Material balance equations have been formulated for the bubble and emulsion phase for O_2 and CO_2 gases as represented by Equations 4.1- 4.4.

Bubble phase for oxygen;

$$\frac{f_{g,b}}{RT}\frac{\partial p_{O_2}{}^{bbl}}{\partial t} = \frac{f_{g,b}u_b}{RT}\frac{\partial p_{O_2}{}^{bbl}}{\partial z} + \frac{\delta K_{BE}}{RT}(p_{O_2}{}^{em} - p_{O_2}{}^{bbl}) \tag{4.1}$$

Emulsion phase for oxygen;

$$\frac{f_{g,e}}{RT}\frac{\partial p_{O_2}{}^{em}}{\partial t} = \frac{f_{g,e}u_e}{RT}\frac{\partial p_{O_2}{}^{em}}{\partial z} + \frac{\delta K_{BE}}{RT}(p_{O_2}{}^{bbl} - p_{O_2}{}^{em}) + \left(\frac{1}{4}\right)\frac{n_{CuO}(-r_{CuO})}{V_R} - \frac{n_C(-r_C)}{V_R} \tag{4.2}$$

Bubble phase for carbon dioxide;

$$\frac{f_{g,b}}{RT}\frac{\partial p_{CO_2}{}^{bbl}}{\partial t} = \frac{f_{g,b}u_b}{RT}\frac{\partial p_{CO_2}{}^{bbl}}{\partial z} + \frac{\delta K_{BE}}{RT}(p_{CO_2}{}^{em} - p_{CO_2}{}^{bbl}) \tag{4.3}$$

Emulsion phase for carbon dioxide;

$$\frac{f_{g,e}}{RT}\frac{\partial p_{CO_2}{}^{em}}{\partial t} = \frac{f_{g,e}u_e}{RT}\frac{\partial p_{CO_2}{}^{em}}{\partial z} + \frac{\delta K_{BE}}{RT}(p_{CO_2}{}^{bbl} - p_{CO_2}{}^{em}) + \frac{n_C(-r_C)}{V_R} \tag{4.4}$$

4.2.3. Rate equations

For modeling the fuel reactor stage of the CLOU process in the batch fluidized reactor, the kinetic equations for fuel oxidation and CuO decomposition are used, as discussed in Chapter 3.

The conversion of petcoke particles with respect to time is provided by rate Equation 4.5 and the reaction rate constant for petcoke oxidation $k_{r,C}$ is provided by Equation 4.6.

$$(-r_C) = \frac{dX_C}{dt} = \frac{3k_{r,C}}{\rho_C R_i} p_{O_{2,em}}^{\frac{1}{2}} (1 - X_C)^{2/3} \tag{4.5}$$

$$k_{r,C} = 930 \exp\left(\frac{-15500}{T}\right) \tag{4.6}$$

The conversion of CuO particles with respect to time is provided by the rate Equation 4.7, and the reaction rate constant for CuO decomposition k_{CuO} is provided by Equation 4.8.

$$(-r_{CuO}) = \frac{dX_{CuO}}{dt} = k_{CuO}(p_{O_2}^e - p_{O_{2,em}})(1 - X_{CuO}) \tag{4.7}$$

$$k_{CuO} = 3 \exp\left(\frac{-2350}{T}\right) \tag{4.8}$$

4.2.4. Reactor and Particle Dimensions

The reactor and particle dimensions which were utilized in the development of the mathematical model for the batch fluidized-bed reactor are provided in Table 4.1.

4.2.5. Semi-empirical correlations and design relationships

The fraction of fluidized-bed volume occupied by the gas in emulsion, $f_{g,e}$ is evaluated by Equation 4.9:

Table 4.1 Reactor and particle dimensions[1]

Parameter	Value
Diameter of the fluidized bed, D_T	22 mm
Superficial Velocity, u_0	0.16 m/s
Temperature range of experiments, T	885-985°C
Density of CuO/ZrO_2 particle,ρ_S	2.145 g/cm^3
Average diameter of CuO/ZrO_2 particle (Size Range = 125-180 μm),d_p	152.5 μm
Density of fuel particle, ρ_C	1.02 g/cm^3
Average diameter of fuel particle(Size Range = 180-250 μm), d_C	215 μm

$$f_{g,e} = (1 - \delta - \alpha\delta)\varepsilon_{mf} \tag{4.9}$$

The fraction of fluidized-bed volume occupied by gas in the bubble, $f_{g,b}$ is evaluated by Equation 4.10:

$$f_{g,b} = \delta(1 + \alpha\varepsilon_{mf}) \tag{4.10}$$

The minimum fluidization velocity, u_{mf} was evaluated with Richardson and Jeronimo's correlation.[2]

$$u_{mf} = \left(\frac{\mu}{d_p\rho_g}\right)\left[\left[(25.7)^2 + \left\{0.0365\left(\frac{d_p^3\rho_g(\rho_S-\rho_g)g}{\mu^2}\right)\right\}\right]^{1/2} - 25.7\right] \tag{4.11}$$

The rise velocity of emulsion through the bed[3], u_e is given by Equation 4.12.

$$u_e = \left(\frac{u_{mf}}{\varepsilon_{mf}}\right) - \frac{\alpha\delta u_b}{(1-\delta-\alpha\delta)} \tag{4.12}$$

The fraction of bed volume occupied by bubbles, δ given by Equation 4.13 and the bubble rise velocity, u_b provided by Equation 4.14 was evaluated with the correlations proposed by Puettmann et al.[4],

$$\delta = 0.8\frac{(u_0 - u_{mf})}{u_b} \tag{4.13}$$

$$u_b = 0.8(u_0 - u_{mf}) + (0.71)(1.18)(gd_b)^{0.5} \tag{4.14}$$

The interchange coefficient for gas between bubble and emulsion phases based on bubble volume[5] (1/s): K_{BE} is given by Equation 4.15.

$$K_{BE} = 2\left(\frac{u_{mf}}{d_b}\right) + 12\left(\frac{(\mathcal{D}\varepsilon_{mf}u_b)^{1/2}}{\pi {d_b}^{3/2}}\right) \tag{4.15}$$

The ratio of height of the fluidized-bed to the minimum fluidized-bed height $\left(\frac{L_f}{L_{mf}}\right)$ has been evaluated by the correlation proposed by Babu et al.[6] for fluidized-bed diameters less than 2.5 inches.

$$\frac{L_f}{L_{mf}} = 1 + \frac{0.762(u_0 - u_{mf})^{0.57}\rho_g^{0.083}}{\rho_s^{0.166}u_{mf}^{0.063}D_T^{0.445}} \tag{4.16}$$

A design approximation proposed by Zenz[7] was used to estimate the variation of bubble diameter, $d_b$with height, h.

$$\left(\frac{d_b}{d_{bi}}\right) = 0.15\left(\frac{h}{d_{bi}}\right) + 0.85 \tag{4.17}$$

The initial bubble size, d_{b0} above the porous plate distributor has been evaluated with Mori and Wen's correlation.[8]

$$d_{b0} = 0.00376\,(u_0 - u_{mf})^2 \tag{4.18}$$

For simplicity of analysis, it has been assumed that the particles are spherical in nature and thus have a voidage at minimum fluidization, ε_{mf} of 0.427.

4.3. Solution Methodology

The model equations were solved for a molar feed of 0.0074 mol C (representing 88.8 wt.% C of a 0.1 g Mexican Petcoke feed) and 0.07547 mol CuO (representing 15 g of 40% CuO supported on ZrO_2 oxygen carrier particles). The value of α (ratio of wake volume to bubble volume) used in the model was 0.05. To capture the effect of temperature increase of 10-15°C occurring in the experiment, the experimental temperature trends was correlated with time using a polynomial correlation.

It is assumed that the length of the batch fluidized-bed reactor is divided into N cells as shown in Figure 4.1. The Equations 4.1 - 4.4 are converted into finite difference approximations.

Equation 4.1 represents a material balance in bubble phase on oxygen which can be written as a forward finite difference approximation in Δz as Equation 4.19.

$$\frac{f_{g,b}}{RT}\frac{dp_{O_2{}^{bbl}}}{dt} = \frac{f_{g,b}u_b}{RT}\left[\frac{p_{O_2{}^{bbl}}\big|_{i+1} - p_{O_2{}^{bbl}}\big|_i}{\Delta z}\right] + \frac{\delta K_{BE}}{RT}\left(p_{O_2{}^{em}}\big|_i - p_{O_2{}^{bbl}}\big|_i\right) \tag{4.19}$$

At z = h, the boundary condition $\frac{dp_{O_2{}^{bbl}}}{dz} = 0$ is employed and a backward difference formulation is used for the last cell to evaluate $p_{O_2{}^{bbl}}$.

$$p_{O_2{}^{bbl}}\big|_N = \frac{4p_{O_2{}^{bbl}}\big|_{N-1} - p_{O_2{}^{bbl}}\big|_{N-2}}{3} \tag{4.20}$$

Equation 4.2 represents a material balance in the emulsion phase on oxygen which can be written as a forward finite difference approximation in Δz as Equation 4.21.

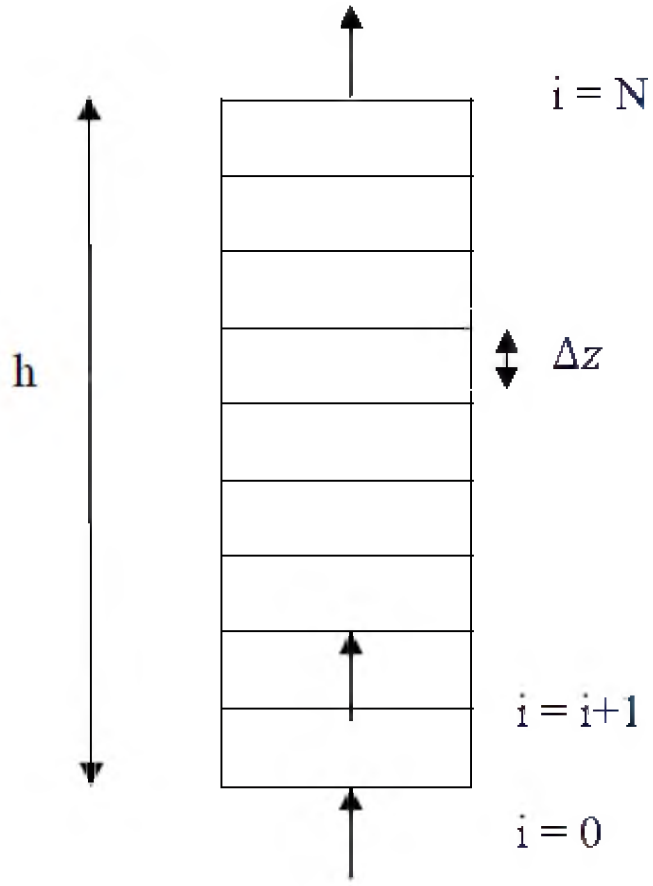

Considerations:

$$At\ z = 0, p_{O_2}{}^{bbl} = p_{O_2}{}^{em} = p_{CO_2}{}^{bbl} = p_{CO_2}{}^{em} = 0$$

$$At\ z = h, \frac{dp_{O_2}{}^{bbl}}{dz} = \frac{dp_{O_2}{}^{em}}{dz} = \frac{dp_{CO_2}{}^{bbl}}{dz} = \frac{dp_{CO_2}{}^{em}}{dz} = 0$$

$$\Delta z = \frac{h}{N}$$

$$h_i = \mathrm{i}\Delta z \ (\text{as } h_0 = 0)$$

Figure 4.1 Schematic to represent the solution scheme

$$\frac{f_{g,e}}{RT}\frac{dp_{O_2}{}^{em}}{dt} = \frac{f_{g,e}u_e}{RT}\left[\frac{p_{O_2}{}^{em}\big|_{i+1} - p_{O_2}{}^{em}\big|_i}{\Delta z}\right] + \frac{\delta K_{BE}}{RT}\left(p_{O_2}{}^{bbl}\Big|_i - p_{O_2}{}^{em}\Big|_i\right) + \left(\frac{1}{4}\right)\frac{n_{CuO}(-r_{CuO})}{V_R} - \frac{n_C(-r_C)}{V_R} \quad (4.21)$$

For fulfilling at z = h, the boundary condition $\frac{dp_{O_2}{}^{em}}{dz} = 0$ is employed and a backward difference formulation is used for the last cell to evaluate $p_{O_2}{}^{em}$.

$$p_{O_2}{}^{em}\big|_N = \frac{4p_{O_2}{}^{em}\big|_{N-1} - p_{O_2}{}^{em}\big|_{N-2}}{3} \quad (4.22)$$

Equation 4.3 represents a material balance in bubble phase on carbon dioxide which can be written as a forward finite difference approximation in Δz, as Equation 4.23.

$$\frac{f_{g,b}}{RT}\frac{dp_{CO_2}{}^{bbl}}{dt} = \frac{f_{g,b}u_b}{RT}\left[\frac{p_{CO_2}{}^{bbl}\big|_{i+1} - p_{CO_2}{}^{bbl}\big|_i}{\Delta z}\right] + \frac{\delta K_{BE}}{RT}\left(p_{CO_2}{}^{em}\big|_i - p_{CO_2}{}^{bbl}\Big|_i\right) \quad (4.23)$$

For fulfilling at z = h, the boundary condition $\frac{dp_{CO_2}{}^{bbl}}{dz} = 0$ is employed and a backward difference formulation is used for the last cell to evaluate $p_{CO_2}{}^{bbl}$.

$$p_{CO_2}{}^{bbl}\Big|_N = \frac{4p_{CO_2}{}^{bbl}\big|_{N-1} - p_{CO_2}{}^{bbl}\big|_{N-2}}{3} \quad (4.24)$$

Equation 4.4 represents a material balance in the emulsion phase on carbon dioxide which can be written as a forward finite difference approximation in Δz as Equation 4.25.

$$\frac{f_{g,e}}{RT}\frac{dp_{CO_2}{}^{em}}{dt} = \frac{f_{g,e}u_e}{RT}\left[\frac{p_{CO_2}{}^{em}\big|_{i+1} - p_{CO_2}{}^{em}\big|_i}{\Delta z}\right] + \frac{\delta K_{BE}}{RT}\left(p_{CO_2}{}^{bbl}\Big|_i - p_{CO_2}{}^{em}\Big|_i\right) + \frac{n_C(-r_C)}{V_R} \quad (4.25)$$

For fulfilling at z = h, the boundary condition $\frac{dp_{CO_2}{}^{em}}{dz} = 0$ is employed and a backward difference formulation is used for the last cell to evaluate $p_{CO_2}{}^{em}$ as provided by Equation 4.26.

$$p_{CO_2}{}^{em}\big|_N = \frac{4p_{CO_2}{}^{em}\big|_{N-1} - p_{CO_2}{}^{em}\big|_{N-2}}{3} \tag{4.26}$$

The reaction rates and reaction rate constants provided by Equations 4.5-4.8 were evaluated at each cell representing a spatially discretized height interval, Δz. Thus for a discretized bed height Δz, the rate of fuel oxidation and CuO decomposition in a cell **i** can be represented by Equations 4.27 and 4.28, respectively.

$$(-r_C)_i = \left[\frac{dX_C}{dt}\right]_i = \left[\frac{3k_{r,C}}{\rho_C R_i} p_{O_2,em}^{\frac{1}{2}} (1 - X_C)^{2/3}\right]_i \quad ; (1 \leq \mathbf{i} \leq \text{N-1}) \tag{4.27}$$

$$(-r_{CuO})_i = \left[\frac{dX_{CuO}}{dt}\right]_i = \left[k_{CuO}(p_{O_2}^e - p_{O_2,em})\,(1 - X_{CuO})\right]_i \quad ; (1 \leq \mathbf{i} \leq \text{N-1}) \tag{4.28}$$

To represent the well-mixed assumption of the reacting fuel and oxygen carrier in the bench-scale batch fluidized-bed reactor, an average rate of reaction was computed for the fuel oxidation reaction, $(-r_C)_{avg}$ in the batch fluidized-bed and CuO decomposition reaction, $(-r_{CuO})_{avg}$. The average was computed over (N-1) cells in the batch fluidized-bed, as the partial pressures for O_2 and CO_2 in the bubble and emulsion phases for the N^{th} cell were evaluated by the backward difference formulations as described earlier.

$$(-r_C)_{avg} = \frac{1}{(N-1)} \sum_{i=1}^{N-1} \left[\frac{dX_C}{dt}\right]_i ; (1 \leq \mathbf{i} \leq \text{N-1}) \tag{4.29}$$

$$(-r_{CuO})_{avg} = \frac{1}{(N-1)} \sum_{i=1}^{N-1} \left[\frac{dX_{CuO}}{dt}\right]_i ; (1 \leq \mathbf{i} \leq \text{N-1}) \tag{4.30}$$

The discretized material balance equations along with the rate equations, semi-empirical correlations and the design parameters were solved using ode15s routine in MATLAB. The MATLAB files for the developed model employed have been included in Appendix A.

4.4. Results and discussion

The model predictions for O_2 have been evaluated at the exit cell of the reactor by:

$$p_{O_2}{}^{exit} = \left[\frac{f_{g,b}p_{O_2}{}^{bbl} + f_{g,e}p_{O_2}{}^{em}}{(f_{g,b}+f_{g,e})}\right]_{exit} \tag{4.31}$$

The initial conditions for the concentration of O_2 are defined by the concentration prevailing in the system before the fuel particles are introduced in the fluidized bed. Figures 4.2 to 4.6 represent the comparison of O_2 concentration trends at 885, 900, 935, 950, and 985°C. The results indicate that the model reasonably predicts the oxygen concentration trends.

As the O_2 concentration data are primarily low in magnitude, and may exhibit more uncertainty, CO_2 trends were also investigated. Figures 4.7 to 4.11 represent the comparison of CO_2 concentration trends at 885, 900, 935, 950, and 985°C. The results indicate that the model reasonably predicts the CO_2 concentration trend, with an error of 20%. The initial conditions for the concentration of CO_2 is zero at t=0 as no fuel particles have been introduced in the fluidized bed. The model predictions for CO_2 have been evaluated at the exit cell of the reactor by:

$$p_{CO_2}{}^{exit} = \left[\frac{f_{g,b}p_{CO_2}{}^{bbl} + f_{g,e}p_{CO_2}{}^{em}}{(f_{g,b}+f_{g,e})}\right]_{exit} \tag{4.32}$$

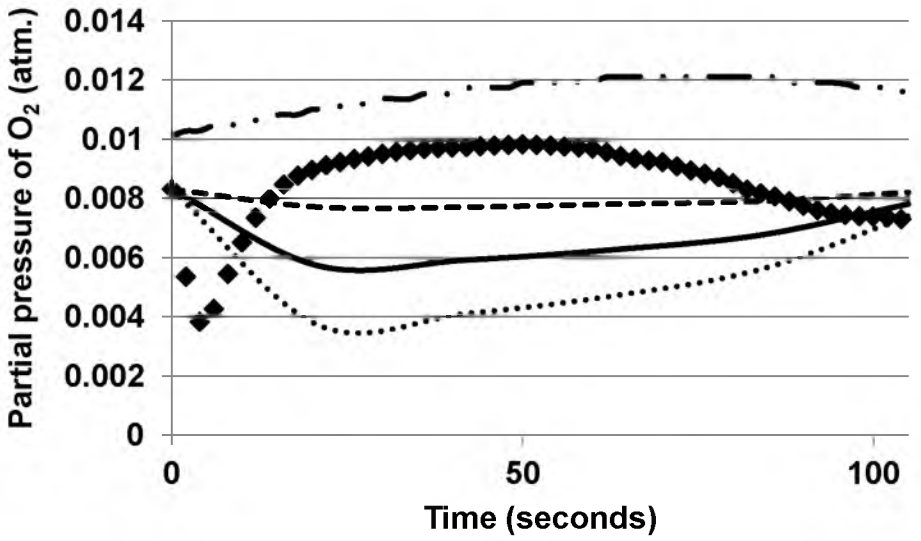

Figure 4.2 O_2 concentration trends at 885°C (♦ Experimental data, — ¨ — O_2 equilibrium concentration for the reaction $4CuO(s) \rightarrow 2Cu_2O(s) + O_2(g)$ determined from experimental temperature measurements, —— Model predictions of the O_2 concentration, - - Model predictions of the O_2 concentration in the bubble phase, ··· Model predictions of the O_2 concentration in the emulsion phase)

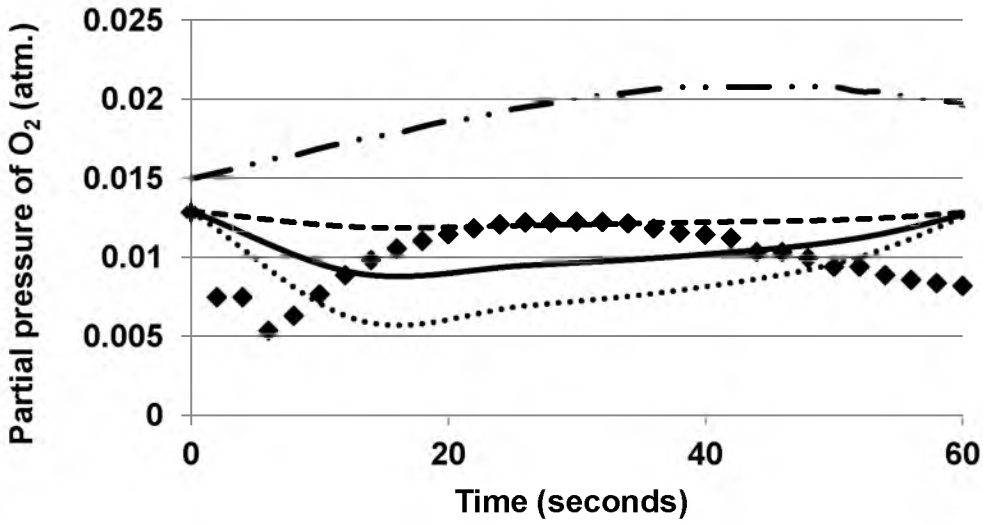

Figure 4.3 O_2 concentration trends at 900°C (♦ Experimental data, — ¨ — O_2 equilibrium concentration for the reaction $4CuO(s) \rightarrow 2Cu_2O(s) + O_2(g)$ determined from experimental temperature measurements, —— Model predictions of the O_2 concentration, - - Model predictions of the O_2 concentration in the bubble phase, ··· Model predictions of the O_2 concentration in the emulsion phase)

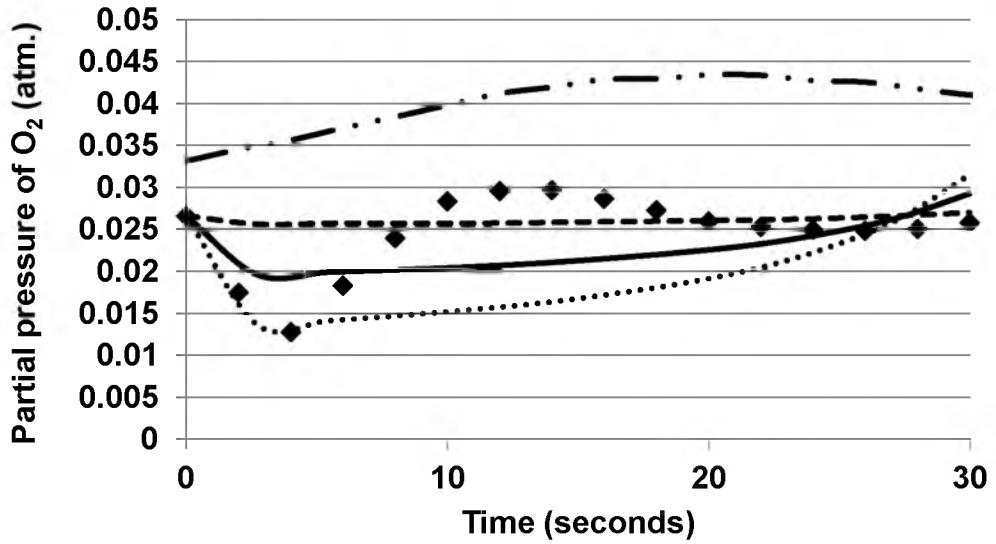

Figure 4.4 O_2 concentration trends at 935°C (♦ Experimental data, — ¨ — O_2 equilibrium concentration for the reaction $4CuO(s) \rightarrow 2Cu_2O(s) + O_2(g)$ determined from experimental temperature measurements, —— Model predictions of the O_2 concentration, - - Model predictions of the O_2 concentration in the bubble phase, ··· Model predictions of the O_2 concentration in the emulsion phase)

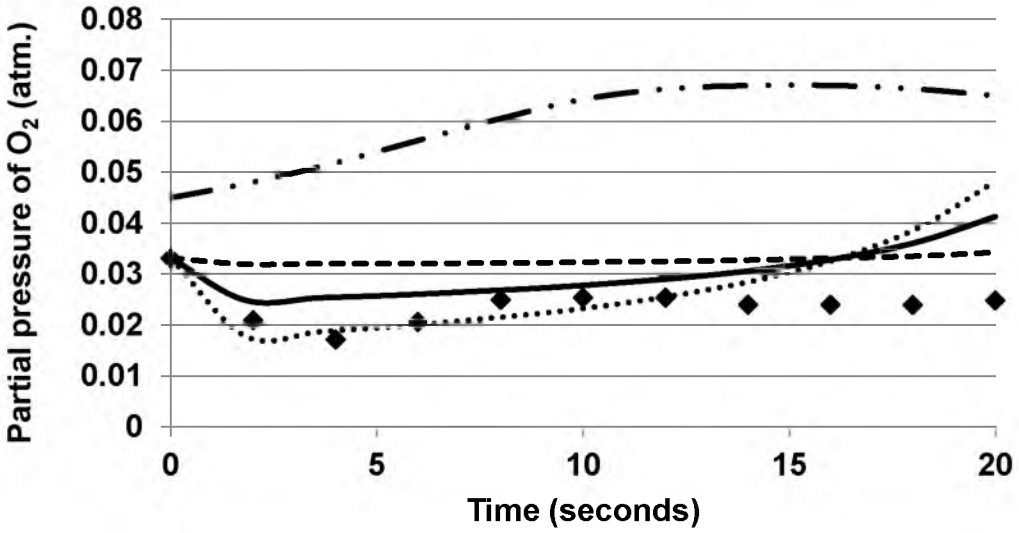

Figure 4.5 O_2 concentration trends at 950°C (♦ Experimental data, — ¨ — O_2 equilibrium concentration for the reaction $4CuO(s) \rightarrow 2Cu_2O(s) + O_2(g)$ determined from experimental temperature measurements, —— Model predictions of the O_2 concentration, - - Model predictions of the O_2 concentration in the bubble phase, ··· Model predictions of the O_2 concentration in the emulsion phase)

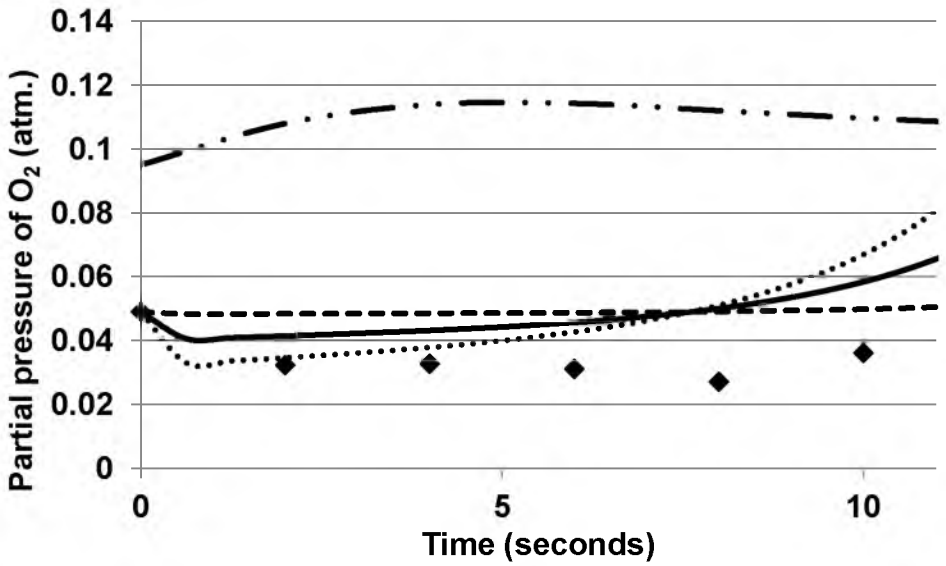

Figure 4.6 O_2 concentration trends at 985°C (♦ Experimental data, — ¨ — O_2 equilibrium concentration for the reaction $4CuO(s) \rightarrow 2Cu_2O(s) + O_2(g)$ determined from experimental temperature measurements, —— Model predictions of the O_2 concentration, - - Model predictions of the O_2 concentration in the bubble phase, ··· Model predictions of the O_2 concentration in the emulsion phase)

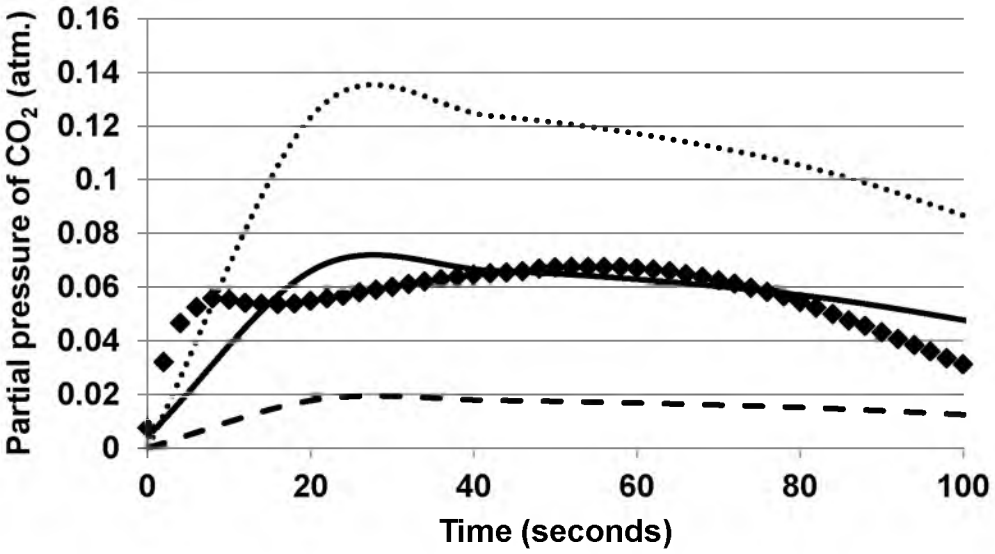

Figure 4.7 CO_2 concentration trends at 885°C (♦ Experimental data, —— Model predictions of the CO_2 concentration, ··· Model predictions of the CO_2 concentration in the emulsion phase, - - Model predictions of the CO_2 concentration in the bubble phase)

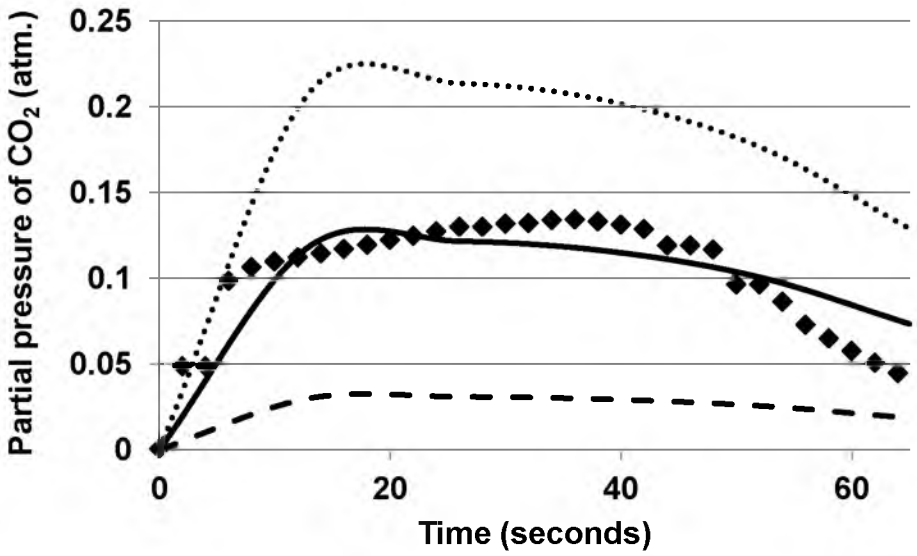

Figure 4.8 CO_2 concentration trends at 900°C (♦ Experimental data, —— Model predictions of the CO_2 concentration, ··· Model predictions of the CO_2 concentration in the emulsion phase, - - Model predictions of the CO_2 concentration in the bubble phase)

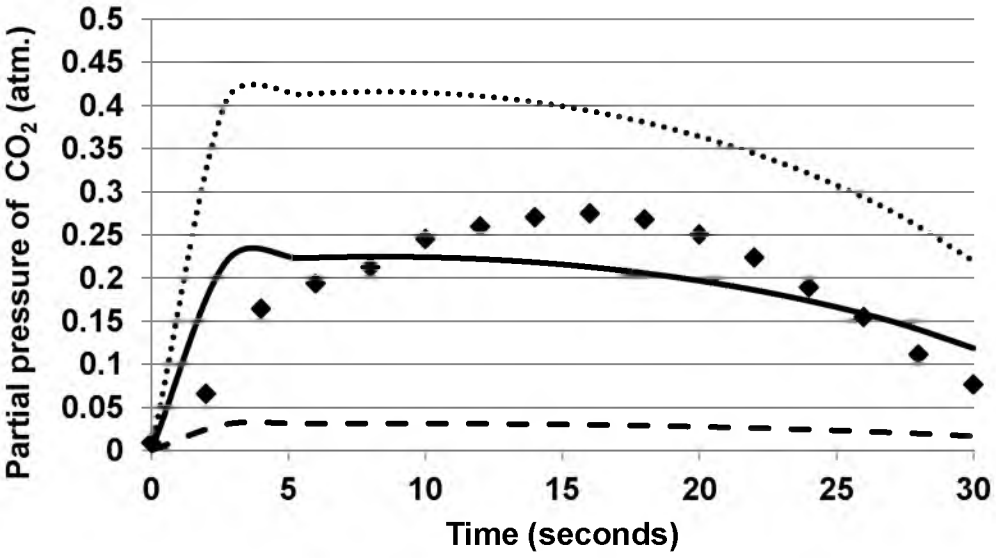

Figure 4.9 CO_2 concentration trends at 935°C (♦ Experimental data, —— Model predictions of the CO_2 concentration, ··· Model predictions of the CO_2 concentration in the emulsion phase, - - Model predictions of the CO_2 concentration in the bubble phase)

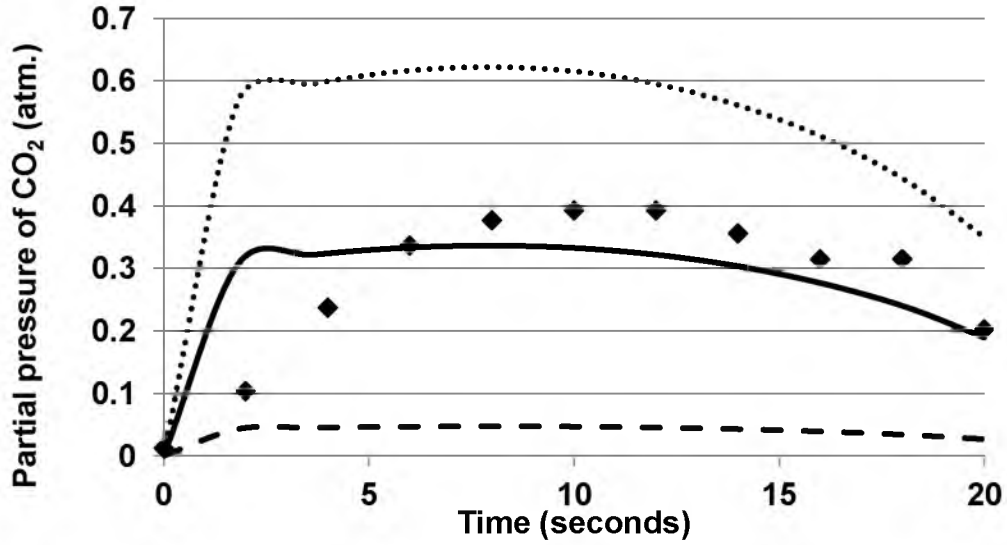

Figure 4.10 CO_2 concentration trends at 950°C (♦ Experimental data, —— Model predictions of the CO_2 concentration, ··· Model predictions of the CO_2 concentration in the emulsion phase, - - Model predictions of the CO_2 concentration in the bubble phase)

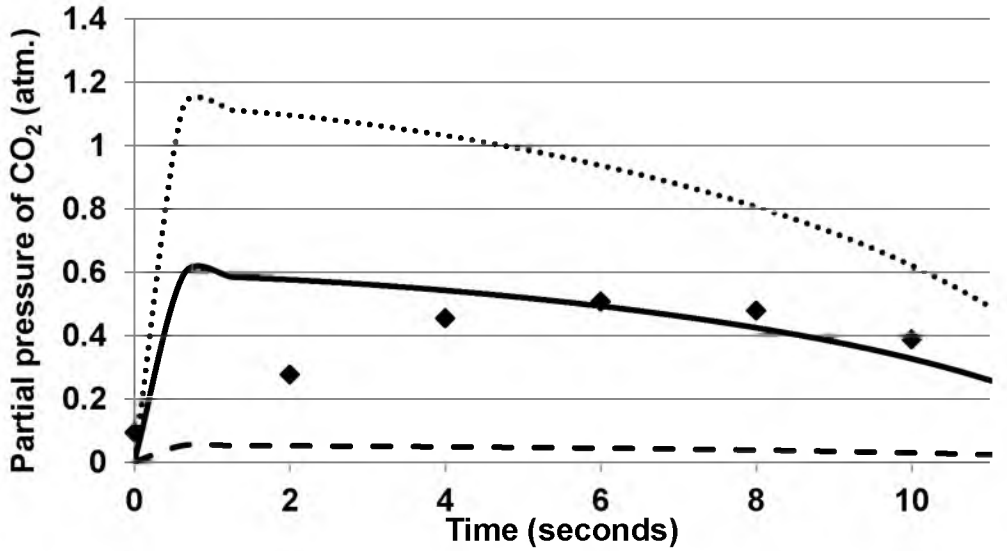

Figure 4.11 CO_2 concentration trends at 985°C (♦ Experimental data, —— Model predictions of the CO_2 concentration, ··· Model predictions of the CO_2 concentration in the emulsion phase, - - Model predictions of the CO_2 concentration in the bubble phase)

The development of a batch-scale fluidized-bed model for the CLOU process where the fuel oxidation and CuO decomposition occur simultaneously is an initial study which holds promise and potential for further analysis.

In this chapter, the model predictions have been compared with experimental data by Mattisson et al.[1] Advanced fluidized-bed modeling considerations for gas-solid reactions will prove vital for future development. Such examples have been reported for rutile chlorination[9,10] for CLC systems using methane combustion by Ni as an oxygen carrier[11] and more recently on coal combustion with ilmenite as an oxygen carrier.[12] These reported studies in conjunction with the present analysis shall prove to be valuable for the analysis of a larger scale CLOU system.

The results of the bench-scale batch fluidized-bed reactor model for the CLOU process presented here show a reasonable prediction of O_2 and CO_2 concentration trends and comparison with independently obtained experimental data, thus indicating that the analysis is satisfactory. The current analysis is based on simplified approximations which can be rigorously analyzed as more data and experience on CLOU is gathered.

4.5. Nomenclature

d_b	diameter of the bubble, cm
d_{b0}	initial diameter of the bubble predicted by Mori and Wen's correlation, cm
d_{bi}	diameter of the bubble at a height interval, cm
d_C	diameter of the fuel particle, μm
d_p	diameter of the oxygen carrier particle, μm
D_T	diameter of the fluidized bed, cm

$\mathcal{D}$	diffusivity of O_2 in CO_2 (A mixture of 10% O_2 and 90% CO_2 is considered), cm^2/s
$f_{g,b}$	fraction of fluidized bed volume occupied by gas in bubble phase
$f_{g,e}$	fraction of fluidized bed volume occupied by gas in emulsion phase
g	gravitational constant, cm/s^2
h	height of the fluidized bed, cm
k_{CuO}	reaction rate constant for CuO decomposition, $atm^{-1}s^{-1}$
$k_{r,C}$	reaction rate constant for petcoke oxidation, g/cm^2 s $atm^{0.5}$
K_{BE}	interchange coefficient for gas between bubble and emulsion phases based on bubble volume, cm/s
L_f	length of fluidized bed, cm
L_{mf}	length of fluidized bed at minimum fluidizing conditions, cm
n_C	moles of C, moles
n_{CuO}	moles of CuO, moles
$p_{O_2}^e$	partial pressure of O_2 at equilibrium, atm
$p_{O_2}{}^{bbl}$	partial pressure of O_2 in bubble phase, atm
$p_{O_2}{}^{em}$	partial pressure of O_2 in emulsion phase, atm
$p_{O_2}{}^{exit}$	partial pressure of O_2 at exit conditions, atm
$p_{CO_2}{}^{bbl}$	partial pressure of CO_2 in bubble phase, atm
$p_{CO_2}{}^{em}$	partial pressure of CO_2 in emulsion phase, atm.
$p_{CO_2}{}^{exit}$	partial pressure of CO_2 at exit conditions, atm.
$(-r_{CuO})$	rate of CuO decomposition [$4CuO(s) \rightarrow 2Cu_2O(s) + O_2(g)$], 1/s
$(-r_C)$	rate of petcoke oxidation [$C(s) + O_2(g) \rightarrow CO_2(g)$], 1/s

R	gas constant, cm^3 atm/mol K
R_i	initial radius of coal char particle, cm
t	time, s
T	temperature, K or °C
u_b	bubble rising velocity, cm/s
u_e	rise velocity of emulsion through the bed, cm/s
u_0	superficial velocity, cm/s
u_{mf}	minimum velocity for fluidization, cm/s
V_R	volume of the fluidized bed, cm^3
X_{CuO}	conversion of CuO particles
X_C	conversion of petcoke particles
z	axial coordinate, cm

Greek Symbols:

α	ratio of wake volume to bubble volume
δ	fraction of fluidized bed volume occupied by bubbles
ε_{mf}	voidage at minimum fluidization conditions
ρ_C	density of coal char particle, g/cm^3
ρ_S	density of oxygen carrier particle, g/cm^3
ρ_g	density of gas, g/cm^3
μ	viscosity, kg/m s

4.6. References

1. Mattisson, T.; Leion, H.; Lyngfelt, A., Chemical-looping with oxygen uncoupling using CuO/ZrO_2 with petroleum coke. *Fuel* **2009,** *88* (4), 683-690.

2. Richardson, J. F.; Jeronimo, M. A., Velocity-voidage relations for sedimentation and fluidization. *Chem. Eng. Sci.* **1979,** *34*, 1419-1422.

3. Kunii, D.; Levenspiel, O., *Fluidization Engineering*. Second ed.; Butterworth-Heinemann: 1991.

4. Puettmann, A.; Hartge, E.-U.; Werther, J., Application of the flowsheet simulation concept to fluidized bed reactor modeling. Part I: Development of a fluidized bed reactor simulation module. *Chemical Engineering and Processing: Process Intensification* **2012,** *60*, 86– 95.

5. Sit, S. P.; Grace, J. R., Effect of bubble interaction on interphase mass transfer in gas fluidized beds. *Chem. Eng. Sci.* **1981,** *36* (2), 327-335.

6. Babu, S. P.; Shah, B.; Talwalkar, A., Fluidization correlations for coal gasification materials-minimum fluidization velocity and fluidized bed expansion ratio. *AIChE Symposium Series* **1978,** *74* (Fluidization: Application to Coal Conversion Processes), 176-186.

7. Zenz, F. A., The Fluid Mechanics of Bubbling Beds. *Fibonacci Quarterly* **1978**, 171-183.

8. Mori, S.; Wen, C. Y., Estimation of bubble diameter in gaseous fluidized beds. *AIChE* **1975,** *21* (1), 109-115.

9. Rhee, K. I.; Sohn, H. Y., The selective chlorination of Iron from Ilmenite Ore by CO-Cl_2 mixtures: Part II Mathematical Modeling of Fluidized Bed Process. *Met. Trans. B* **1990,** *21B*, 331-340.

10. Zhou, L.; Sohn, H. Y., Mathematical Modeling of Fluidized-Bed Chlorination of Rutile. *AIChE* **1996,** *42* (11), 3102-3112.

11. Iliuta, I.; Tahoces, R.; Patience, G. S.; Rifflart, S.; Luck, F., Chemical-Looping Combustion Process: Kinetics and Mathematical Modeling. *AIChE* **2010,** *56* (4), 1063-1079.

12. Abad, A.; Gayan, P.; De Diego, L.; Garciá-Labiano, F.; Adanez, J., Fuel reactor modelling in chemical-looping combustion of coal: 1. model formulation. *Chem.Eng. Sci.* **2013,** *87*, 277-293.

CHAPTER 5

PROCESS ANALYSIS OF CHEMICAL-LOOPING WITH OXYGEN UNCOUPLING (CLOU) AND CHEMICAL-LOOPING COMBUSTION (CLC) FOR SOLID FUELS

5.1. Abstract

Chemical-looping with oxygen uncoupling (CLOU) offers a potential advantage as it facilitates combustion reactions for solid fuels with the help of released O_2 from the decomposition of a metal oxide (e.g. CuO). Based on the rate analysis discussed in the third chapter, a process design for CLOU has been conceptualized by identifying a residence time, optimal circulation rate, and a temperature difference between the air and fuel reactors. The objective of the CLOU process model is to evaluate the material and energy requirements for a process development unit which will be operated on a Wyoming Powder River Basin (PRB) coal as one of the initial feedstocks. Insights from previously reported kinetic studies on lab-scale units have been incorporated for conceptualizing process models.

Iron-based materials are being considered as one of the primary candidates for oxygen carriers in chemical-looping combustion (CLC), where a syngas is generated through the gasification of coal. The transition from Fe_2O_3 to Fe_3O_4 has been identified as a potential route for facilitating carbon dioxide capture from a thermodynamical standpoint. ASPEN PLUS process engineering models have been developed for CLOU using a copper-based carrier, and CLC using an iron-based carrier, and a comparison of material and energy balance scenarios for both CLOU and CLC has been made.

5.2. CLOU: Determination of an optimum circulation rate and residence time

The circulation rate of the oxygen carrier, together with the total mass of oxygen-carrier, is an important parameter in the economical design of a chemical looping system.[1-4] The magnitude of circulation rate is governed by the need to supply the fuel reactor with

oxygen needed to consume the fuel. In Chapter 3, the methodology used for determining the kinetic parameters for CuO decomposition and solid fuel oxidation during the fuel reactor stage and for Cu_2O oxidation in the air reactor stage has been discussed. In this chapter, the insights derived from the rate analysis will be employed to determine the requisite residence times and parameters for the design of the CLOU process. These parameters were determined from the batch fluidized-bed CLOU experiments with Mexican petcoke as reported by Mattisson et al.[1] and Leion.[5]

The analysis assumes complete fuel consumption, which will be justified later in this section. The moles (or mass) of Cu circulating between the fuel and air reactor has been chosen as the basis for calculation since it is independent of the oxygen state of the oxygen-carrier. The calculations are based on the moles of copper associated with the oxygen-carrier.

$$Y_{CuO} = \frac{\dot{N}_{CuO}}{\dot{N}_{CuO}+2\dot{N}_{Cu_2O}} = \frac{\dot{N}_{CuO}}{\dot{N}_{Cu}} \tag{5.1}$$

where $\dot{N}_{CuO}$, $\dot{N}_{Cu_2O}$ and $\dot{N}_{Cu}$ are the molar flow rates of CuO, Cu_2O, and Cu, respectively. For the fuel reactor, the difference in the oxygen content of the oxygen-carrier entering and leaving the reactor is consumed in the combustion of coal.

The purpose of this investigation is to support the development of a 150-200 kW_{th} CLOU process development unit at the University of Utah which will be operated on Wyoming Powder River Basin (PRB) North Antelope coal as an initial fuel. The properties of PRB North Antelope coal are provided in Table 5.1 and are compared with Mexican petcoke. If Ω_{coal} is defined as the stoichiometric moles of O_2 required to convert 1 kg coal to CO_2, H_2O, NO and SO_2,[6]

Table 5.1 Ultimate analysis for fuels used for comparison

Coal	C(wt% d.a.f)	H (wt% d.a.f)	O(wt % d.a.f)	N(wt % d.a.f)	S(wt% d.a.f)	Cl(wt % d.a.f)	Heating Value (MJ/kg)
Mexican Petcoke	88.8	3.1	0.5	1.0	6.6	-	30.9(as recd.)
North Antelope PRB	75.3	5.0	18.3	1.1	0.3	-	27.7(dry basis)

$$\Omega_{coal} = \frac{f_c}{M_c} + \left(\frac{1}{4}\right)\frac{f_h}{M_h} + \left(\frac{1}{2}\right)\frac{f_n}{M_n} + \frac{f_s}{M_s} - \left(\frac{1}{2}\right)\frac{f_o}{M_o} \tag{5.2}$$

For a stoichiometric equation of $4CuO(s) \rightarrow 2Cu_2O(s) + O_2(g)$, the following relation exists between the oxygen released by CuO decomposition and consumption of O_2 by coal. Equation 5.3 relates the mass flow rate of coal feed, $\dot{m}_{coal}$, Ω_{coal} and the difference in flow of $\dot{N}_{CuO}$, expressed in terms of a mole ratio Y entering and leaving the reactor,

$$\dot{m}_{coal}\,\Omega_{coal} = \frac{\dot{N}_{Cu}(Y_{CuO,AR} - Y_{CuO,FR})}{4} \tag{5.3}$$

where AR and FR refer to the air and fuel reactor, respectively. Rearrangement yields

$$\frac{\dot{N}_{Cu}}{\dot{m}_{coal}\,\Omega_{coal}} = \frac{4}{(Y_{CuO,AR} - Y_{CuO,FR})} \tag{5.4}$$

The difference in mole ratio Y_{CuO} at the exit of the air and fuel reactors is defined as $\Delta Y_S = (Y_{CuO,AR} - Y_{CuO,FR})$.

Equation 5.5 provides the mass flow rate of Cu per megawatt of thermal energy introduced in the fuel reactor as fuel, $\hat{m}_{Cu}$ (kg Cu s^{-1} MW_{th} $fuel^{-1}$),

$$\hat{m}_{Cu} = \frac{4\,\Omega_{coal} M_{Cu}}{\Delta Y_S Q_c} \tag{5.5}$$

where M_{Cu} represents the molecular mass of copper.

This relation is shown in Figure 5.1 in which the mass flow rate of copper in kg/s circulated in the system per MW_{th} of coal introduced in the fuel reactor is plotted against the difference in mole ratio ΔY_S for different values of $Y_{CuO,FR}$ (Figure 5.1**).** It should be noted that the circulation mass in Figure 5.1 needs to be corrected for both oxidation of the Cu (increases by a factor of 1.13 to 1.25 depending on the oxidation state of the Cu), and on the percent of copper loading on the oxygen-carrier when calculating the total mass of oxygen carrier. Supported oxygen-carriers with CuO loadings of up to 80% have been prepared with binders (substrates) of Al_2O_3, Sepiolite, SiO_2, TiO_2, and ZrO_2.[7] In order to compare oxygen-carrier circulation rates on a common basis, the rates will be converted to the rates of CuO circulated on a support free basis. Given the results of Figure 5.1, a circulation of approximately 1.8 kg/(s)(MW_{th}) is required on a support-free basis for a ΔY_S (difference of mole ratio) of 0.35. The difference of mole ratio is related to the choice of an optimal circulation rate which has been described later in this section. The total rate of material circulated is equal to this value divided by the weight percent of CuO for oxygen carriers consisting of supported CuO. In order to compare the present result with results reported in the literature, the data need to be converted to a support-free basis by multiplying the reported rates by the weight percent of active material on the supported oxygen carrier.

A temperature of 950°C was selected to approximate the highest temperatures used in laboratory reactors with solid fuels without bed agglomeration and attrition.[1,8-13]

A design temperature of 935°C was used for the air reactor by maintaining a temperature difference of 15°C. The rationale of this decision is explained in section 5.3.

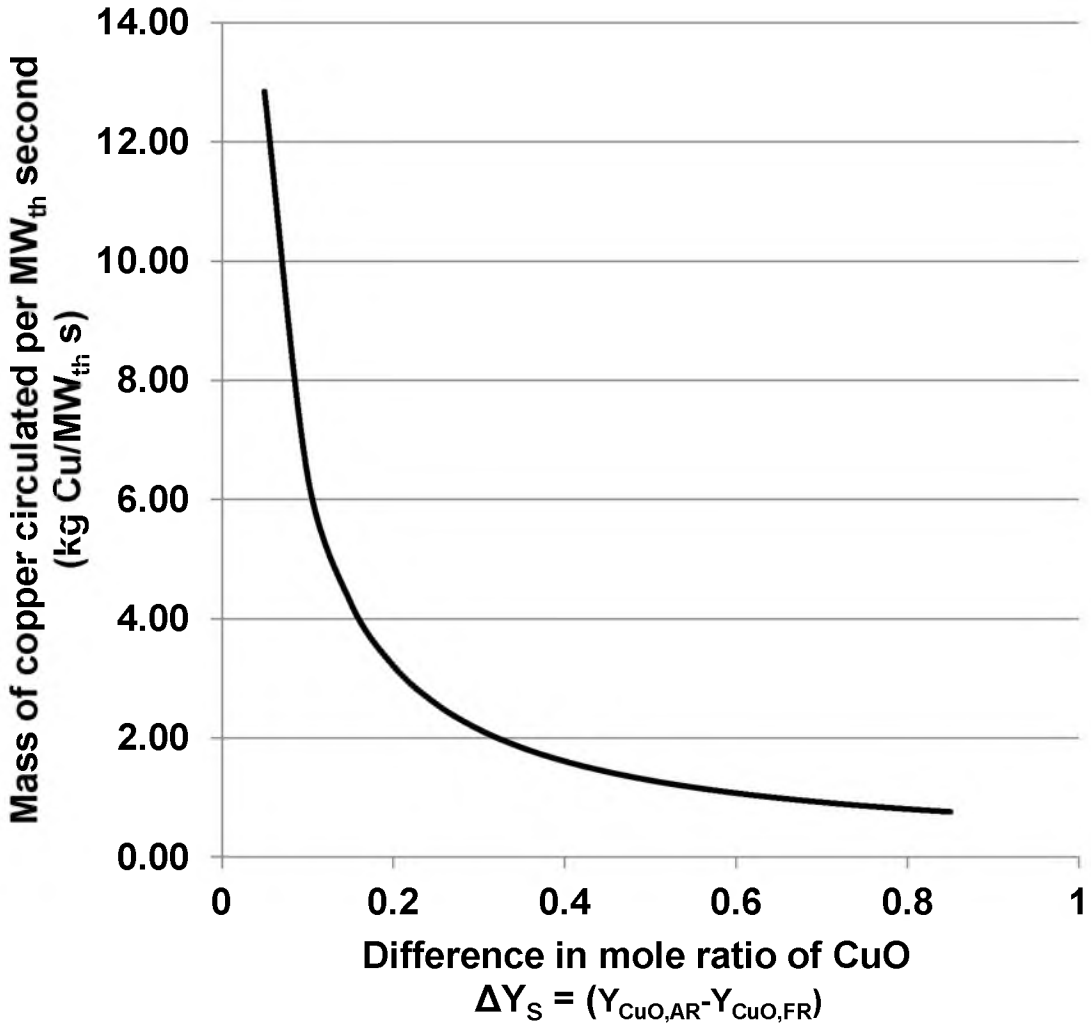

Figure 5.1 Variation in mass flow rate (kg/s) of copper circulated per MW_{th} fuel with variation in difference of CuO mole ratio.

The residence time for the decomposition of CuO to release oxygen is calculated by:

$$\tau_{FR} = \frac{1}{k_{CuO}\overline{(p_{O_{2,e}} - p_{O_2})_{avg}}} \, ln[1/\{1 - X_{CuO}\}] \tag{5.6}$$

where X_{CuO} is the conversion of CuO in the fuel reactor.

In terms of variation between an inlet mole ratio of $Y_{CuO,AR}$ to an exit mole ratio of $Y_{CuO,FR}$ the residence time could be expressed by Equation 5.7 as:

$$\tau_{FR} = \frac{1}{k_{CuO}\overline{(p_{O_{2,e}} - p_{O_2})_{avg}}} \, ln\left[1/\left\{1 - \left(\frac{\Delta Y_S}{Y_{CuO,AR}}\right)\right\}\right] \tag{5.7}$$

where k_{CuO} is the CuO decomposition rate constant. The equation for k_{CuO} and the magnitude of $\overline{(p_{O_{2,e}} - p_{O_2})_{avg}}$ for experiments at 950°C have been provided in Table 5.2.

As discussed in Chapter 3, it was demonstrated that the rate of Cu_2O oxidation under chemical reaction control can be approximated by:

$$t \cong \left[\left(\frac{RT_{avg}\alpha_S \tilde{\rho}_{S,Cu_2O}}{2k_{Cu_2O,app}\overline{(p_{O_2} - p_{O_{2,e}})_{avg}}}\right)\left\{1 - \left(1 - X_{Cu_2O}\right)^{\frac{1}{3}}\right\}\right] \tag{5.8}$$

Table 5.3 provides the values used to evaluate the residence times by Equation 5.8.

The value of $k_{Cu_2O,app}$ calculated for the oxidation experiment with air conducted by Leion[5] at 935°C is 18.0 s^{-1}. Figure 5.2 represents the comparison between the prediction of Equation 5.8 and experimental data. The methodology of the analysis of experimental data on Cu_2O oxidation has been explained in Chapter 3.

In terms of the mole ratio, the residence time for the air reactor could be expressed by Equation 5.9 as:

Table 5.2 Data utilized for analyzing the rate equation for CuO decomposition[1,14]

param.	value
k_{CuO}	$3\ exp\left(\frac{-2350}{T}\right)$
$\overline{(p_{O_2}-p_{O_{2,e}})_{avg}}$ for CuO decomposition experiments at 950°C (T_{avg} = 962°C)	0.052 atm

Table 5.3 Data utilized for analyzing the rate equation for Cu_2O oxidation[1,14]

param.	value
r_p	76.5 μm (Diameter was evaluated by taking the average of 125 and 180 μm)
$\tilde{\rho}_{S,Cu_2O}$	41931.6 mol/m^3
α_S	0.1425
$p_{O_{2,in}}$	0.21 atm
$\overline{(p_{O_2}-p_{O_{2,e}})_{avg}}$ for oxidation experiments at 935°C (T_{avg} = 956°C)	0.089 atm

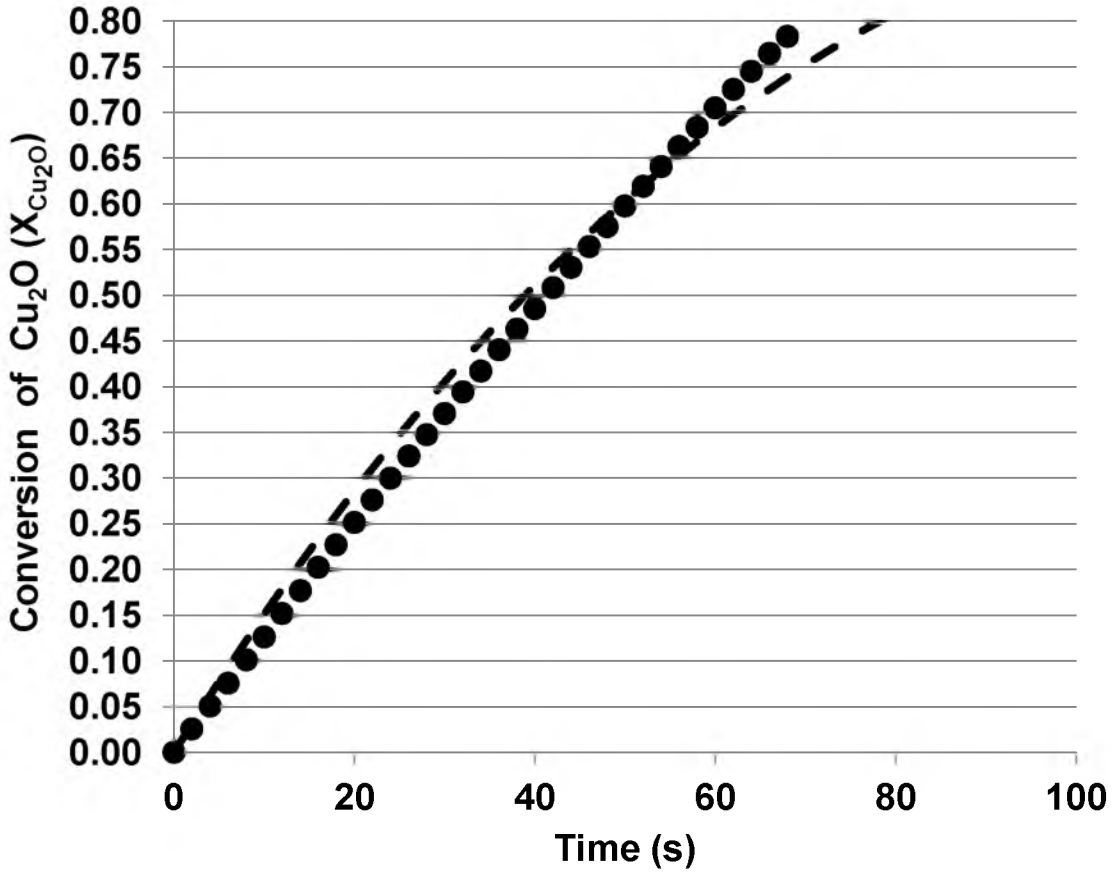

Figure 5.2 Comparison of experimental data for conversion of Cu_2O vs. time at temperatures of 935°C (oxidation with air) with Equation 5.8 derived by the Law of Additive Reaction Times for $k_{Cu2O,\ app} = 18.00\ s^{-1}$ (● experimental data points, - - - conversion for chemical reaction control)

$$\tau_{AR} = \left[\left(\frac{RT_{avg}\alpha_S\tilde{\rho}_{S,Cu_2O}}{2k_{Cu_2O,app}\overline{(p_{O_2}-p_{O_2,e})_{avg}}}\right)\left\{1-\left(1-\left(\frac{\Delta Y_S}{(1-Y_{CuO,FR})}\right)\right)^{\frac{1}{3}}\right\}\right] \quad (5.9)$$

The mass of Cu metal required per MW_{th} of coal burnt in a CLOU system, m_{Cu} can be obtained from Equation 5.10:

$$m_{Cu} = \widehat{m}_{Cu}(\tau_{FR} + \tau_{AR})|_{\Delta Y_S, Y_{CuO,FR}} \quad (5.10)$$

where the residence times are determined by Equations 5.7 and 5.9 as a function of $Y_{CuO,AR}$ and $Y_{CuO,FR}$, or alternatively, $Y_{CuO,FR}$ and ΔY_S. The resulting mass of the copper in the oxygen carrier per MW_{th} input of fuel is provided in Figure 5.3, mapping similar to those developed previously.[2,3,15]

The results in Figure 5.3 indicate a minimum copper metal loading for both fuel and air reactor of 127 kg Cu/MW_{th} fuel (or 159 kg CuO/ MW_{th} fuel) for a $Y_{CuO,FR}$ of 0.3 and ΔY_S of 0.35. The estimated magnitude of CuO loading per MW_{th} fuel for both the air and fuel reactors is higher than the recently reported value of 28-56 kg CuO per MW_{th}. obtained using devolatilized wood char and a 40% CuO supported on a $MgAl_2O_4$ carrier.[16] Previous literature studies have reported inventory values for the fuel reactor of 48-80 kg CuO/MW_{th} with 40% CuO supported on ZrO_2 and petcoke as a fuel[1] and 141 kg CuO/MW_{th} using a 60% CuO supported on $MgAl_2O_4$ and bituminous coal as a fuel.[6] All the CuO loading values have been reported on a support-free basis. The mole ratio of CuO at exit of the fuel reactor $Y_{CuO,FR}$ of 0.3 and a difference of mole ratio ΔY_S of 0.35 translates to a stoichiometric conversion of 54% in the fuel reactor and 50% in the air reactor (derivations discussed in Appendix B).

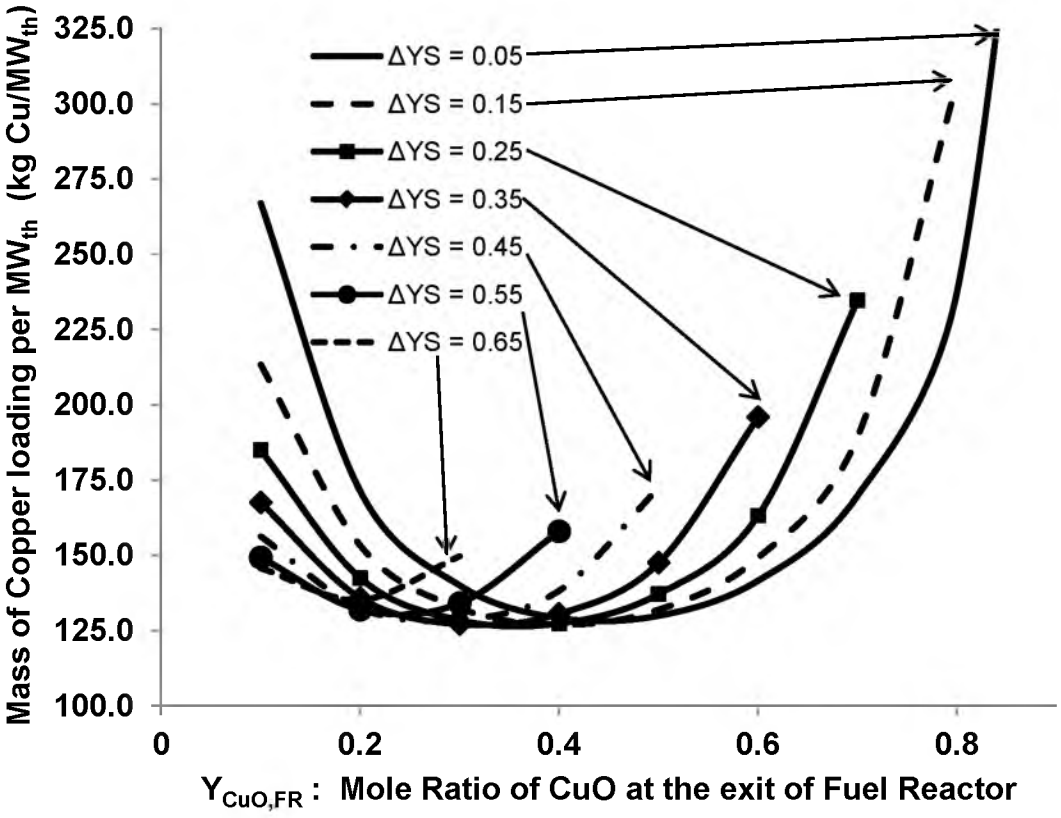

Figure 5.3 Mass of copper loading per MW_{th} vs mole ratio of CuO at the exit of fuel reactor for different values of ΔY_S.

For the highest ΔY_S of 0.65 shown on the plot, the minimum carrier loading is 135 kg/MW_{th}. The shape of each curve is determined by the increase in reaction time in the fuel reactor as the value of $Y_{CuO,FR}$ decreases at a given ΔY_S (see Equation 5.7). The reaction times for the air reactor by contrast increases with increasing $Y_{CuO,FR}$ at a fixed ΔY_S (see Equation 5.9). Selection of the optimum values of conditions depends on selecting a high value of ΔY_S to reduce the circulation rate of oxygen carrier (see Figure 5.3) as well as to minimize oxygen carrier loading. An optimization would be based on an economic analysis. A value of ΔY_S (often referred to in CLC literature as ΔX_S[3]) between 0.2-0.4 has been cited for low circulation rates and low solid inventories.

A plot of residence time with respect to temperature based on the experimental data of Leion[5] is shown in Figure 5.4. The time for 54% CuO decomposition in the presence of fuel particles decreases with an increase in temperature from 342 seconds at 885°C to 19 seconds at 985°C. For a fuel reactor operating at 950°C, the residence time is 35 seconds.

However, in the air reactor, the time required to attain 50% conversion, with air as a reactant for Cu_2O oxidation, increases with increasing temperature, ranging from 30 seconds at 885°C to 132 seconds at 985°C. The residence time for an air reactor operating at 935°C is 42 seconds. For PRB coal, the rate of coal char burnout was determined by applying the shrinking sphere model to fuel particles having an average diameter of 200 μm and a density of 0.4 g/cm^3. The kinetic rate constant (in g/cm^2 s) for PRB coal char oxidation is provided by Equation 5.11 as: [17]

$$k_{r,c} = 145\ exp\left(\frac{-19970}{R_g T}\right) \tag{5.11}$$

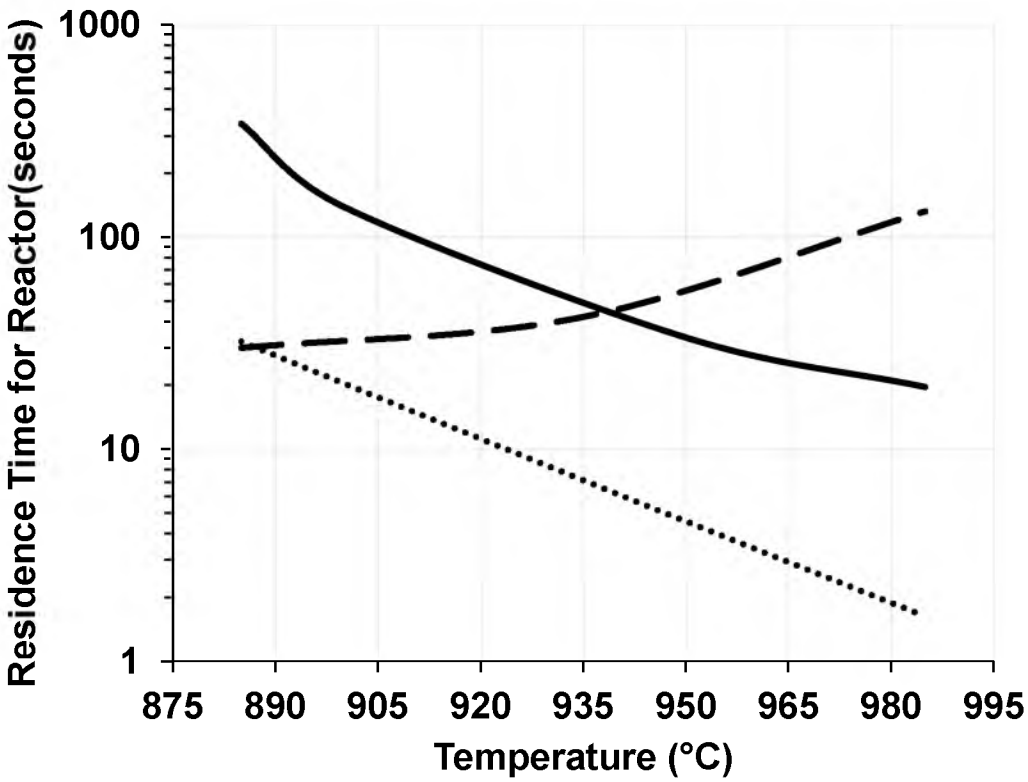

Figure 5.4 Residence time in a reactor (on a logarithmic scale) versus temperature (— CuO reduction (54%), - - Cu_2O oxidation (50%), •• PRB coal char burnout time)

As can be observed from Figure 5.4, the time required for oxidation of PRB coal char particles is substantially less than the time required by CuO/ZrO_2 particles to release O_2.

5.3. CLOU: Determination of an appropriate temperature difference

An ASPEN PLUS process model was developed to envision the importance of an appropriate temperature difference for the CLOU process with the parameters as mentioned in Table 5.4.

Figure 5.5 is a schematic of the ASPEN PLUS process model developed for analyzing the CLOU process. Coal combustion has been modeled by a combination of RYIELD and RGIBBS reactor models. The oxygen for combusting coal is supplied by an RSTOIC reactor with a specified CuO conversion of 54% as discussed in the previous section. The Cu_2O formed after CuO decomposition is regenerated in an air reactor with a specified Cu_2O conversion of 50%. The air reactor has been modeled with a RSTOIC reactor model. The magnitude of the mass flow rates of the inlet metal oxide stream to the fuel reactor and the outlet metal oxide stream from the air reactor in the ASPEN PLUS model are equated to accomplish recirculation of metal oxide for the process models of chemical-looping combustion systems discussed in this dissertation.

The coal feed and the inlet air enter at 25°C in this simulation. An energy analysis from the following five sources / sinks has been conducted to understand the importance of temperature difference between the air reactor and the fuel reactor.

1. Fuel Reactor – The energy associated with the simultaneous exothermic

Table 5.4 Process parameters for ASPEN PLUS process model

Coal feed rate	100 kg/h
Air flow rate varied in accordance to the partial pressure of O_2 at outlet of the reactor corresponding to equilibrium conditions	825-902 kg/h
Temperature range of Fuel Reactor investigated	885°C - 985°C
Temperature range of Air Reactor investigated	885°C - 950°C
Mass flow rate of CuO at the inlet of fuel reactor	3392 kg/h
Mass flow rate of Cu_2O at the inlet of fuel reactor	1648 kg/h
Mass flow rate of ZrO_2 circulating in the system	7836 kg/h

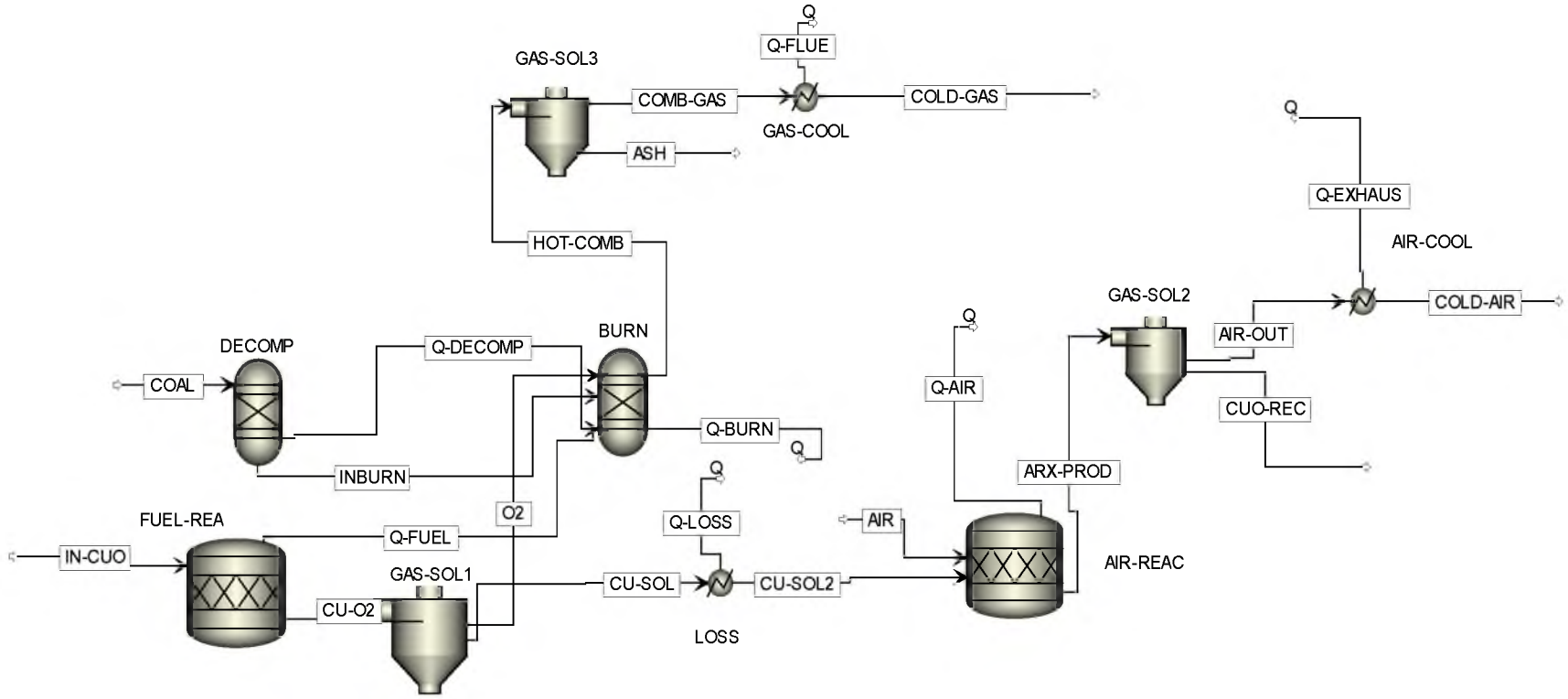

Figure 5.5 Schematic of ASPEN PLUS process model used to analyze the significance of temperature differential between air and fuel reactors

combustion and endothermic CuO reduction is considered.

2. Air Reactor – The energy associated with the exothermic Cu_2O oxidation reaction is taken into account.

3. Flue Gas – The energy associated with the products of combustion cooled down to a temperature of 150°C is taken into account. A HEATER block has been used in the ASPEN PLUS model to evaluate the energy obtained by cooling the flue gas.

4. Air Exhaust – The energy associated with the cooling of nitrogen-enriched stream, after oxygen has been consumed by the Cu_2O oxidation reaction, is evaluated. The temperature of the stream is reduced to 150°C with the help of a HEATER block.

5. Loss – The energy associated with the temperature differential between the fuel and air reactor is evaluated through this parameter. A HEATER block has been used in the ASPEN PLUS model to evaluate the energy associated with the temperature differential. For the purpose of analysis, the energy associated with the process model block is being visualized as a loss, since the fuel reactor will be at a higher temperature than the air reactor in order to support faster CuO decomposition and fuel oxidation reactions in the CLOU process. The intention of documenting this parameter is to analyze the implication of energy associated with the cooling of oxygen carrier particles on the design process.

Table 5.5 represents the energy which is associated with various process units in the ASPEN PLUS process model at different temperature differentials between the fuel and the air reactor. The energy associated with the temperature differential between the fuel and air reactor is referred to as “loss” which increases with increasing temperature differences.

Table 5.5 Energy associated with various units with respect to temperature of reactors

Fuel Reactor Temp. (°C)	Air Reactor Temp. (°C)	ΔT between Fuel and Air Reactor (°C)	Heat duty for Air Reactor (kW_{th})	Heat duty for Fuel Reactor (kW_{th})	Energy associated with Flue Gas(kW_{th})	Energy associated with Loss(kW_{th})	Energy associated with exhaust from air reactor (kW_{th})	Total (kW_{th})
885	885	0	181	110	76	0	146	513
950	935	15	144	75	84	-33	176	446
935	885	50	181	-5	82	-110	146	294
985	935	50	144	-7	88	-111	176	290
950	885	65	181	-41	84	-143	146	227
985	885	100	181	-122	88	-221	146	72

A 15°C temperature difference between the fuel reactor and the air reactor results in an energy differential of 33 kW_{th} and a 100°C difference between the fuel and air reactor has an energy differential of 221 kW_{th}. These results highlight the necessity of designing an efficient energy recovery and reheating system for the oxygen carrier. The loss in this study is a result of the oxygen carrier cooling to a lower temperature to obtain a faster Cu_2O oxidation rate, and then being reheated back to a higher temperature to take advantage of a faster CuO decomposition. This information is valuable in the design phase of the process development unit.

The 15°C temperature difference between the fuel reactor and the air reactor results in a recoverable energy of 446 kW_{th} and a 100°C difference between the fuel and air reactor has a recoverable energy of 72 kW_{th}. The recoverable energy in this section has been determined, assuming energy is not adequately extracted from the oxygen carrier stream. In the case of particles coming out of the air reactor at 885°C, they have to be heated by 100°C to 985°C before entering the fuel reactor which requires energy and reduces the recoverable energy content substantially. This analysis adds another dimension to the optimization, the major consideration being taking advantage of kinetics at different temperatures and minimizing energy loss through heating and cooling of oxygen carriers.

Figure 5.6 represents the distribution of energy associated with the fuel reactor (a combination of CuO decomposition, coal char oxidation, and oxygen carrier reheating requirement), flue gas cooling, air exhaust cooling, loss (energy associated with lowering the temperature of oxygen carrier) and the air reactor (energy associated with Cu_2O oxidation) through a stacked diagram of parameters.

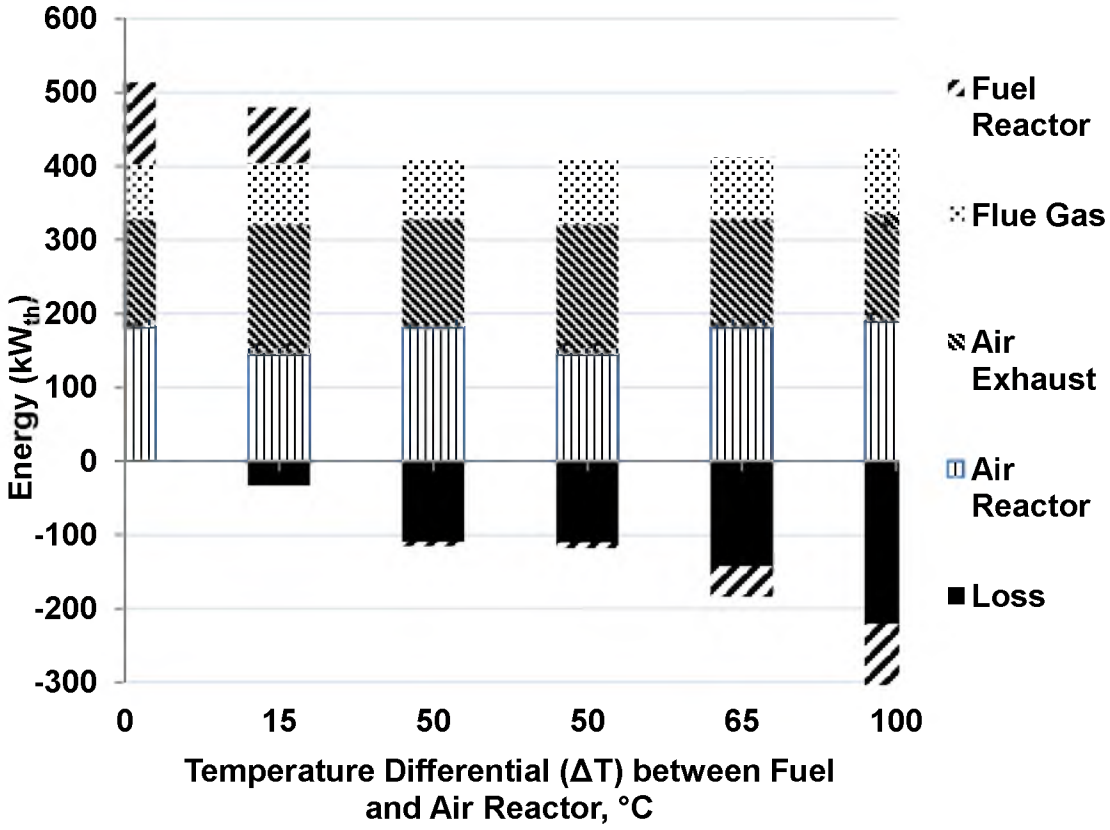

Figure 5.6 Stacked diagram representing energy associated with the various components with respect to the temperature differential (ΔT).

For the case of CLOU with CuO/ZrO_2 oxygen carrier and Mexican Petcoke, the results indicated in Figure 5.4 and Figure 5.6 suggest that a temperature difference of 15°C between the fuel and air reactor in the temperature range of 920°C-960°C will result in residence time of reactors below 100 seconds.

5.4. CLOU: Process model

In the previous sections of this chapter, the rationale of determining an optimum circulation rate, residence time, and temperature difference have been discussed. The following design considerations could further be taken into account.

Firstly, a design based on the circulating fluidized bed concept could be envisaged with a thermal output of 3 MW/m^2. A ratio of superficial to terminal velocity of two was employed, as a design assumption which is common for circulating fluidized-bed coal combustors.[18] The correlations employed to evaluate the fluidized-bed velocities are based on design correlations in circulating fluidized-bed coal combustion literature[18] and are mentioned in Table 5.6.

Secondly, the flue gas containing CO_2 and H_2O has been recirculated in the fuel reactor to fluidize the bed.

Thirdly, the air flow rate has been established by considering a design outlet oxygen concentration of 5%, which corresponds to approximately 25% excess air and keeps the exhaust gas higher than the partial pressure of O_2 in a $CuO-Cu_2O$ system at 935°C (~0.032 atm.).

Lastly, the amount of CuO required takes into account a design factor of supplying 15% excess oxygen in the fuel reactor.

Table 5.6 Correlations employed for determining the velocities in the fluidized bed [18]

Reynolds number at minimum fluidizing conditions	$Re_{mf} = \frac{d_p u_{mf} \rho_g}{\mu} = [(22.7)^2 + 0.0408Ar]^{0.5} - 22.7$
Archimedes Number (Ar)	$Ar = \frac{\rho_g(\rho_p - \rho_g) g d_p^3}{\mu}$
Minimum bubbling velocity for Group A particles	$u_{mb} = 2.07\exp(.716F) d_p \left(\frac{\rho_g^{0.06}}{\mu^{0.347}}\right)$
Reynolds number based on terminal settling velocity for spherical particles (for $0.4 < Re_t < 500$)	$Re_t = \frac{d_p u_t \rho_g}{\mu} = \left[\frac{Ar}{7.5}\right]^{0.666}$

Figure 5.7 represents a schematic of the ASPEN Plus model developed for analyzing the CLOU process which takes into account a CO_2 recycle, and process models representing the energy requirements for fluidizing the bed. Table 5.7 outlines the parameters for the process model for CLOU. The conversion of CuO in the fuel reactor is 54%, and a Cu_2O conversion of 50% for the air reactor has been selected for the ASPEN PLUS RSTOIC model. The solid fuel combustion process is modeled with the combination of RYIELD and RGIBBS reactor models. The pressure drop is evaluated by multiplying the circulation rate with the residence time (35 seconds in the fuel reactor, and 42 seconds in the air reactor).

Table 5.8 provides the relationships used for determining the energy requirements for fluidization. In Table 5.9, the energy contributions and requirements associated with the various process units in the ASPEN PLUS process model are outlined. According to the table, approximately 513 kW_{th} of energy could be recovered in CLOU with lower

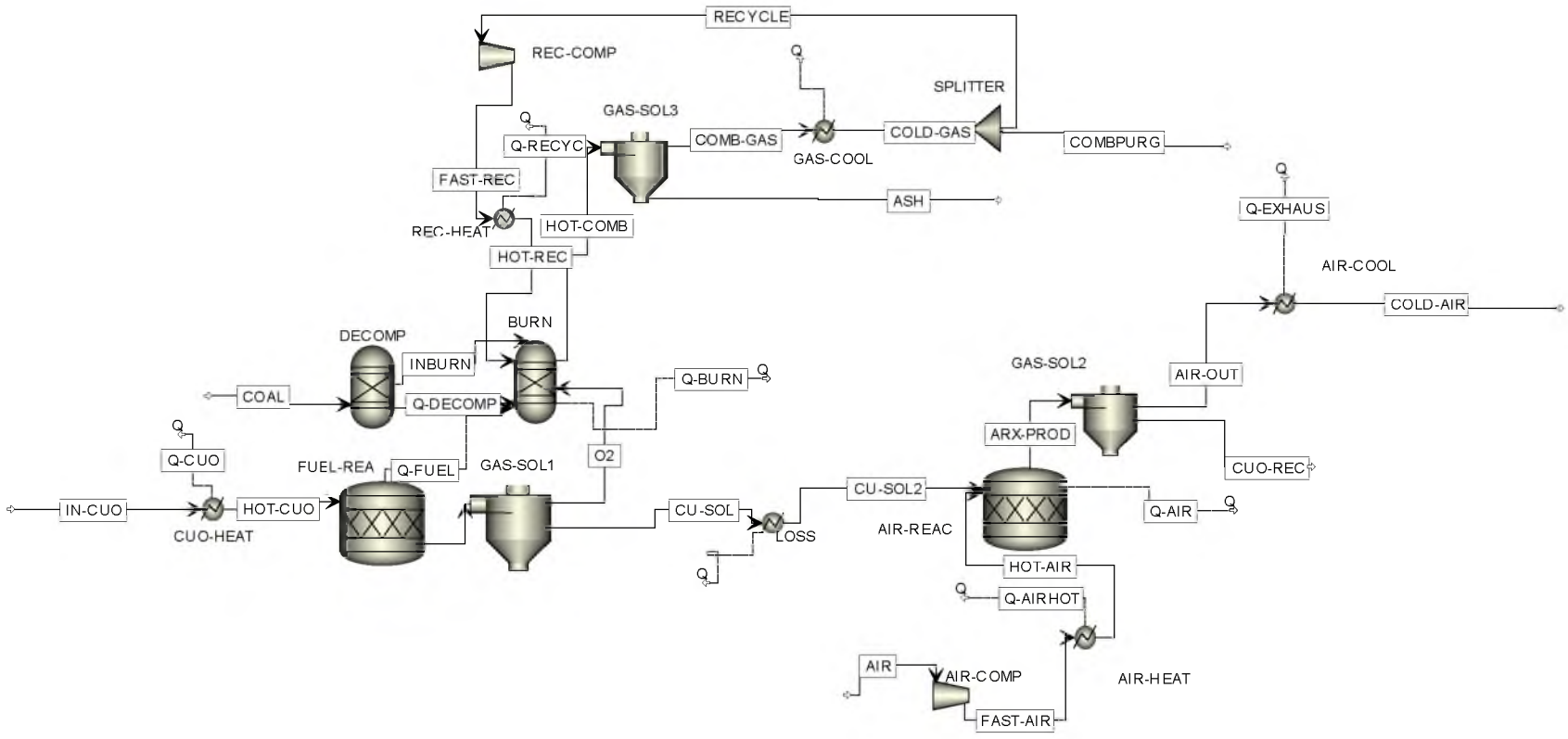

Figure 5.7 Schematic of ASPEN PLUS process model for CLOU with $CuO\text{-}ZrO_2$ as an oxygen carrier

Table 5.7 Parameters for ASPEN PLUS process model and pressure drop calculations for CLOU

Air flow rate	986 kg/h
Temperature of fuel reactor investigated	950°C
Temperature of air reactor investigated	935°C
Mass flow rate of CuO at the inlet of the fuel reactor	3392 kg/h
Mass flow rate of Cu_2O at the inlet of the fuel reactor	1648 kg/h
Mass flow rate of CuO at the exit of the fuel reactor	1560 kg/h
Mass flow rate of Cu_2O at the exit of the fuel reactor	3295 kg/h
Amount of ZrO_2 circulating in the system	7836 kg/h
Fraction of flue gas stream recycled for fluidization for fuel reactor particles	0.69
Particle density	2140 kg/m^3
Design superficial velocity for fuel reactor calculated based on particle properties	2.1 m/s
Design superficial velocity for air reactor calculated based on particle properties	2.4 m/s

Table 5.8 Relationships and parameters employed for determining energy requirements for fluidization[4,19]

Bed voidage, ϕ	0.6
Unfluidized bed height, h_{bed}	$h_{bed} = \frac{m_{bed}}{\rho_p(1-\phi)A_{reactor}}$
ΔP across the bed	$\Delta p_{bed} = (1-\varepsilon_{mf})(\rho_p - \rho_g)gh_{bed}$
ΔP across the bed and grate	$\Delta p = (1.4)\Delta p_{bed}$
Fan power	$\frac{n}{(n-1)}\frac{p_{inlet}v_{inlet}\dot{m}_{inlet}}{\eta_{fan}}\left[\left[\frac{p_{inlet}+\Delta p}{p_{inlet}}\right]^{(n-1)/n} - 1\right]$
Isentropic coefficient	1.4
Fan efficiency, η_{fan}	0.9

Table 5.9 Energy requirements and contributions for ASPEN PLUS process model for CLOU

Fuel reactor operation at 950°C(combustion of coal and CuO decomposition)	109
Thermal energy required by oxygen carrier(OC) to attain fuel reactor operation temperature	-35
Air reactor operation (oxidation of OC)	394
Thermal energy provided by OC to attain air reactor operation temperature of 935°C	33
Energy required for heating air from 25°C to air reactor temperature of 935°C	-265
Energy associated with cooling air reactor exhaust to 25°C	196
Energy associated with cooling flue gas from fuel reactor temperature to 150°C	271
Energy required to heat recycled gas from 150°C to fuel reactor temperature for fluidization	-185
Requirements for fluidizing the gas in the fuel and air reactors and for compressing steam	-5
Total	513

energy requirement of fluidizing the particles of 5 kW_{th} owing to a substantially lower residence time in the fuel reactor process.

A possible scheme is conceptualized for the CLOU process development unit according to the process parameters mentioned in Table 5.7 and 5.9 where CO_2 would be used as a fluidizing gas for the fuel reactor. CO_2 will have to be cooled to 150°C to be recompressed, and 69% of the flue gas stream would be recycled. The mass flow rate of CO_2 has been evaluated based on the energy requirements for fluidizing the fuel reactor. For reheating the CO_2 back to fuel reactor temperature, energy could be exchanged with the air reactor exhaust stream.

Table 5.10 indicates the possibility of recovering energy from both the fuel and air reactors in a CLOU process, even if the heating requirements of the oxygen carrier from the lower air reactor temperature of 935°C and air from ambient conditions are taken into consideration. In this scenario, 74 kW_{th} energy can be recovered from the fuel reactor and 162 kW_{th} from the air reactor. The air exhaust and the flue gas cooling streams also serve as a source for recovering thermal energy. The potential energy recovery is 513 kW_{th}. The scenario of operating the fuel reactor at a higher temperature than the air reactor in CLOU contrasts with that in CLC using an iron-based oxygen carrier using coal as a fuel, where it is essential to maintain the air reactor at a higher temperature. The details of the analysis with CLC using an iron-based oxygen carrier (OC) are presented in the next section.

5.5. CLC: ASPEN PLUS process model with Fe_2O_3-Fe_3O_4 system

Iron oxides such as hematite have been identified as one of the candidate oxygen carrier materials for chemical-looping combustion (CLC) applications.[20-26] The complete

Table 5.10 Analysis of energy recovery (in kW_{th}) from reactors in the CLOU process

Cumulative contribution of energy associated with fuel reactor operation and energy associated with oxygen carrier(OC)	74
Energy associated with cooling flue gas from fuel reactor temperature to 150°C	271
Cumulative contribution of energy associated with air reactor operation, energy associated with OC and heating air from 25°C	162
Energy associated with cooling air reactor exhaust to 25°C	196
Energy required to heat recycled gas from 150°C to fuel reactor temperature for fluidization	-185
Pump/compressor work	-5
Total	513

conversion of a carbonaceous fuel to achieve a high percentage of carbon dioxide capture could only be achieved by the transition from Fe_2O_3 to Fe_3O_4 from a thermodynamic standpoint.[27,28] Fixed bed reactor experiments on baorixile lignite in the presence of steam as a gasification agent and Fe_2O_3 as an oxygen carrier, which demonstrated the reduction of Fe_2O_3 to Fe_3O_4 by coal pyrolysis and steam char gasification intermediates, has been reported.[29] Hematite has also been investigated for combustion of a Shenhua bituminous coal and Huabei anthracite in a 1 kW_{th} interconnected fluidized bed laboratory set-up.[30,31]

For analyzing material and energy balance scenarios for the CLC process with PRB coal, a 60% Fe_2O_3 on Al_2O_3 was used as an oxygen carrier with a particle size of 150 microns, as studied previously by other researchers.[32,33] The reactions (5.12) and (5.13) take place in the fuel reactor:

$$3Fe_2O_3\,(s) + CO\,(g) \rightarrow 2Fe_3O_4\,(s) + CO_2\,(g) \qquad (5.12)$$

$$3Fe_2O_3\,(s) + H_2\,(g) \rightarrow 2Fe_3O_4\,(s) + H_2O\,(g) \quad (5.13)$$

An estimate of the gasification kinetics for the PRB coal was derived through comparisons with two coals which have been previously studied, a Colombian coal and Illinois #6 bituminous coal. The Colombian coal was recently tested in the 100 kW_{th} unit using ilmenite as an oxygen carrier at Chalmers.[34,35] The properties of the coals are compared in Tables 5.11 and 5.12.

The data presented in the tables suggest that the Colombian and Illinois #6 coals are similar. In addition, experimental studies on entrained flow gasification showed that the relative reactivity of a PRB coal char was 1.17 times greater than the Illinois #6 coal.[36] Hence, the kinetic data from the Colombian coal used in this analysis are likely to be more conservative in terms of gasification rates than the PRB coal.

Table 5.11 Proximate analysis for fuels used for comparison (wt. %)

Coal	Moisture	Volatile Matter	Ash
North Antelope PRB (Sub-Bituminous)	23.7	49.8	6.5
Colombian Coal (Bituminous)	3.3	37.0	5.2
Illinois #6 (Bituminous)	6.7	39.4	10.4

Table 5.12 Ultimate analysis for fuels used for comparison

Coal	C(wt% d.a.f)	H (wt% d.a.f)	O(wt % d.a.f)	N(wt % d.a.f)	S(wt% d.a.f)	Heating Value (MJ/kg)
PRB	75.3	5.0	18.3	1.1	0.3	27.7(dry basis)
Colombian Coal	80.7	5.5	11.5	1.5	0.6	29.1
Illinois#6 Coal	75.3	5.3	13.0	1.6	4.8	27.4 (dry basis)

The simulations for the CLC process were carried out for two different temperatures. In the first scenario, the fuel reactor temperature was considered to be at 950°C and the air reactor temperature as 935°C. This estimate was based on the optimum temperature which was found for the CLOU process as described in a previous section of this chapter (Sections 5.3 and 5.4). Another scenario (Scenario 2) for the CLC process was investigated based on the design temperatures of the 1 MW_{th} pilot at Technische Universität Darmstadt, Germany. The design temperature of the fuel reactor is 970°C and for the air reactor is 1050°C.[37] The conversion of CO and H_2 is almost complete when Fe_2O_3 is converted to Fe_3O_4 with an equilibrium concentration of $CO/(CO_2 + CO) \sim 0.005\%$ and that of $H_2/(H_2 + H_2O) \sim 0.003\%$ at 900 °C.[38] In this study, Al_2O_3 has been considered as an inert to facilitate order of magnitude calculations, though Kidambi et al.[39] have demonstrated the significance of the reaction of iron and Al_2O_3 through the formation of hercynite ($FeAl_2O_4$). In the air reactor, the oxidation reaction occurs by the following pathway:

$$2Fe_3O_4\,(s) + 1/2\,O_2(g) \rightarrow 3Fe_2O_3\,(s) \qquad (5.14)$$

The ASPEN PLUS flow sheet in Figure 5.8 shows the various unit blocks. Gasification and metal oxide reduction processes occur in the fuel reactor. The gasification process has been modeled by a combination of a RYIELD reactor and a RGIBBS equilibrium reactor with steam as an inlet stream. The steam/carbon mole ratio was maintained at unity for the process model. The resulting syngas was converted to CO_2 and H_2O in a RSTOIC reactor with a ~99.9% conversion of Fe_2O_3 to Fe_3O_4.

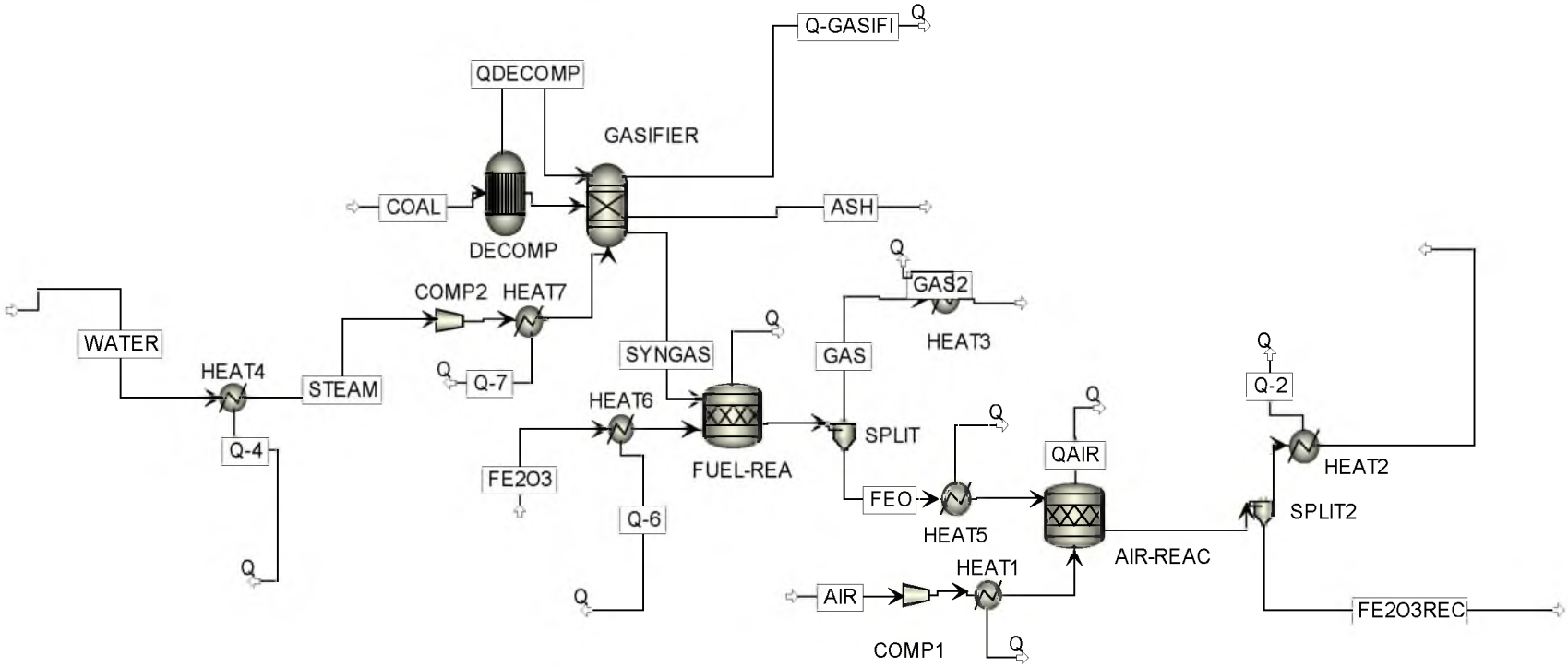

Figure 5.8 Schematic of ASPEN PLUS process model for CLC with Fe_2O_3-Al_2O_3 as an oxygen carrier

A RSTOIC reactor with an 80% conversion of Fe_3O_4 to Fe_2O_3 has been considered for modeling the oxidation process in the air reactor.

The rate of 95% conversion for Colombian coal in CLC fluidized-bed experiments with Fe-based ilmenite as an oxygen carrier was reported to be 9.6% $minute^{-1}$ at 970°C.[40] Syngas reduction rates of 8-30% min^{-1} have been reported for Fe_2O_3 supported on Al_2O_3 oxygen carriers.[33] Since the coal gasification reaction takes a longer time than the syngas reduction reaction, the fuel reactor has been designed considering the coal gasification reaction as a rate limiting step. A residence time on the order of 10 minutes was employed as an initial design approximation for the fuel reactor.

A residence time of 4 minutes was used for the oxidation reaction of OC in the air reactor. This assumption is in with line with the reported data of Zetterstrom with pellets and 80% conversion of Fe_3O_4 to Fe_2O_3 at 900°C.[41] This is a conservative estimate for the process design of a CLC air reactor employing iron oxide as an oxygen carrier, as Mattisson et al.[20] have reported high rates of 90% min^{-1} in their batch fluidized-bed oxidation experiments on natural hematite (α-Fe_2O_3) particles sized between 0.180 and 0.250 mm. at 950°C. For the ASPEN PLUS model for CLC, the pertinent parameters investigated for both scenarios are listed in Table 5.13. The energy requirements for various units and streams obtained from the ASPEN PLUS process model for both scenarios where the reactors are operating at different temperatures are listed in Table 5.14. The composition of the syngas at the outlet of the gasifier fuel reactor operating at 950°C consists of 31.8% CO, 5.2% CO_2, 50.2% H_2, and 12.5% H_2O. It can be noticed from Table 5.14 that there is a requirement to supply energy to the fuel reactor if its temperature is greater than that of the air reactor. The endothermic

Table 5.13 Parameters for ASPEN PLUS process model and pressure drop calculations for CLC

Air flow rate	714 kg/h
Mass flow rate of Fe_2O_3 at the inlet of the fuel reactor	4740 kg/h
Mass flow rate of Fe_3O_4 at the inlet of the fuel reactor	1145 kg/h
Mass flow rate of Fe_2O_3 at the exit of the fuel reactor	0.02 kg/h
Mass flow rate of Fe_3O_4 at the exit of the fuel reactor	5728 kg/h
Amount of Al_2O_3 circulating in the system	3951 kg/h
Particle density	3200 kg/m^3
Design superficial velocity for fuel reactor at 950°C calculated based on particle properties	3.9 m/s
Design superficial velocity for air reactor at 935°C calculated based on particle properties	3.1 m/s
Design superficial velocity for fuel reactor at 970°C calculated based on particle properties	3.9 m/s
Design superficial velocity for air reactor at 1050°C calculated based on particle properties	3.3 m/s

Table 5.14 Energy requirements and contributions (in kW_{th}) for ASPEN PLUS process model for CLC

	Scenario 1(Fuel Reactor Temperature = 950°C, Air Reactor Temperature = 935°C)	Scenario 2(Fuel Reactor Temperature = 970°C, Air Reactor Temperature =1050°C)
Fuel reactor operation (gasifying coal and reducing metal oxide)	-160	-161
Thermal energy required/provided by oxygen carrier(OC) to attain fuel reactor operation temperature	-42	212
Heat steam from 150°C to fuel reactor temperature	-96	-97
Air reactor operation (oxidation of OC)	663	658
Thermal energy provided/required by OC to attain air reactor operation temperature	41	-205
Heat air from 25°C to air reactor temperature	-188	-215
Energy associated with cooling air reactor exhaust to 25°C	137	158
Cool flue gas from fuel reactor temperature to 150°C	117	121
Requirements for fluidizing the gas in the fuel and air reactors and for compressing steam	-43	-43
Total	429	428

gasification and metal oxide reduction reactions require 160 kW_{th}, and 42 kW_{th} is required to heat the oxygen carrier from 935°C to 950°C for fuel reactor operation. Thus, 202 kW_{th} of energy has to be supplied. The relationships mentioned in Table 5.6 were employed to determine the energy requirements for fluidization.

To avoid the addition of thermal energy to the fuel reactor, the temperature of the air reactor has to be higher than that of the fuel reactor. The results in Table 5.15 demonstrate the cumulative contribution of the energy associated with fuel reactor operation and oxygen carrier heating/cooling requirements. The requirement of supplying 202 kW_{th} for the endothermic gasification and metal oxide reduction reactions in the fuel reactor is accomplished by the transfer of oxygen carrier from the air reactor operating at a higher temperature of 1050°C to the fuel reactor (Scenario 2). As the air reactor is maintained at a higher temperature, it is possible to operate the fuel reactor in an "auto-thermal" operation with 51 kW_{th} available from it. Thermal energy could still be recovered from the air reactor for the case when the air reactor is operated at a higher temperature than the fuel reactor. The concept of an "auto-thermal" mode of operation where the process development unit does not require external heating has been proposed for CLC reactors for coal combustion with Ca-based carriers[42] and natural gas combustion with Ni-based carriers.[43]

A preliminary estimate for an oxygen carrier inventory of 2000 kg/MW_{th} for CLC with petroleum coke with a 60% Fe_2O_3 supported on 40% inert $MgAl_2O_4$ oxygen carrier has been reported by Leion et al.[13] The reported residence time of the fuel reactor was 5 minutes which could be achieved if the fuel conversion is conducted in the presence of 100% steam, and a significant amount of un-reacted char is adequately separated and recycled.

Table 5.15 Analysis of energy recovery (in kW_{th}) from reactors in the CLC process

	Scenario 1(Fuel Reactor Temperature = 950°C, Air Reactor Temperature = 935°C)	Scenario 2(Fuel Reactor Temperature = 970°C, Air Reactor Temperature =1050°C)
Cumulative contribution of energy associated with fuel reactor operation, and energy change associated with the oxygen carrier introduced in fuel reactor	-202	51
Cumulative contribution of energy associated with air reactor operation, energy associated with oxygen carrier introduced in the air reactor, and heating air from 25°C	516	238
Cooling of air reactor exhaust	137	158
Cooling of flue gas	117	121
Heating of steam	-96	-97
Pump/compressor work	-43	-43
Total	429	428

The analysis conducted in this chapter takes into account a fuel reactor residence time of 10 minutes, based on experimental observations in batch fluidized-bed experiments.[44] As more operational experience is gathered with CLC experiments with solid fuels on Fe_2O_3-based oxygen carriers in continuous units, this design assumption could be suitably modified.

5.6. Conclusions

The CLOU system supports energy recovery from both the air and fuel reactor. In contrast to CLOU, operating the fuel reactor at a higher temperature than the air reactor in CLC shall require identification of appropriate means to supply energy from the air reactor to the fuel reactor for supporting the endothermic reduction and solid fuel gasification reactions. A strategy that could be employed and has been reported[35,37,43] is to operate the air reactor at a higher temperature than the fuel reactor, which shall result in the oxygen carrier serving as a source of energy supply for the endothermic fuel gasification and metal oxide reduction reactions in the CLC fuel reactor.

Based on the analysis of batch-scale experimental fluidized-bed data with CuO/ZrO_2 oxygen carrier,[14] it was identified that a temperature difference of 15°C between the fuel reactor operating at a higher temperature and air reactor at a lower temperature in the range of 920°C-960°C could be a viable range for operation for the CLOU process.

The slower gasification reactions in CLC require a large residence time which result in larger hold-up times for oxygen carrier (OC) particles. This indicates a larger pressure drop across the fuel reactor bed for CLC and a higher energy cost in fluidizing the particles (43 kW_{th} versus 5 kW_{th} for CLOU).

Finally, for CLC, with an 60% Fe_2O_3 on Al_2O_3, a circulation rate of 98.4 kg OC/kg coal has been determined and for CLOU, with 40% CuO on ZrO_2 ,a circulation rate of 128.8 kg OC/kg coal has been evaluated. It is important to note that the calculation for Fe is based on the transition from Fe_2O_3 to Fe_3O_4. A process scheme exploring the transition from Fe_2O_3 to a lower oxidation state has promise to lower these circulation rates. This is currently being explored with ilmenite. In the case of CLOU, optimizing the oxygen carrier loading is the key to take advantage of faster reaction rates for CuO to Cu_2O, which has the promise to lower the fuel reactor volume.

5.7. Nomenclature

$A_{reactor}$	cross sectional area of reactor
Ar	Archimedes Number
d_p	diameter of particle, m
f	mass fraction
F	fraction of particles above 45μm
g	acceleration due to gravity, m/s^2
h_{bed}	height of bed, m
k_{CuO}	reaction rate constant of CuO decomposition, $atm^{-1}s^{-1}$
$k_{Cu_2O,app}$	apparent reaction rate constant of Cu_2O oxidation, s^{-1}
$k_{r,C}$	reaction rate constant of coal char oxidation, $g/cm^2atm^{0.5}s$
$\dot{m}$	mass flow rate, kg/s
m	mass of metal required per MW_{th} fuel
m_{bed}	mass of the fluidized bed, kg
$\hat{m}$	mass flow rate per MW_{th}, kg/MW_{th} s

M	molecular weight
n	isentropic coefficient
$\dot{N}$	molar flow rate, mole/s
p_{inlet}	pressure at inlet of reactor, atm
$p_{O_{2,in}}$	partial pressure of oxygen at inlet of reactor, atm
$p_{O_{2,e}}$	partial pressure of oxygen at the equilibrium conditions of CuO decomposition, atm
$p_{O_{2,out}}$	partial pressure of oxygen at the exit of reactor, atm
Δp	pressure drop across bed, atm
Δp_{bed}	pressure drop across bed and grate, atm
r_C	radius of the carbonaceous fuel particle, m
r_p	radius of the oxygen carrier particle, m
Q	heating value of fuel, MJ/kg
R	gas constant, J/mol K
R_g	gas constant, cal/mol K
Re_{mf}	Reynolds number at minimum fluidization conditions
t	time, s
T	temperature, K
T_{avg}	average of the temperature, K
u_{mb}	minimum bubbling velocity for Group A particles, m/s
u_{mf}	velocity at minimum fluidization conditions, m/s
u_t	terminal velocity, m/s
v_{inlet}	specific volume at inlet of reactor, m^3/kg
X_{CuO}	conversion of CuO

X_{Cu_2O}	conversion of Cu_2O
Y	mole ratio (defined in Equation.5.1)

Subscripts

avg	average
AR	air reactor
FR	fuel reactor
c	carbon
coal	coal
Cu	copper
Cu_2O	cuprous oxide
CuO	cupric oxide
h	hydrogen
n	nitrogen
s	sulphur
o	oxygen
S	solids
th	thermal

Greek Symbols

α_S	fraction of particle volume initially occupied by solid reactant
ε_{mf}	voidage at minimum fluidization
ρ_C	density of carbonaceous particle, g/cm^3
ρ_g	density of gas, g/cm^3

ρ_p	density of particle, kg/m^3
$\tilde{\rho}_S$	molar density of solid reactant, mol/m^3
$\tilde{\rho}_{S,Cu_2O}$	molar density of Cu_2O, mol/m^3
τ_{AR}	residence time of an air reactor,s
τ_{FR}	residence time of an fuel reactor,s
μ	viscosity of gas, kg/ms
Ω_{coal}	stoichiometric moles of O_2 required to convert 1 kg coal to CO_2, H_2O, NO and SO_2
ϕ	bed voidage
η_{fan}	fan efficiency

Abbreviations

CLOU	chemical-looping with oxygen uncoupling
CLC	chemical-looping combustion
d.a.f.	dry ash free
kW_{th}	kilowatt thermal
MW_{th}	megawatt thermal
OC	oxygen carrier

5.8. References

1. Mattisson, T.; Leion, H.; Lyngfelt, A., Chemical-looping with oxygen uncoupling using CuO/ZrO_2 with petroleum coke. *Fuel* **2009,** *88* (4), 683-690.

2. García-Labiano, F.; De Diego, L. F.; Adánez, J.; Abad, A.; Gayán, P., Reduction and oxidation kinetics of a copper-based oxygen carrier prepared by impregnation for chemical-looping combustion. *Industrial and Engineering Chemistry Research* **2004,** *43* (26), 8168-8177.

3. Abad, A.; Adánez, J.; García-Labiano, F.; de Diego, L. F.; Gayán, P.; Celaya, J., Mapping of the range of operational conditions for Cu-, Fe-, and Ni-based oxygen carriers in chemical-looping combustion. *Chemical Engineering Science* **2007,** *62* (1–2), 533-549.

4. Lyngfelt, A.; Leckner, B.; Mattisson, T., A fluidized-bed combustion process with inherent CO_2 separation: Application of chemical-looping combustion. *Chemical Engineering Science* **2001,** *56* (10), 3101-3113.

5. Leion, H., Chemical-Looping Combustion with Solid Fuels. Ph.D. Dissertation, Chalmers University of Technology, Göteborg, Sweden, 2007.

6. Abad, A.; Adánez-Rubio, I.; Gayán, P.; García-Labiano, F.; de Diego, L. F.; Adánez, J., Demonstration of chemical-looping with oxygen uncoupling (CLOU) process in a 1.5 kW_{th} continuously operating unit using a Cu-based oxygen-carrier. *International Journal of Greenhouse Gas Control* **2012,** *6*, 189-200.

7. de Diego, L. F.; García-Labiano, F.; Adánez, J.; Gayán, P.; Abad, A.; Corbella, B. M.; María Palacios, J., Development of Cu-based oxygen carriers for chemical-looping combustion. *Fuel* **2004,** *83* (13), 1749-1757.

8. Lewis, W. K.; Gilliland, E. R.; Sweeney, M. P., Gasification of Carbon, Metal Oxides in a Fluidized Powder Bed. *Chem. Eng. Prog.* **1951,** *47*, 251-256.

9. Lewis, W. K.; Gilliland, E. R., US Patent 2665972, 1954.

10. Mattisson, T.; Lyngfelt, A.; Leion, H., Chemical-looping with oxygen uncoupling for combustion of solid fuels. *International Journal of Greenhouse Gas Control* **2009,** *3* (1), 11-19.

11. Leion, H.; Mattisson, T.; Lyngfelt, A., Solid fuels in chemical-looping combustion. *International Journal of Greenhouse Gas Control* **2008,** *2* (2), 180-193.

12. Leion, H.; Mattisson, T.; Lyngfelt, A., Combustion of a German Lignite Using Chemical-looping with oxygen uncoupling (CLOU). In *The 33rd International Technical Conference on Coal Utilization & Fuel Systems*, Clearwater,FL, **2008**.

13. Leion, H.; Mattisson, T.; Lyngfelt, A., The use of petroleum coke as fuel in chemical-looping combustion. *Fuel* **2007,** *86* (12-13), 1947-1958.

14. Sahir, A.H.; Sohn, H. Y.; Leion, H.; Lighty, J. S., Rate Analysis of Chemical-Looping with oxygen uncoupling (CLOU) for Solid Fuels. *Energy Fuels* **2012,** *26* (7), 4395-4404.

15. Eyring, E. M.; Konya, G.; Lighty, J. S.; Sahir, A. H.; Sarofim, A. F.; Whitty, K., Chemical Looping with Copper Oxide as Carrier and Coal as Fuel. *Oil Gas Sci. Technol. Rev. IFP Energies nouvelles* **2011,** *66* (2), 209-221.

16. Arjmand, M.; Keller, M.; Leion, H.; Mattisson, T.; Lyngfelt, A., Oxygen Release and Oxidation Rates of $MgAl_2O_4$-Supported CuO Oxygen Carrier for Chemical-Looping Combustion with oxygen uncoupling (CLOU). *Energy Fuels* **2012,** *26* (11), 6528-6539.

17. Bartok, W.; Sarofim, A.F., *Fossil Fuel Combustion A Source Book*. John Wiley & Sons: 1991.

18. Basu, P.; Fraser, S.A., *Circulating Fluidized Bed Boilers-Design and Operations*. Butterworth-Heinemann: 1991.

19. Kunii, D.; Levenspiel, O., *Fluidization Engineering*. Second ed.; Butterworth-Heinemann: 1991.

20. Mattisson, T.; Lyngfelt, A.; Cho, P., The use of iron oxide as an oxygen carrier in chemical-looping combustion of methane with inherent separation of CO_2. *Fuel* **2001,** *80* (13), 1953-1962.

21. Mattisson, T.; Lyngfelt, A.; Cho, P., Possibility of using iron oxide as an oxygen carrier for combustion of methane with removal of CO_2-Application of chemical-looping combustion. *Proc. 5th Int Conf Greenhouse Gas Control Technologies (GHGT-5)* **2000**.

22. Johansson, M.; Mattisson, T.; Lyngfelt, A., Investigation of Fe_2O_3 with $MgAl_2O_4$ for chemical-looping combustion. *Industrial and Engineering Chemistry Research* **2004,** *43* (22), 6978-6987.

23. Mattisson, T.; Johansson, M.; Lyngfelt, A., Multicycle reduction and oxidation of different types of iron oxide particles-application to chemical-looping combustion. *Energy Fuels* **2004,** *18* (3), 628-637.

24. Ishida, M.; Takeshita, K.; Suzuki, K.; Ohba, T., Application of Fe_2O_3-Al_2O_3 composite particles as solid looping material of the chemical-loop combustor. *Energy Fuels* **2005,** *19* (6), 2514-2518.

25. Dennis, J. S.; Scott, S. A.; Hayhurst, A. N., In situ gasification of coal using steam with chemical looping: A technique for isolating CO_2 from burning a solid fuel. *Journal of the Energy Institute* **2006,** *79* (3), 187-190.

26. Abad, A.; Mattisson, T.; Lyngfelt, A.; Johansson, M., The use of iron oxide as oxygen carrier in a chemical-looping reactor. *Fuel* **2007,** *86* (7-8), 1021-1035.

27. Mattisson, T.; Lyngfelt, A., Capture of CO_2 using chemical-looping combustion. In *Scandinavian-Nordic Section of the Combustion Institute*, Goteborg, Sweden, 2001; pp 163-168.

28. Jerndal, E.; Mattisson, T.; Lyngfelt, A., Thermal analysis of chemical-looping combustion. *Chemical Engineering Research and Design* **2006,** *84* (9 A), 795-806.

29. Yang, J. B.; Cai, N. S.; Li, Z. S., Reduction of iron oxide as an oxygen carrier by coal pyrolysis and steam char gasification intermediate products. *Energy Fuels* **2007,** *21* (6), 3360-3368.

30. Song, T.; Wu, J.; Zhang, H.; Shen, L., Characterization of an Australia hematite oxygen carrier in chemical looping combustion with coal. *International Journal of Greenhouse Gas Control* **2012,** *11* (0), 326-336.

31. Song, T.; Shen, T.; Shen, L.; Xiao, J.; Gu, H.; Zhang, S., Evaluation of hematite oxygen carrier in chemical-looping combustion of coal. *Fuel* **2013,** *104* (0), 244-252.

32. Cho, P.; Mattisson, T.; Lyngfelt, A., Comparison of iron-, nickel-, copper- and manganese-based oxygen carriers for chemical-looping combustion. *Fuel* **2004,** *83* (9), 1215-1225.

33. Abad, A.; García-Labiano, F.; de Diego, L. F.; Gayán, P.; Adánez, J., Reduction Kinetics of Cu-, Ni-, and Fe-Based Oxygen Carriers Using Syngas ($CO + H_2$) for Chemical-Looping Combustion. *Energy Fuels* **2007,** *21* (4), 1843-1853.

34. Markstrom, P.; Lyngfelt, A.; Linderholm, C., Chemical-looping Combustion in a 100 kW_{th} unit for solid fuels. In *21st International Conference on Fluidized Bed Combustion*, Naples, 2012.

35. Markstrom, P.; Lyngfelt, A.; Linderholm, C., Operation of a 100 kW_{th} chemical-looping combustor with Mexican petroleum coke and Cerrejon coal In *Proceedings of the 2nd International Conference on Chemical-looping*, Darmstadt; Germany, 2012.

36. Brown, B. W., Smoot, L.D.,Hedman, P.O., Effect of coal type on entrained gasification. *Fuel* **1986,** *65*, 673-678.

37. Orth, M.; Strohle, J.; Epple, B., Design and operation of a $1MW_{th}$ Chemical-looping plant. In *Proceedings of the 2nd International Conference on Chemical Looping*, Darmstadt, Germany, 2012.

38. Xue, Z.; Chen, S.; Wang, D.; Xiang, W., Design and Fluid Dynamic Analysis of a Three-Fluidized-Bed Reactor System for Chemical-Looping Hydrogen Generation. *Industrial & Engineering Chemistry Research* **2012,** *51* (11), 4267-4278.

39. Kidambi, P. R.; Cleeton, J. P. E.; Scott, S. A.; Dennis, J. S.; Bohn, C. D., Interaction of Iron Oxide with Alumina in a Composite Oxygen Carrier during the Production of Hydrogen by Chemical Looping. *Energy Fuels* **2011,** *26* (1), 603-617.

40. Leion, H.; Mattisson, T.; Lyngfelt, A., Using chemical-looping with oxygen uncoupling (CLOU) for combustion of six different solid fuels. *Energy Procedia* **2009,** *1*, 447-453.

41. Zetterstrom, J. D., *Oxidation of magnetite concentrates*. U.S. Dept. of the Interior, Bureau of Mines: 1950.

42. Andrus, H. E.; Chiu, J. H.; Thibeault, P. R.; Brautsch, A., Alstom's calcium oxide chemical looping combustion coal power technology development. In *Proceedings of the 34th International Technical Conference on Clean Coal & Fuel Systems*, Clearwater, FL, 2009.

43. Marx, K.; Bolhàr-Nordenkampf, J.; Pröll, T.; Hofbauer, H., Chemical looping combustion for power generation—Concept study for a 10 MW_{th} demonstration plant. *International Journal of Greenhouse Gas Control* **2011,** *5* (5), 1199-1205.

44. Leion, H.; Mattisson, T.; Lyngfelt, A., Using chemical-looping with oxygen uncoupling (CLOU) for combustion of six different solid fuels. *Energy Procedia* **2009,** *1* (1), 447-453.

CHAPTER 6

CONCLUSIONS

6.1. Conclusions

Chemical-looping combustion (CLC) is one of the carbon capture technologies which offers considerable promise and potential for solid fuels. As of early 2013, CLC demonstration units for solid fuels at the 3 MW_{th} scale have been constructed.[1,2] Chemical-looping with oxygen uncoupling (CLOU) offers several opportunities and challenges for implementation. This research exploring CLC and CLOU found the following:

- The relative importance of chemical reaction, external mass transfer, and internal mass transfer for typical operating conditions of a CLC system through the Law of Additive Reaction Times was investigated. In the present work, reported experimental studies for Cu oxidation in the air reactor were reanalyzed, and the importance of porous solid reaction modulus in identifying the appropriate controlling regime (chemical reaction, internal/external mass transfer) was demonstrated. In the analysis of the experimental study of copper oxidation on 10% CuO supported on alumina by Garcia-Labiano et al.,[3] the magnitude of porous solid reaction modulus was determined to be less than 0.1 for the particles used in their study (sized between 0.1 to 0.3 mm.), indicating control under the chemical-reaction regime. The Law of Additive Reaction Times further predicted that for the particles (10% CuO supported on alumina used by Garcia-Labiano et al.[3]) in the size range of 0.8 to 1 mm., external and/or internal mass transfer effects were significant and should be duly considered in the analysis, as the magnitude of porous solid reaction modulus was of the order of unity. On the other end, the reanalysis of copper oxidation with 1.3% O_2 in an O_2-N_2 mixture, for one of the experimental datasets from Chuang et al.[4] at 700°C (for 82.5% CuO supported on alumina particles, sized between 0.85 – 1 mm.) by the Law of Additive Reaction Times, it was demonstrated that

their experiment was controlled by a combination of external and internal mass transfer. This observation made with the help of the law was consistent with one of the conclusions drawn by Chuang et al.[4] that the oxidation reaction in their experiment was controlled by external mass transfer. The application of the Law of Additive Reaction Times offers an approximate solution which is valuable in providing a quantitative basis for design and optimization for CLC systems and obviates the need of a numerical solution, and thus will prove to be important for technology development.

- The detailed rate analysis for chemical-looping with oxygen uncoupling (CLOU), utilizing reported experimental data for combustion of Mexican petcoke particles with the help of a CuO/ZrO_2 oxygen carrier, found that the apparent activation energy for CuO decomposition reaction was 280 kJ/mol. It was further identified that the energy requirements to overcome the thermodynamic barrier for CuO decomposition are substantially larger than the kinetic barrier. The activation energy for petcoke oxidation was estimated to be 129 kJ/mol. The apparent kinetic rate constants for Cu_2O oxidation were also determined. The rate analysis of the experimental data through the concepts investigated will facilitate the pilot-scale development of CLOU process for solid carbonaceous fuels.
- The kinetics of CuO reduction and petcoke oxidation determined from the rate analysis of CLOU process were utilized in developing a fluidized-bed model for the fuel reactor. The results showed a reasonable prediction of O_2 and CO_2 concentration trends with independently obtained experimental data of Mattisson et al.[5]. The model equations and the solution procedure utilized to analyze the bench-scale CLOU fluidized-bed reactor experiment in this dissertation is an initial attempt, which will be refined further in future

efforts to analyze the experimental CO_2 and O_2 concentration profiles from the fuel reactor of a CLOU process development unit.

- ASPEN PLUS process models were developed for a solid fuel-based chemical looping process development unit using a copper-based oxygen carrier for CLOU, and for CLC employing an iron-based oxygen carrier. Based on kinetic considerations and process model results, a temperature difference of 15°C between the fuel reactor operating at a higher temperature, and the air reactor at a lower temperature in the range of 920°C-960°C for the CLOU process was identified as a viable range of operation. An oxygen carrier circulation rate for CLOU of 128.8 kg OC/kg coal with 40% CuO on ZrO_2 was determined based on an optimum conversion of 54% in the fuel reactor and 50% in the air reactor. The results of an ASPEN PLUS models for CLC based on the transition from Fe_2O_3 to Fe_3O_4 indicates a circulation rate of 98.4 kg OC/kg coal for combustion with 60% Fe_2O_3 on Al_2O_3 oxygen carrier. The process model results for CLC reiterate the relevance of operating the air reactor at higher temperatures to supply energy for the endothermic metal oxide reduction and fuel gasification reactions, as has also been suggested by other researchers.[6-8] The results also indicate a larger pressure drop across the fuel reactor bed for CLC and a higher energy cost in fluidizing the particles (43 kW_{th} versus 5 kW_{th}) versus the CLOU process for a 100 kg/hr coal feed rate.

6.2. Future Work

The work performed as a part of this dissertation lays the initial foundation for the some of the important concepts which will be required to conceptualize a process for chemical-looping combustion for solid fuels. At the University of Utah, a 150-200 kW_{th}

process development unit (PDU) for a CLOU system is currently under construction, where the investigations presented in this dissertation will find application.[9,10]

Cost of the oxygen carrier and attrition rates are a major consideration for CLOU. For copper-based oxygen carriers, agglomeration is also a concern. Investigations on oxygen carrier materials like $MgAl_2O_4$[11-12], cement supports[13], copper ores[14], sol-gel derived $CuO/CuAl_2O_4$[15], and Cu–Al layered double hydroxide (LDH) precursors[16] are being undertaken by various research groups worldwide. These studies highlight the potential for future development. The methodology of determining kinetics proposed in this dissertation could be applied to other copper-based CLOU oxygen carriers, which will help in determining the equipment sizes and relevant process scenarios.

Based on the process model evaluation for CLC using iron-based oxygen carriers for a Fe_2O_3 to Fe_3O_4 transition reported in this work, strategies to reduce the fuel reactor residence time in chemical-looping combustion (CLC) for solid fuel combustion are of vital importance. One of the possibilities which is currently being investigated by researchers is the enhancement of gasification rates by incorporating potassium-based additives in iron-based oxygen carriers for solid fuel CLC.[17-19] The reduction of fuel reactor residence time in CLC will have an impact on solid fuel and oxygen carrier hold up, reactor dimensions, and energy requirements for fluidization.

While the fluidized-bed model developed for CLOU reported in this work does not take into account segregation, segregation of particles is observed when solid particles of differing densities or size distribution are introduced in a circulating fluidized bed system.[20] Recently, researchers have reported investigations on mixing and segregation for CLC with the help of cold flow models, discrete element models (DEM) and computational fluid

dynamic (CFD) predictions [21,22], where it was shown that binary mixtures of oxygen carrier particles employed to improve the overall reduction and oxidation characteristics of the system have the tendency to segregate under certain operating conditions. The CLOU process involves two solid materials in the fuel reactor, the carbonaceous fuel and an oxygen carrier. For the CLOU process, it has been shown that the ratio of coal particles to CuO-based oxygen carrier particles, and solid fuel reactivity have an effect on the oxygen concentration trends at the outlet of a fuel reactor in the CLOU process.[23] The identification of fuel reactor operation regimes for the CLOU process where segregation could affect system performance is a study which merits attention, as the distribution of oxygen through the height of the fuel reactor could be impacted by variation in coal to CuO-based oxygen carrier ratio. The variation in oxygen concentration in the fuel reactor may impact the evolution of CO and CO_2, and the role of segregation in the phenomenon needs to be analyzed further.

The process engineering insights and principles presented in this dissertation will help in conducting energy integration studies and techno-economic analysis, which will be refined further as more data and experience are gathered.

6.3. References

1. Henderson, C. IEA Clean Coal Centre ,Visit to 2nd International Conference on Chemical Looping, 26-28 Sep, Darmstadt, Germany. http://www.iea-coal.org.uk/site/2010/blog-section/blog-posts/visit-to-2nd-international-conference-on-chemical-looping-darmstadt-germany (accessed March 19, 2013).

2. Bullis, K. MIT Technology Review, A Cleaner Way to Use Coal. http://www.technologyreview.com/news/510736/a-cleaner-way-to-use-coal/ (accessed March 19, 2013).

3. García-Labiano, F.; De Diego, L. F.; Adánez, J.; Abad, A.; Gayán, P., Reduction and oxidation kinetics of a copper-based oxygen carrier prepared by impregnation for

chemical-looping combustion. *Industrial and Engineering Chemistry Research* **2004,** *43* (26), 8168-8177.

4. Chuang, S. Y.; Dennis, J. S.; Hayhurst, A. N.; Scott, S. A., Kinetics of the oxidation of a co-precipitated mixture of Cu and Al_2O_3 by O_2 for chemical-looping combustion. *Energy and Fuels* **2010,** *24* (7), 3917-3927.

5. Mattisson, T.; Lyngfelt, A.; Leion, H., Chemical-looping with oxygen uncoupling for combustion of solid fuels. *International Journal of Greenhouse Gas Control* **2009,** *3* (1), 11-19.

6. Markstrom, P.; Lyngfelt, A.; Linderholm, C., Operation of a 100 kW_{th} chemical looping combustor with Mexican petroleum coke and Cerrejon coal In *Proceedings of the 2nd International Conference on Chemical-looping*, Darmstadt; Germany, **2012**.

7. Orth, M.; Strohle, J.; Epple, B., Design and operation of a $1MW_{th}$ Chemical looping plant. In *Proceedings of the 2nd International Conference on Chemical Looping*, Darmstadt, Germany, **2012**.

8. Marx, K.; Bolhàr-Nordenkampf, J.; Pröll, T.; Hofbauer, H., Chemical looping combustion for power generation—Concept study for a 10 MW_{th} demonstration plant. *International Journal of Greenhouse Gas Control* **2011,** *5* (5), 1199-1205.

9. Lighty, J. S., Chemical Looping with Oxygen Uncoupling (CLOU) for coal combustion. In *2012 NETL CO_2 capture technology meeting*, Pittsburgh, Pennsylvania, USA, **2012**.

10. Whitty, K. J., Practical Challenges of System Design for a CLOU-Based System for Chemical Looping Combustion of Coal In *2nd International Conference on Chemical Looping*, Darmstadt, Germany, **2012**.

11. Arjmand, M.; Keller, M.; Leion, H.; Mattisson, T.; Lyngfelt, A., Oxygen Release and Oxidation Rates of $MgAl_2O_4$-Supported CuO Oxygen Carrier for Chemical-Looping Combustion with Oxygen Uncoupling (CLOU). *Energy Fuels* **2012,** *26* (11), 6528-6539.

12. Adánez-Rubio, I.; Abad, A.; Gayán, P.; de Diego, L. F.; García-Labiano, F.; Adánez, J., Performance of CLOU process in the combustion of different types of coal with CO_2 capture. *International Journal of Greenhouse Gas Control* **2013,** *12* (0), 430-440.

13. Xu, L.; Wang, J.; Li, Z.; Cai, N, Experimental Study of Cement-Supported CuO Oxygen Carriers in Chemical Looping with Oxygen Uncoupling(CLOU). *Energy Fuels* **2013,** *27,* 1522-1530.

14. Wen, Y.-Y.; Li, Z.-s.; Xu, L.; Cai, N.-s., Experimental Study of Natural Cu Ore Particles as Oxygen Carriers in Chemical Looping with Oxygen Uncoupling (CLOU). *Energy Fuels* **2012,** *26* (6), 3919-3927.

15. Mei, D.; Zhao, H.; Ma,Z; Zheng, C., Using sol-gel derived $CuO/CuAl_2O_4$ oxygen carrier in chemical-looping with oxygen uncoupling for three coals. *Energy Fuels* **2013, DOI:** 10.1021/ef3021602

16. Song, Q.; Liu,Z.; Bohn,C.D.; Harper, R.N.; Sivaniah, E.; Scott, S.A. ; Dennis, J.S. A high performance oxygen storage material for chemical looping processes with CO_2 capture, *Energy Environ. Sci.*, **2013**, *6*, 288-298.

17. Yu, Z.; Li, C.; Fang, Y.; Huang, J.; Wang, Z. Reduction Rate Enhancements for Coal Direct Chemical Looping Combustion with an Iron Oxide Oxygen Carrier, *Energy Fuels* **2012**, *26*, 2505-2511.

18. Gu, H.; Shen, L.; Xiao, J.; Zhang, S.; Song, T.; Chen, D. Iron Ore as Oxygen Carrier Improved with Potassium for Chemical Looping Combustion of Anthracite Coal, *Combust. Flame* **2012**, *159*, 2480-2490.

19. Keller, M.; Leion, H.; Mattisson, T. Mechanisms of Solid Fuel Conversion by Chemical-looping combustion(CLC) using Manganese Ore: Catalytic Gasification by Potassium Compounds, *Energy Technology* **2013**,*1*,273-282.

20. Hirschberg, B.; Werther, J. Factors affecting solids segregation in circulating fluidized-bed riser, *AIChE. J.* **1998**, *44* 25–34.

21. Alghamdi, Y.A.; Doroodchi, E.; Moghtaderi, B. Mixing and segregation of binary oxygen carrier mixtures in a cold flow model of a chemical looping combustor, *Chemical Engineering Journal*, **2013**, *223*, 772–784.

22. Peng, Z.; Doroodchi,E.; Alghamdi,Y.; Moghtaderi.B. Mixing and segregation of solid mixtures in bubbling fluidized beds under conditions pertinent to the fuel reactor of a chemical looping system, *Powder Technology* **2013**, *235*, 823–837.

23. Eyring, E. M.; Konya, G.; Lighty, J. S.; Sahir, A. H.; Sarofim, A. F.; Whitty, K.,Chemical Looping with Copper Oxide as Carrier and Coal as Fuel. *Oil Gas Sci. Technol. Rev. IFP Energies nouvelles* **2011,** *66* (2), 209-221.

APPENDIX A

MATLAB PROGRAM FOR THE FLUIDIZED BED MODEL

```
% Program to analyze the fluidized bed reactor for CLOU process
% Author: Asad H. Sahir

% Program Structure:
% FBR - Main Program
% pde.m - Function where the partial differential equations have been
%         solved in time by discretizing the z-Coordinate
% umf.m - Function for minimum fluidization velocity
% ue.m - Function to calculate rise velocity of emulsion gas
% delta.m - Function to calculate the fraction of bed volume occupied by
%           bubbles
% kbe.m - Function to evaluate the Interchange coefficient for gas between
%         bubble and emulsion phases based on bubble volume
% fgb.m - Function to calculate the fraction of gas in the bubble phase
% fge.m - Function to calculate the fraction of gas in emulsion phase
% fse.m - Function to calculate the fraction of solid in emulsion phase
% db.m - Function to evaluate the bubble diameter
% ub.m - Function to calculate the local bubble rise velocity
% diff_coeff.m - Function to calculate the diffusion coefficient based on
%                 90% CO2 and 10% O2
% viscosity.m - Function to calculate viscosity of gas based on 90% CO2
and
%               10% O2


% Clear Previous Files
    clear all
    clc

% Parameters shared with the ODE routine
    global n ncvr nCuOvr ri rhoc h nc vr  nCuO rcuo


% Determination of volume of fluidized bed
d0 = 0.022;% d0 : Diameter of the bed: (m)
h = 0.045;% h:  Height of the reactor(m); based on Babu, Shah and
Talwalkar's correlation(1978)
vr = 4.209+((3.14/4)*((d0*100)^2)*((h-0.02)*100));% vr - Volume of the
fluidized bed(cm3)


% Moles of C in the fluidized bed
nc = 0.0074;% nc: Moles of C in fuel
mass_c =0.1;% mass_c:Mass of C particles in fuel introduced
rhoc = 1.02;%rhoc: Particle Density in g/cm3
ncvr = nc/vr; % ncvr: Moles of carbon per unit volume
ri = 107.5*1e-4; % ri: Fuel particle radius in cm.

% nCuO: Moles of CuO introduced in the fluidized bed
nCuO = 0.07547 ;% nCuO - Moles of CuO introduced in the reactor(mol CuO)
nCuOvr = nCuO/vr; % ncvr: Moles of CuO per unit volume
rcuo = 76.25*1e-4;% rcuo: Oxygen carrier particle radius in cm.

% Initial and Final Times for reaction
% For all  Temperatures: ti=0
% tf : For 885 C:105 seconds , For 900 C:65 seconds, For 935 C:30 s
%      For 950 C:20 s, For 985 C:12 s
```

```
ti = 0; % ti: Initial Time(s)
tf = 12;%tf: Final Time(s)

% Number of cells
% This parameter has been varied accordingly for different temperatures
% and for different values of alpha
% For 885 C: Number of cells=6, alpha=0.05(mentioned in pde.m), time = 105
% seconds, pO2i = 0.00831, appropriate time-temperature correlation to be
% selected in pde.m
% For 900 C: Number of cells=6 and alpha=0.05(mentioned in pde.m), time =
65
% seconds, pO2i = 0.01285, appropriate time-temperature correlation to be
% selected in pde.m
% For 935 C: Number of cells=12 and alpha=0.05(mentioned in pde.m), time =
% 30 seconds, pO2i = 0.02659, appropriate time-temperature correlation to
be
% selected in pde.m
% For 950 C: Number of cells=12 and alpha=0.05(mentioned in pde.m), time =
% 20 seconds, pO2i = 0.03305, appropriate time-temperature correlation to
be
% selected in pde.m
% For 985 C: Number of cells=20 and alpha=0.05(mentioned in pde.m), time =
% 11 seconds, pO2i = 0.04894, appropriate time-temperature correlation to
be
% selected in pde.m

% Specify number of cells
n =20;

% Independent variable for ODE integration
    tout = linspace(ti,tf,n);



% Initial conditions for the equations
    p = zeros(6,n);
    for i = 1:n
    p(1,i)=0.04894; %p(1,i):pO2e: Partial pressure of O2 in the emulsion
    p(2,i)=0.04894; %p(2,i):pO2b: Partial pressure of O2 in the bubble
    p(3,i)=0; %p(3,i):pCO2e: Partial pressure of CO2 in the emulsion
    p(4,i)=0; %p(4,i):pCO2b: Partial pressure of CO2 in the bubble
    p(5,i)=0; %p(4,i):XC: Conversion of fuel
    p(6,i)=0; %p(4,i):XCuO: Conversion of CuO
    end

pini=reshape(p,6*n,1);% pini: Rearranging the initial condition for pde.m
    % options = odeset('RelTol',1e-5,'AbsTol',1e-6);
    [t,p]=ode15s(@pde,tout,pini);

% Reshaping the answer
P = reshape(p,length(t),6,n);

% Evaluating the last partial pressures and conversions by the boundary
condition
P(:,:,n) = (4*P(:,:,n-1)-P(:,:,n-2))/3;

% Reproducing results
```

```
disp('Time:')
disp(t)
disp('Partial Pressure of O2 in emulsion corresponding to time t')
disp(P(:,1,n))
disp('Partial Pressure of O2 in bubble corresponding to time t')
disp(P(:,2,n))
disp('Partial Pressure of CO2 in emulsion corresponding to time t')
disp(P(:,3,n))
disp('Partial Pressure of CO2 in bubble corresponding to time t')
disp(P(:,4,n))
disp('Fractional conversion of fuel corresponding to time t')
disp(P(:,5,n))
disp('Fractional conversion of CuO corresponding to time t')
disp(P(:,6,n))

% Plotting for the top compartment
subplot(3,3,1)
plot(t,P(:,1,n))
xlabel('Time(seconds)')
ylabel('Partial pressure of O2 in emulsion')
title('O2 in Emulsion')
hold on
subplot(3,3,2)
plot(t,P(:,2,n))
xlabel('Time(seconds)')
ylabel('Partial pressure of O2 in bubble')
title('O2 in Bubble')
hold on
subplot(3,3,3)
plot(t,P(:,3,n))
xlabel('Time(seconds)')
ylabel('Partial pressure of CO2 in emulsion')
title('CO2 in Emulsion')
hold on
subplot(3,3,4)
plot(t,P(:,4,n))
xlabel('Time(seconds)')
ylabel('Partial pressure of CO2 in bubble')
title('CO2 in Bubble')
hold on
subplot(3,3,5)
plot(t,P(:,5,n))
xlabel('Time(seconds)')
ylabel('Conversion of fuel')
title('Conversion of fuel')
hold on
subplot(3,3,6)
plot(t,P(:,6,n))
xlabel('Time(seconds)')
ylabel('Conversion of CuO')
title('Conversion of CuO')
hold on
```

```
function rhs=pde(t,p)
% pde: This function is for evaluating the partial differential equation
%      RHS

% Problem parameters
    global h n ncvr nCuOvr rhoc ri nc vr  nCuO  v_c v_cuo v_zrO2 rcuo

    z1 = 0.0;%z1: Initial Height
    zu = h*100;%zu: Final Height
    dz = (zu-z1)/n;%dz:Height Interval

% Temperature-Time Correlations derived from experimental data
% T: Temperature (in Deg C)
% t: Time (in seconds)

% Select appropriate temperature-time correlation
% T = -0.0015*(t^2) + (0.2131*t) + 1158.1;%For 885 C
% T = -0.0069*(t^2) + (0.6275*t) + 1175;% For 900 C
% T = -0.0265*(t^2) + (1.1297*t) + 1209.3; % For 935 C
% T = -0.0697*(t^2) + (2.2634*t) + 1222.2; % For 950 C
T = -0.0901*(t^2) + (1.4583*t) + 1257.5; % For 985 C


% p1: It is a variable whose indices are being used for solve various
% variables with respect to time
%p1(1,i);i=1 to n cells:pO2e: Partial pressure of O2 in the emulsion
%p1(2,i);i=1 to n cells::pO2b: Partial pressure of O2 in the bubble
%p1(3,i);i=1 to n cells::pCO2e: Partial pressure of CO2 in the emulsion
%p1(4,i);i=1 to n cells::pCO2b: Partial pressure of CO2 in the bubble
%p1(5,i);i=1 to n cells::XC: Conversion of fuel
%p1(6,i);i=1 to n cells::XCuO: Conversion of CuO
   p1 = reshape(p,6,n);


% rhs1 representing the RHS of the material balance equation
rhs1 = zeros(6,n);

%  Introducing the boundary conditions for each of the variables
   p1(1,1)=0;
   p1(2,1)=0;
   p1(3,1)=0;
   p1(4,1)=0;
   p1(5,1)=0;
   p1(6,1)=0;

for ind=1:n-1
% Forward Difference Formula Code
% if(1<=ind<=n-1)% For statement to be changed to n-1
ibottom  = ind;    % index for i
itop = ind+1;      % index for cell i+1


% Defining variables:
% emf: Function to calculate minimum voidage for Fluidization:
% umf: Function to calculate minimum velocity in Fluidization(cm/s)
% ub: Velocity of bubble rising through the bed(cm/s)
% delta: Bubble fraction in a fluidized bed(dimensionless)
```

```
% ue: Gas velocity in emulsion (cm/s)
% fgb: Function to calculate volumetric gas fraction in bubble
% fge: Function to calculate volumetric gas fraction in emulsion
% fse: Function to calculate volumetric solid fraction in emulsion

% Parameters for evaluating emf,umf,ub,delta,ue,fgb,fge,fse
% which is employed to evaluate bed properties at a particular height

mu = viscosity(T) ;% mu: Viscosity (kg/m s)
dp = (2*rcuo)*1e-2;% dp: Diameter of CuO/ZrO2 particle(m)
rhog = (101325*43.4*1e-3)/(8.314*T);% rhog: Density of gas
(kg/m3)considered
                                    % for a 90%CO2 and 10% O2 mixture
rhos = 2140;% rhos: Density of solid(kg/m3)
u0= 0.16;% u0: Superficial velocity(m/s)
d0 =0.022;% d0 : Diameter of the bed: (m)
alpha = 0.05;% alpha: Ratio of wake volume to bubble volume
diff = diff_coeff(T);% diff: Diffusivity of O2 in CO2(m2/s)
R = 82.05746;% Value of Universal Gas Constant in (cm3 atm/mol K)

% v1,v2,v3,v4: Arrays for evaluating different properties based on
% information required by different parameters
v1=[mu,dp,rhog,rhos];% v1: Array for emf,umf
v2=[mu,dp,rhog,rhos,u0,d0,h];% v2: Array for ub,delta
v3=[mu,dp,rhog,rhos,u0,d0,alpha,h];% v3: Array for ue,us,fgb,fge,fsb,fse
v4=[mu,dp,rhog,rhos,u0,d0,alpha,diff,h];% v4: Array for kbe

% As the height of the bed is varied,hence the last element in each array
% is changed to accomodate changes in bed height
v2(1,7)=(ind*dz)/100;
v3(1,8)=(ind*dz)/100;
v4(1,9)=(ind*dz)/100;

% Checks introduced during program run
   min_v = umf(v1);
   height = v2(1,7);
   bub_fr = delta(v2);
   voidage = emf(v1);
   height = (ind*dz)/100
   fr_gb = fgb(v3)
   fr_ge=fge(v3)
   bub_vel=ub(v2);
   emul_vel=ue(v3);
   bubble_dia=db(v2);
   mass_t = kbe(v4);
   vol_fr = delta(v2);

% An IF-ELSE Statement is accomodated to run the program at t =0
% and other times at average reaction rate for fuel and CuO conversion
if(t==0)
   rhs1(1,ind) = (ue(v3)*(p1(1,itop)-p1(1,ibottom))/dz)-
(((delta(v2)*kbe(v4))/fge(v3))*(p1(1,ibottom)-p1(2,ibottom)))...
                +nCuOvr*0.25*kCuO(T)*(pO2eq(T)-((p1(1,ibottom)/2)))*(1-
p1(6,ibottom))*(1/fge(v3))*(R*T)...

ncvr*((3*kc(T))/(rhoc*ri))*(0.5*(p1(1,ibottom)^0.5))*((1-
p1(5,ibottom))^(2/3))*(1/fge(v3))*(R*T);
```

```
   rhs1(2,ind) = (ub(v2)*(p1(2,itop)-p1(2,ibottom))/dz)-
(((delta(v2)*kbe(v4))/fgb(v3))*(p1(2,ibottom)-p1(1,ibottom)));
   rhs1(3,ind) = (ue(v3)*(p1(3,itop)-p1(3,ibottom))/dz)-
(((delta(v2)*kbe(v4))/fge(v3))*(p1(3,ibottom)-p1(4,ibottom)))...

+ncvr*((3*kc(T))/(rhoc*ri))*(0.5*(p1(1,ibottom)^0.5))*((1-
p1(5,ibottom))^(2/3))*(1/fge(v3))*(R*T);
   rhs1(4,ind) = (ub(v2)*(p1(4,itop)-p1(4,ibottom))/dz)-
(((delta(v2)*kbe(v4))/fgb(v3))*(p1(4,ibottom)-p1(3,ibottom)));
   rhs1(5,ind) = ((3*kc(T))/(rhoc*ri))*((p1(1,ibottom)^0.5))*((1-
p1(5,ibottom))^(2/3));
   rhs1(6,ind) = kCuO(T)*(pO2eq(T)-(p1(1,ibottom)/2))*(1-p1(6,ibottom));
else
   sumpO2e = sum(p1(1,1:n-1));%sumpO2e: Sum of partial pressure of O2 in
emulsion
   avgpO2e = sumpO2e/(n-1);%avgpO2e: Average of partial pressure of O2 in
emulsion
   sumCuOx = sum(1-p1(6,1:n-1));%sumCuOx: Sum of (1-X)for CuO over (n-
1)intervals
   avgCuOx = sumCuOx/(n-1);%avgCuOx: Average of (1-X) for CuO over (n-
1)intervals
   avgCuOrate = kCuO(T)*(pO2eq(T)-(avgpO2e/2))*avgCuOx;%avgCuOrate:
Average of CuO reaction rate
   sumpO2h = sum((0.5*p1(1,1:(n-1))).^0.5);%sumpO2h: Sum of partial
pressure of O2 raised to half power in emulsion
   avgpO2h = sumpO2h/(n-1);%avgpO2h: Average of partial pressure of O2 in
emulsion raised to half power over (n-1)intervals
   sumCx = sum((1-p1(5,1:n-1)).^(2/3));%sumCx: Sum of (1-X)^(2/3)
   avgCx = sumCx/(n-1);%avgCx: Average of (1-X)^(2/3)over (n-1)intervals
   avgCrate = ((3*kc(T))/(rhoc*ri))*(avgpO2h)*avgCx;  %avgCrate: Average
of fuel conversion rate
   rhs1(1,ind) = (ue(v3)*(p1(1,itop)-p1(1,ibottom))/dz)-
(((delta(v2)*kbe(v4))/fge(v3))*(p1(1,ibottom)-p1(2,ibottom)))...
                +nCuOvr*0.25*avgCuOrate*(1/fge(v3))*(R*T)...
                -ncvr*avgCrate*(1/fge(v3))*(R*T);
   rhs1(2,ind) = (ub(v2)*(p1(2,itop)-p1(2,ibottom))/dz)-
(((delta(v2)*kbe(v4))/fgb(v3))*(p1(2,ibottom)-p1(1,ibottom)));
   rhs1(3,ind) = (ue(v3)*(p1(3,itop)-p1(3,ibottom))/dz)-
(((delta(v2)*kbe(v4))/fge(v3))*(p1(3,ibottom)-p1(4,ibottom)))...
                 +ncvr*avgCrate*(1/fge(v3))*(R*T);
   rhs1(4,ind) = (ub(v2)*(p1(4,itop)-p1(4,ibottom))/dz)-
(((delta(v2)*kbe(v4))/fgb(v3))*(p1(4,ibottom)-p1(3,ibottom)));
   rhs1(5,ind) = avgCrate;
   rhs1(6,ind) = avgCuOrate;
end
end
% Reshaping the obtained ns-1*nz matrix of the rhs1 as a column vector
rhs = reshape(rhs1,6*n,1);
```

```
 function u3=db(r2)
% db or u3(in this program): Effective Bubble Diameter(m)
% mu = Viscosity of Gas Mixture (kg/m s)
% dp = Diameter of particle (m)
% rhog = Density of gas (kg/m3)
% rhos = Density of solid (kg/m3)
% u0 = Superficial velocity(m/s)
% h = Height of the bed(m)
% d0 = Diameter of the bed(m)
mu=r2(1);
dp=r2(2);
rhog=r2(3);
rhos=r2(4);
u0 = r2(5);
d0 = r2(6);
h= r2(7);

g = 9.8;% g = Gravitational Constant (m/s2)
val1 = (mu/(dp*rhog));% val1 : A variable used for computing umf
val2 = ((dp^3)*rhog*(rhos-rhog)*g)/(mu^2);% val2 : A variable used for
computing umf
% Richardson and Jeronimo's Correlation(1979)
% umf: Minimum Velocity for fluidization(m/s)
% emf: Voidage at minimum fluidization
umf = val1*((((25.7^2)+(0.0365*val2))^0.5)-25.7);% u1 in m/s
emf = 0.42;%Value taken for spherical particles based on Wen and Yu(1966)
%          Sourced from p.22 - Couderc (Chapter 1:Incipient Fluidization
and
%          Particulate Systems), Fluidization 2nd. ed. : Davidson, Clift
%          and Harrison

umfcm = umf*100;%umfcm:  umf in cm/s
d0cm = d0*100; %d0cm: Diameter of bed in cm.
u0cm = u0*100; %u0cm: Superficial velocity in cm/s
hcm = h*100; % hcm: Height of fluidized bed in cm.

db0 = 0.00376*((u0cm-umfcm)^2);% db0: Bubble Diameter above
distributor,cm.(Sourced from Mori and Wen-AIChE,1975)
u3 = db0*((0.15*(hcm/db0))+0.85);%u3: Variation of bubble dimensions with
height-Zenz(1978)
```

```
function u5=delta(r2)
% delta: Function to evaluate the fraction occupied by bubbles
%        in a fluidized bed
% mu = Viscosity of Gas Mixture (kg/m s)
% dp = Diameter of particle (m)
% rhog = Density of gas (kg/m3)
% rhos = Density of solid (kg/m3)
% u0 = Superficial velocity(m/s)
% h = Height of the bed(m)
% d0 = Diameter of the bed(m)
mu=r2(1);
dp=r2(2);
rhog=r2(3);
rhos=r2(4);
u0 = r2(5);
d0 = r2(6);
h= r2(7);

g = 9.8;% g = Gravitational Constant (m/s2)
val1 = (mu/(dp*rhog));% val1 : A variable used for computing umf
val2 = ((dp^3)*rhog*(rhos-rhog)*g)/(mu^2);% val2 : A variable used for
computing umf
% umf: Minimum Velocity for fluidization
% Correlation based on Babu,Shah and Talwalkar(1978)
% emf: Voidage at minimum fluidization
umf = val1*((((25.7^2)+(0.0365*val2))^0.5)-25.7);% u1 in m/s
emf = 0.42;%Value taken for spherical particles based on Wen and Yu(1966)
%          Sourced from p.22 - Couderc (Chapter 1:Incipient Fluidization
and
%          Particulate Systems), Fluidization 2nd. ed. : Davidson, Clift
%          and Harrison
umfcm = umf*100;%umfcm:  umf in cm/s
d0cm = d0*100; %d0cm: Diameter of bed in cm.
u0cm = u0*100; %u0cm: Superficial velocity in cm/s
hcm = h*100; % hcm: Height of fluidized bed in cm.

db0 = 0.00376*((u0cm-umfcm)^2);% db0: Bubble Diameter above
distributor,cm.(Sourced from Mori and Wen-AIChE,1975)
u3 = db0*((0.15*(hcm/db0))+0.85);%u3: Variation of bubble dimensions with
height-Zenz(1978)
ub = (0.8*(u0cm-umfcm))+(0.838*((981*u3)^0.5));% Velocity of the bubble in
cm/s-Puettmann et al.(2012)
u5 = 0.8*((u0cm-umfcm)/ub);% delta: Volume Fraction of bubble in bed-
Puettmann et al.(2012)
```

```
function diff = diff_coeff(T)
% Diffusion Coefficient in m2/s
% Calculated using Fuller's correlation sourced from
% Poling, Prausnitz and O'Connell(Properties of Gases and Liquids)
patm = 1.01325;%patm - Pressure in atm
mO2 = 32;% mO2 - Molecular Mass of O2
mCO2 = 44;% mCO2- Molecular Mass of CO2
avgmw =2*((1/mO2)+(1/mCO2))^(-1);%Average Mol. Wt. of Mixture
diffvolO2 = 16.3 ;%diffvolO2 - Diffusion volume of O2
diffvolCO2 = 26.9 ;%diffvolCO2 - Diffusion volume of CO2
diffvol = ((diffvolO2^(1/3))+(diffvolCO2^(1/3)))^2;
diff = (0.00143*(T^1.75))/(patm*(avgmw^0.5)*diffvol)*1e-4;
```

```
function u2=emf(r1)
mu=r1(1);
dp=r1(2);
rhog=r1(3);
rhos=r1(4);
% emf: Function to calculate minimum voidage for Fluidization
% mu = Viscosity of Gas Mixture (kg/m s)
% dp = Diameter of particle (m)
% rhog = Density of gas (kg/m3)
% rhos = Density of solid (kg/m3)

g = 9.8;% g = Gravitational Constant (m/s2)
u2 = 0.42;%Value taken for spherical particles based on Wen and Yu(1966)
%          Sourced from p.22 - Couderc (Chapter 1:Incipient Fluidization
and
%          Particulate Systems), Fluidization 2nd. ed. : Davidson, Clift
%          and Harrison
```

```
function u8=fgb(r3)
% fgb: Function to calculate volumetric gas fraction in bubble
% mu = Viscosity of Gas Mixture (kg/m s)
% dp = Diameter of particle (m)
% rhog = Density of gas (kg/m3)
% rhos = Density of solid (kg/m3)
% u0 = Superficial velocity(m/s)
% h = Height of the bed(m)
% d0 = Diameter of the bed(m)

mu=r3(1);
dp=r3(2);
rhog=r3(3);
rhos=r3(4);
u0 = r3(5);
d0 = r3(6);
alpha = r3(7);
h= r3(8);

g = 9.8;% g = Gravitational Constant (m/s2)
val1 = (mu/(dp*rhog));% val1 : A variable used for computing umf
```

```
val2 = ((dp^3)*rhog*(rhos-rhog)*g)/(mu^2);% val2 : A variable used for
computing umf
% umf: Minimum Velocity for fluidization
% emf: Voidage at minimum fluidization
umf = val1*((((25.7^2)+(0.0365*val2))^0.5)-25.7);% u1 in m/s
% Richardson and Jeronimo's Correlation(1979)
emf = 0.42;%Value taken for spherical particles based on Wen and Yu(1966)
%          Sourced from p.22 - Couderc (Chapter 1:Incipient Fluidization
and
%          Particulate Systems), Fluidization 2nd. ed. : Davidson, Clift
%          and Harrison
umfcm = umf*100;% umf in cm/s
d0cm = d0*100; %d0cm: Diameter of bed in cm.
u0cm = u0*100; %u0cm: Superficial velocity in cm/s
hcm = h*100; % hcm: Height of fluidized bed in cm.

db0 = 0.00376*((u0cm-umfcm)^2);% db0: Bubble Diameter above
distributor,cm.(Sourced from Mori and Wen-AIChE,1975)
u3 = db0*((0.15*(hcm/db0))+0.85);%u3: Variation of bubble dimensions with
height-Zenz(1978)
ub = (0.8*(u0cm-umfcm))+(0.838*((981*u3)^0.5));% Velocity of the bubble in
cm/s-Puettmann et al.(2012)
delta = 0.8*((u0cm-umfcm)/ub);% delta: Volume Fraction of bubble in bed-
Puettmann et al.(2012)
u8 = delta*(1+(alpha*emf));



function u7=fge(r3)
% fge: Function to calculate volumetric gas fraction in emulsion
% mu = Viscosity of Gas Mixture (kg/m s)
% dp = Diameter of particle (m)
% rhog = Density of gas (kg/m3)
% rhos = Density of solid (kg/m3)
% u0 = Superficial velocity(m/s)
% h = Height of the bed(m)
% d0 = Diameter of the bed(m)

mu=r3(1);
dp=r3(2);
rhog=r3(3);
rhos=r3(4);
u0 = r3(5);
d0 = r3(6);
alpha = r3(7);
h= r3(8);

g = 9.8;% g = Gravitational Constant (m/s2)
val1 = (mu/(dp*rhog));% val1 : A variable used for computing umf
val2 = ((dp^3)*rhog*(rhos-rhog)*g)/(mu^2);% val2 : A variable used for
computing umf
% umf: Minimum Velocity for fluidization
% emf: Voidage at minimum fluidization
umf = val1*((((25.7^2)+(0.0365*val2))^0.5)-25.7);% u1 in m/s
% Richardson and Jeronimo's Correlation(1979)
emf = 0.42;%Value taken for spherical particles based on Wen and Yu(1966)
```

```
%          Sourced from p.22 - Couderc (Chapter 1:Incipient Fluidization
and
%          Particulate Systems), Fluidization 2nd. ed. : Davidson, Clift
%          and Harrison
umfcm = umf*100;% umf in cm/s
d0cm = d0*100; %d0cm: Diameter of bed in cm.
u0cm = u0*100; %u0cm: Superficial velocity in cm/s
hcm = h*100; % hcm: Height of fluidized bed in cm.

db0 = 0.00376*((u0cm-umfcm)^2);% db0: Bubble Diameter above
distributor,cm.(Sourced from Mori and Wen-AIChE,1975)
u3 = db0*((0.15*(hcm/db0))+0.85);%u3: Variation of bubble dimensions with
height-Zenz(1978)
ub = (0.8*(u0cm-umfcm))+(0.838*((981*u3)^0.5));% Velocity of the bubble in
cm/s-Puettmann et al.(2012)
delta = 0.8*((u0cm-umfcm)/ub);% delta: Volume Fraction of bubble in bed-
Puettmann et al.(2012)
u7 = (1-delta-(alpha*delta))*emf;




function u4=kbe(r4)
% kbe.m - Function to evaluate the Interchange coefficient for gas between
%         bubble and emulsion phases based on bubble volume
% Sit SP, Grace JR. Effect of bubble interaction on interphase mass
transfer in
% gas fluidized beds. Chem Eng Sci 1981;36:327-35.
% Sourced from: Gomez-Barea,A. and  Modeling of biomass gasification
% in fluidized bed
% Progress in Energy and Combustion Science 36 (2010) 444-509

% mu = Viscosity of Gas Mixture (kg/m s)
% dp = Diameter of particle (m)
% rhog = Density of gas (kg/m3)
% rhos = Density of solid (kg/m3)
% u0 = Superficial velocity(m/s)
% h = Height of the bed(m)
% d0 = Diameter of the bed(m)
% alpha = Ratio of wake volume to bubble volume
% Df = Diffusivity of O2 in CO2 (m2/s)

mu=r4(1);
dp=r4(2);
rhog=r4(3);
rhos=r4(4);
u0 = r4(5);
d0 = r4(6);
alpha = r4(7);
Df = r4(8);
h= r4(9);

g = 9.8;% g = Gravitational Constant (m/s2)
val1 = (mu/(dp*rhog));% val1 : A variable used for computing umf
val2 = ((dp^3)*rhog*(rhos-rhog)*g)/(mu^2);% val2 : A variable used for
computing umf
```

```
% umf: Minimum Velocity for fluidization
% emf: Voidage at minimum fluidization
umf = val1*((((25.7^2)+(0.0365*val2))^0.5)-25.7);% u1 in m/s
% Richardson and Jeronimo's Correlation(1979)
emf = 0.42;%Value taken for spherical particles based on Wen and Yu(1966)
%          Sourced from p.22 - Couderc (Chapter 1:Incipient Fluidization
and
%          Particulate Systems), Fluidization 2nd. ed. : Davidson, Clift
%          and Harrison
umfcm = umf*100;% umf in cm/s
d0cm = d0*100; %d0cm: Diameter of bed in cm.
u0cm = u0*100; %u0cm: Superficial velocity in cm/s
hcm = h*100; % hcm: Height of fluidized bed in cm.

db0 = 0.00376*((u0cm-umfcm)^2);% db0: Bubble Diameter above
distributor,cm.(Sourced from Mori and Wen-AIChE,1975)
db = db0*((0.15*(hcm/db0))+0.85);%u3: Variation of bubble dimensions with
height-Zenz(1978)
ub = (0.8*(u0cm-umfcm))+(0.838*((981*db)^0.5));% Velocity of the bubble in
cm/s-Puettmann et al.(2012)
Dfcm = Df*1e4; % Dfcm: Diffusivity in cm2/s
gcm = g*1e2;% gcm: g in cm/s2
u4 = ((2*umfcm)/db)+ (12*((Dfcm*emf*ub)^0.5))/(3.14*(db^1.5));
```

```
% ------------------------------------------
% Kinetic rate constants for Mexican Petcoke
% Derived from Chalmers Date
% Ac exp (-E/RT)
% Ac = g/(cm2*atm^0.5)
% E/R = 15500 (Determined from Chalmers)- Energy and Fuels paper
% Sahir, Sohn, Leion and Lighty(2012)
% ------------------------------------------------
function k1=kc(T)
k1 = 930* exp(-15500/T);% % kc  = g/(cm2*atm^0.5)s



% ------------------------------------------
% Kinetic rate constants for CuO Depomposition
% Sahir, Sohn, Leion and Lighty(2012)-Energy and Fuels
% ------------------------------------------------
function k2=kCuO(T)
% kCuO: Rate of CuO decomposition(atm-1s-1)
k2 = 3*exp(-2350/T);



function f4=pO2eq(T)
% Approximated from data from Pankrantz
% Pankratz, L. B. Thermodynamic Properties of Elements and
% Oxides Bulletin 672; U.S. Department of the Interior, Bureau of
% Mines: Washington, DC, 1982.
% pO2eq: Equilibrium partial pressure of Oxygen (atm.)
% T: Temperature (K)
f4 = 2.867848e-14*exp(2.295839e-02*(T));
```

```
function u9=ub(r2)
% ue : Gas velocity in emulsion(m/s)
% mu = Viscosity of Gas Mixture (kg/m s)
% dp = Diameter of particle (m)
% rhog = Density of gas (kg/m3)
% rhos = Density of solid (kg/m3)
% u0 = Superficial velocity(m/s)
% h = Height of the bed(m)
% d0 = Diameter of the bed(m)
mu=r2(1);
dp=r2(2);
rhog=r2(3);
rhos=r2(4);
u0 = r2(5);
d0 = r2(6);
h= r2(7);

g = 9.8;% g = Gravitational Constant (m/s2)
val1 = (mu/(dp*rhog));% val1 : A variable used for computing umf
val2 = ((dp^3)*rhog*(rhos-rhog)*g)/(mu^2);% val2 : A variable used for
computing umf
% umf: Minimum Velocity for fluidization
% Correlation based on Babu,Shah and Talwalkar(1978)
% emf: Voidage at minimum fluidization
umf = val1*((((25.7^2)+(0.0365*val2))^0.5)-25.7);% u1 in m/s
emf = 0.42;%Value taken for spherical particles based on Wen and Yu(1966)
%          Sourced from p.22 - Couderc (Chapter 1:Incipient Fluidization
and
%          Particulate Systems), Fluidization 2nd. ed. : Davidson, Clift
%          and Harrison
umfcm = umf*100;%umfcm:  umf in cm/s
d0cm = d0*100; %d0cm: Diameter of bed in cm.
u0cm = u0*100; %u0cm: Superficial velocity in cm/s
hcm = h*100; % hcm: Height of fluidized bed in cm.

db0 = 0.00376*((u0cm-umfcm)^2);% db0: Bubble Diameter above
distributor,cm.(Sourced from Mori and Wen-AIChE,1975)
u3 = db0*((0.15*(hcm/db0))+0.85);%u3: Variation of bubble dimensions with
height-Zenz(1978)
u9 = (0.8*(u0cm-umfcm))+(0.838*((981*u3)^0.5));% Velocity of the bubble in
cm/s-Puettmann et al.(2012)
```

```
function u7=ue(r3)
% ue : Gas velocity in emulsion(m/s)
% mu = Viscosity of Gas Mixture (kg/m s)
% dp = Diameter of particle (m)
% rhog = Density of gas (kg/m3)
% rhos = Density of solid (kg/m3)
% u0 = Superficial velocity(m/s)
% h = Height of the bed(m)
% d0 = Diameter of the bed(m)

mu=r3(1);
dp=r3(2);
rhog=r3(3);
rhos=r3(4);
u0 = r3(5);
d0 = r3(6);
alpha = r3(7);
h= r3(8);

g = 9.8;% g = Gravitational Constant (m/s2)
val1 = (mu/(dp*rhog));% val1 : A variable used for computing umf
val2 = ((dp^3)*rhog*(rhos-rhog)*g)/(mu^2);% val2 : A variable used for
computing umf

% umf: Minimum Velocity for fluidization
% Richardson and Jeronimo's Correlation(1979)
% emf: Voidage at minimum fluidization
u1 = val1*((((25.7^2)+(0.0365*val2))^0.5)-25.7);% u1 in m/s
umfcm = u1*100;% umf in cm/s
emf = 0.42;%Value taken for spherical particles based on Wen and Yu(1966)
%          Sourced from p.22 - Couderc (Chapter 1:Incipient Fluidization
and
%          Particulate Systems), Fluidization 2nd. ed. : Davidson, Clift
%          and Harrison

% Converting dimensions of diameter and height in cm.
d0cm = d0*100; %d0cm: Diameter of bed in cm.
u0cm = u0*100; %u0cm: Superficial velocity in cm/s
hcm = h*100; % hcm: Height of fluidized bed in cm

% Determination of bubble rise velocity
db0 = 0.00376*((u0cm-umfcm)^2);% db0: Bubble Diameter above
distributor,cm.(Sourced from Mori and Wen-AIChE,1975)
u3 = db0*((0.15*(hcm/db0))+0.85);%u3: Variation of bubble dimensions with
height
ub = (0.8*(u0cm-umfcm))+(0.838*((981*u3)^0.5));% Velocity of the bubble in
cm/s
delta = 0.8*((u0cm-umfcm)/ub);% delta: Volume Fraction of bubbles in
fluidized bed
u7 = (umfcm/emf)-((alpha*delta*ub)/(1-delta-(alpha*delta)));% u7: Rise
velocity in emulsion (cm/s)
```

```
function u1=umf(r1)
% umf: Function to calculate Minimum velocity in Fluidization
% mu = Viscosity of Gas Mixture (kg/m s)
% dp = Diameter of particle (m)
% rhog = Density of gas (kg/m3)
% rhos = Density of solid (kg/m3)
mu=r1(1);
dp=r1(2);
rhog=r1(3);
rhos=r1(4);
g = 9.8;% g = Gravitational Constant (m/s2)
val1 = (mu/(dp*rhog));% val1 : A variable used for computing umf
val2 = ((dp^3)*rhog*(rhos-rhog)*g)/(mu^2);% val2 : A variable used for
computing umf
u1m = val1*((((25.7^2)+(0.0365*val2))^0.5)-25.7);% Velocity in m/s
% Richardson and Jeronimo's Correlation(1979)
u1 = u1m*100;% Velocity in cm/s

function visc =viscosity(T)
% Implementation of gas viscosity Neufeld correlation
% Sourced from
% Poling, Prausnitz and O'Connell(Properties of Gases and Liquids)
A=1.16145;
B=0.14874;
C=0.52487;
D=0.77320;
E=2.16178;
F=2.43787;
yCO2 = 0.95;
yO2 = 0.05;
 % For CO2
% eps/k
% Chapman Enskog Correlation
epskco2 =  195.2;
sigmaco2 = 3.941;
TCO2 = T/epskco2;
coll_CO2=(A*(TCO2^(-B)))+(C*exp(-D*TCO2))+(E*exp(-F*TCO2));
MCO2 =  44.00;
viscCO2 = (26.69*((MCO2*T)^0.5))/((sigmaco2^2)*(coll_CO2))*1e-7;

% For O2
% eps/k
% Chapman Enskog Correlation
epsko2 =  106.7;
sigmao2 = 3.467;
TO2 = T/epsko2;
coll_O2=(A*(TO2^(-B)))+(C*exp(-D*TO2))+(E*exp(-F*TO2));
MO2 =   32.00;
viscO2 = (26.69*((MO2*T)^0.5))/((sigmao2^2)*(coll_O2))*1e-7;

% Gas Mixture Viscosity estimation of CO2 and O2 from Wilke et al.
term1 = ((1+(((viscO2/viscCO2)^0.5)*((MCO2/MO2)^0.25))))^0.5;
phi12 = term1/(8*((MO2/MCO2)+1))^0.5;
phi21 = phi12*(viscCO2/viscO2)*(MO2/MCO2);
visc = (viscO2*yO2)/(yO2+(yCO2*phi12))+(viscCO2*yCO2)/(yCO2+(yO2*phi21));
```

APPENDIX B

ESTABLISHING A RELATIONSHIP BETWEEN MOLE RATIO AND CONVERSION

Case 1: Conversion of CuO in the fuel reactor

The conversion of CuO in the fuel reactor is represented by X_{CuO} which can also be defined as:

$$X_{CuO} = \frac{Moles\ of\ CuO\ reacted\ in\ the\ fuel\ reactor}{Moles\ of\ CuO\ introduced\ in\ the\ fuel\ reactor} \quad \text{(B.1)}$$

$$(1 - X_{CuO}) = 1 - \frac{Moles\ of\ CuO\ reacted\ in\ the\ fuel\ reactor}{Moles\ of\ CuO\ introduced\ in\ the\ fuel\ reactor} \quad \text{(B.2)}$$

Equation B.2 can also be expressed as:

$$(1 - X_{CuO})$$

$$= \frac{(Moles\ of\ CuO\ introduced\ in\ the\ fuel\ reactor) - (Moles\ of\ CuO\ reacted\ in\ the\ fuel\ reactor)}{Moles\ of\ CuO\ introduced\ in\ the\ fuel\ reactor} \quad \text{(B.3)}$$

$$(1 - X_{CuO}) = \frac{Moles\ of\ CuO\ exiting\ the\ fuel\ reactor}{Moles\ of\ CuO\ introduced\ in\ the\ fuel\ reactor} \quad \text{(B.4)}$$

In terms of Cu, Equation B.4 could also be written as:

$$(1 - X_{CuO}) = \frac{Moles\ of\ Cu\ associated\ with\ CuO\ exiting\ the\ fuel\ reactor}{Moles\ of\ Cu\ associated\ with\ CuO\ introduced\ in\ the\ fuel\ reactor} \quad \text{(B.5)}$$

Multiplying and dividing by the total moles of Cu circulating in the system

$$(1 - X_{CuO}) = \left[\frac{Moles\ of\ Cu\ associated\ with\ CuO\ exiting\ the\ fuel\ reactor}{Moles\ of\ Cu\ \ circulating\ in\ the\ system}\right] \times$$

$$\left[\frac{Moles\ of\ Cu\ \ circulating\ in\ the\ system}{Moles\ of\ Cu\ associated\ with\ CuO\ introduced\ in\ the\ fuel\ reactor}\right] \quad \text{(B.6)}$$

The mole ratio has been defined as:

$$Y_{CuO} = \frac{N_{CuO}}{N_{CuO}+2N_{Cu_2O}} = \frac{N_{CuO}}{N_{Cu}} \quad \text{(B.7)}$$

where N_{CuO} are moles of CuO, N_{Cu_2O} are moles of Cu_2O, and N_{Cu} are the moles of Cu.

If the mole ratio is defined at the exit of a reactor stream, then in accordance to Equation B.7, a mole ratio at the outlet of the fuel reactor stream could be defined as:

$$Y_{CuO,FR} = \left[\frac{Moles\ of\ Cu\ associated\ with\ CuO\ exiting\ the\ fuel\ reactor}{Moles\ of\ Cu\ \ circulating\ in\ the\ system}\right] \quad \text{(B.8)}$$

If the mole ratio is defined at the exit of a reactor stream, then in accordance to Equation B.7, a mole ratio at the outlet of the air reactor stream (or at the inlet of the fuel reactor) could be defined as:

$$Y_{CuO,AR} = \left[\frac{Moles\ of\ Cu\ associated\ with\ CuO\ exiting\ the\ air\ reactor}{Moles\ of\ Cu\ \ circulating\ in\ the\ system}\right] \quad \text{(B.9)}$$

Thus,
$$(1 - X_{CuO}) = \frac{Y_{CuO,FR}}{Y_{CuO,AR}} \quad \text{(B.10)}$$

If ΔY_S is defined as the difference between the mole ratios between the fuel and the air reactor, $\Delta Y_S = Y_{CuO,FR} - Y_{CuO,AR}$, then:

$$X_{CuO} = \frac{\Delta Y_S}{Y_{CuO,AR}} \quad \text{(B.11)}$$

Case 2: Conversion of Cu_2O in the air reactor

The conversion of Cu_2O in the air reactor is represented by X_{Cu_2O} which can also be defined as:

$$X_{Cu_2O} = \frac{Moles\ of\ Cu_2O\ reacted\ in\ the\ air\ reactor}{Moles\ of\ Cu_2O\ introduced\ in\ the\ air\ reactor} \quad (B.12)$$

By the reaction $Cu_2O + ½\ O_2 \rightarrow 2CuO$

$$\frac{N_{Cu_2O,in\ AR} - N_{Cu_2O,out\ AR}}{1} = \frac{N_{CuO,in\ AR} - N_{CuO,out\ AR}}{-2} \quad (B.13)$$

where $N_{Cu_2O,in\ AR}$ are the moles of Cu_2O at the air reactor inlet.

$$N_{CuO,out\ AR} - N_{CuO,in\ AR} = 2(N_{Cu_2O,in\ AR} - N_{Cu_2O,out\ AR}) \quad (B.14)$$

$$N_{CuO,out\ AR} = N_{CuO,in\ AR} + 2N_{Cu_2O,in\ AR}X_{Cu_2O} \quad (B.15)$$

as $N_{Cu_2O,out\ AR} = N_{Cu_2O,in\ AR}(1 - X_{Cu_2O})$

considering that 1 mole of CuO has 1 mole of Cu atoms and 1 mole of Cu_2O has 2 moles of Cu atoms. For analyzing, it is further considered that Cu exists in two forms, only CuO and Cu_2O, in a CLOU system.

Interpreting Equation B.15 in terms of an element balance for Cu

$$N_{Cu,out\ AR} =$$

$$N_{Cu,in\ AR} + 2X_{Cu_2O}\left[\frac{(Total\ moles\ of\ Cu) - (Cu\ associated\ in\ CuO\ at\ the\ air\ reactor\ inlet)}{2}\right] \quad (B.16)$$

Applying the definition of the mole ratio as mentioned in Equation B.7 and dividing Equation B.16 by the total moles of Cu circulating in the system yields:

$$Y_{CuO,out\ AR} = Y_{CuO,in\ AR} + X_{Cu_2O}(1 - Y_{CuO,in\ AR}) \quad (B.17)$$

As the inlet of the air reactor has identical conditions to the fuel reactor outlet, hence

$$Y_{CuO,out\ AR} = Y_{CuO,out\ FR} + X_{Cu_2O}(1 - Y_{CuO,out\ FR}) \quad \text{(B.18)}$$

Thus the conversion can be expressed as:

$$X_{Cu_2O} = \frac{Y_{CuO,out\ AR} - Y_{CuO,out\ FR}}{(1 - Y_{CuO,out\ FR})} \quad \text{(B.19)}$$

Equation B.19 could be also expressed in terms of a difference of mole ratio ΔY_S as:

$$X_{Cu_2O} = \frac{Y_{CuO,AR} - Y_{CuO,FR}}{(1 - Y_{CuO,FR})} = \frac{\Delta Y_S}{(1 - Y_{CuO,FR})} \quad \text{(B.20)}$$

APPENDIX C

A PRELIMINARY FRAMEWORK FOR EXPLORING THE CLOU PROCESS WITH SOLID FUELS

A preliminary conceptual framework for the fuel reactor in the CLOU process based on engineering approximations has been investigated by considering the effect of equilibrium and taking into consideration global coal char kinetic models. The significant assumptions for the framework are the following.

The solid fuel has been assumed to be carbon for simplicity of analysis. This eliminates complications associated with the combustion of the volatiles that would be released by most solid fuels. The emphasis on carbon is motivated by the fact that carbon gasification has been shown to be the limiting factor in the combustion of coals and petroleum cokes[1-7] and significant progress has been made in developing CLC for gaseous compounds representative of volatiles.

It is assumed that the partial pressure of O_2 at the surface of the CuO particle is at equilibrium conditions. In this study, the case of mass transfer of O_2 from the CuO particle is assumed to be rate controlling as a first approximation for design.

The effect of chemical reaction of the carbon is included by using the empirical fit of data on carbon burnout based on its external surface area developed by Hurt and Mitchell[8] and Hamor and Smith.[9]

The mass transfer coefficient is calculated assuming a Sherwood Number of 2 and obtaining the diffusivity of oxygen in carbon-dioxide using Fuller's correlation.[10]

A mathematical relationship accounting for the equilibrium oxygen concentration at the CuO surface, followed by the transfer of O_2 through the boundary layer around the surface of the CuO and C particles and the subsequent consumption of O_2 at the C surface was developed. Figure C.1 is a schematic representing the various oxygen concentrations taken into account in the analysis.

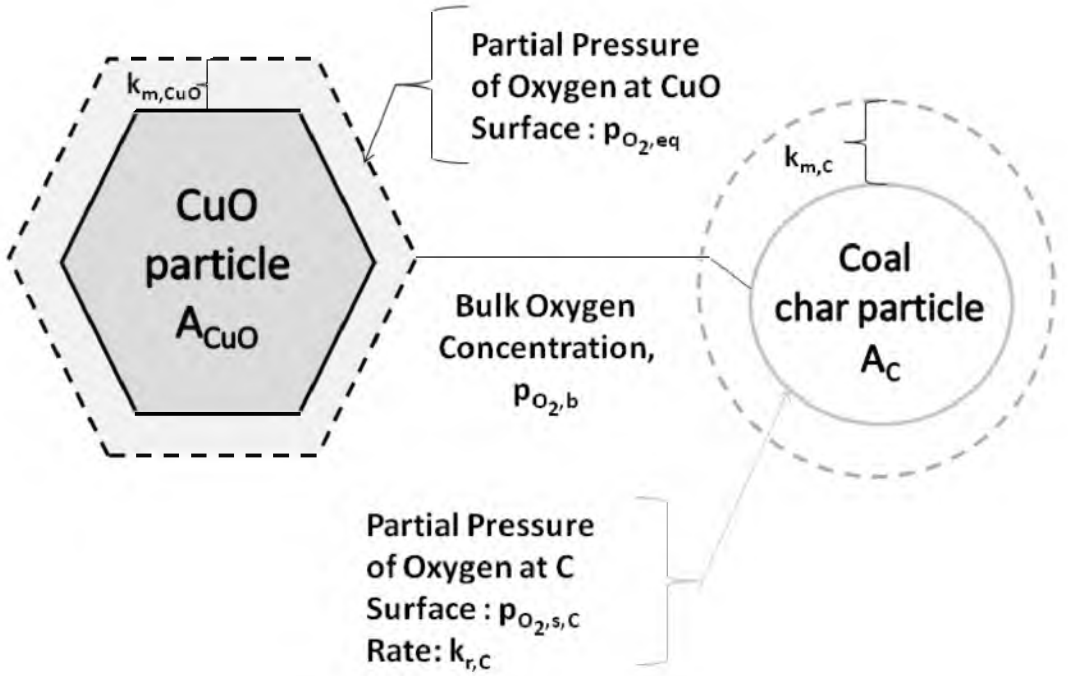

Figure C.1 Schematic representing oxygen concentrations utilized in the analysis

For the case when the release of O_2 from the CuO is controlled by mass transfer, the molar rate of oxygen transferred from CuO particles in a fuel reactor is then given by:

$$\dot{N}_{O_2,CuO} = k_{m,CuO}A_{CuO}\left(\frac{p_{O_{2,e}}}{RT} - \frac{p_{O_{2,b}}}{RT}\right)\left(\left(\frac{\sigma_{P,CuO}}{V_R}\right)V_R\right) \quad \text{(C.1)}$$

The surface oxygen partial pressure on a carbon particle and the bulk oxygen partial pressure around the particle can be related by equating the mass rate of oxygen transfer from bulk environment to the surface of the carbon particle and the mass consumption of oxygen at the surface of the carbon particle,

$$k_{m,C}A_C M_C\left(\frac{p_{O_{2,b}}}{RT} - \frac{p_{O_{2,s}}}{RT}\right) = k_{r,C}A_C {p_{O_{2,s}}}^{1/2} \quad \text{(C.2)}$$

Consequently, the molar rate of oxygen mass transfer to the surface of carbon particles in a fuel reactor can be expressed as:

$$\dot{N}_{O_2,C} = k_{m,C}A_C\left(\frac{p_{O_{2,b}}}{RT} - \frac{p_{O_{2,s}}}{RT}\right)\left(\left(\frac{\sigma_{P,C}}{V_R}\right)V_R\right) \quad \text{(C.3)}$$

The bulk oxygen concentration can be obtained by equating the molar rate of oxygen release from the CuO particles to the mass transfer at the carbon surface; that is, equating the right hand sides of Equations C.1 and C.3:

$$\left(p_{O_{2,e}} - p_{O_{2,b}}\right) = \left(\frac{k_{m,C}A_C}{k_{m,CuO}A_{CuO}}\right)\left[\frac{\left(\frac{\sigma_{P,C}}{V_R}\right)}{\left(\frac{\sigma_{P,CuO}}{V_R}\right)}\right]\left(p_{O_{2,b}} - p_{O_{2,s}}\right) \quad \text{(C.4)}$$

Equation C.4 can be simplified to yield an expression in surface oxygen partial pressure, $p_{O_{2,s}}$.

$$p_{O_{2,s}} = \frac{\left((\lambda+1)p_{O_{2,b}} - p_{O_{2,e}}\right)}{\lambda} \tag{C.5}$$

where, $\lambda = \left(\frac{k_{m,C}A_C}{k_{m,CuO}A_{CuO}}\right)\left[\frac{\left(\frac{\sigma_{P,C}}{V_R}\right)}{\left(\frac{\sigma_{P,CuO}}{V_R}\right)}\right]$ (C.6)

By equating the surface oxygen partial pressures which are obtained from Equations C.3 and C.5, Equation C.7 is obtained:

$$\frac{2}{\lambda}p_{O_{2,b}} + \left(\frac{k_{r,C}RT}{k_{m,C}M_C}\right)\left[4p_{O_{2,b}} + \left(\frac{k_{r,C}RT}{k_{m,C}M_C}\right)^2\right]^{1/2} - \frac{2}{\lambda}p_{O_{2,e}} - \left(\frac{k_{r,C}RT}{k_{m,C}M_C}\right)^2 = 0 \tag{C.7}$$

This equation can be solved to obtain the bulk oxygen concentration as a function of two coefficients, λ, which provides a measure of the ratio of loadings of carbon to CuO and $\left(\frac{k_{r,C}RT}{k_{m,C}M_C}\right)$ which provides a measure of the ratio of reaction rate to the mass transfer coefficient for the carbon. Table C.1 represents the magnitudes of pre-exponential factors and activation energies of the coals used in the analysis.

Figure C.2 represents the bulk partial pressure of oxygen vs. λ for three coals – Pittsburgh#8,[8] Pocahontas,[8] and Australian brown coal.[9] Examining this figure yields the following important conclusions.

Table C.1 Magnitudes of pre-exponential factors and activation energies of coal chars employed in analysis

Coal	Pre-exponential factor ($g\ C/cm^2 s\ atm^{0.5}$)	Activation energy (kcal/mol)
Pittsburgh#8 (Hurt and Mitchell) [8]	29	24
Pocahontas (Hurt and Mitchell) [8]	114	30
Australian Brown Coal (Hamor and Smith) [9]	9.3	16.2

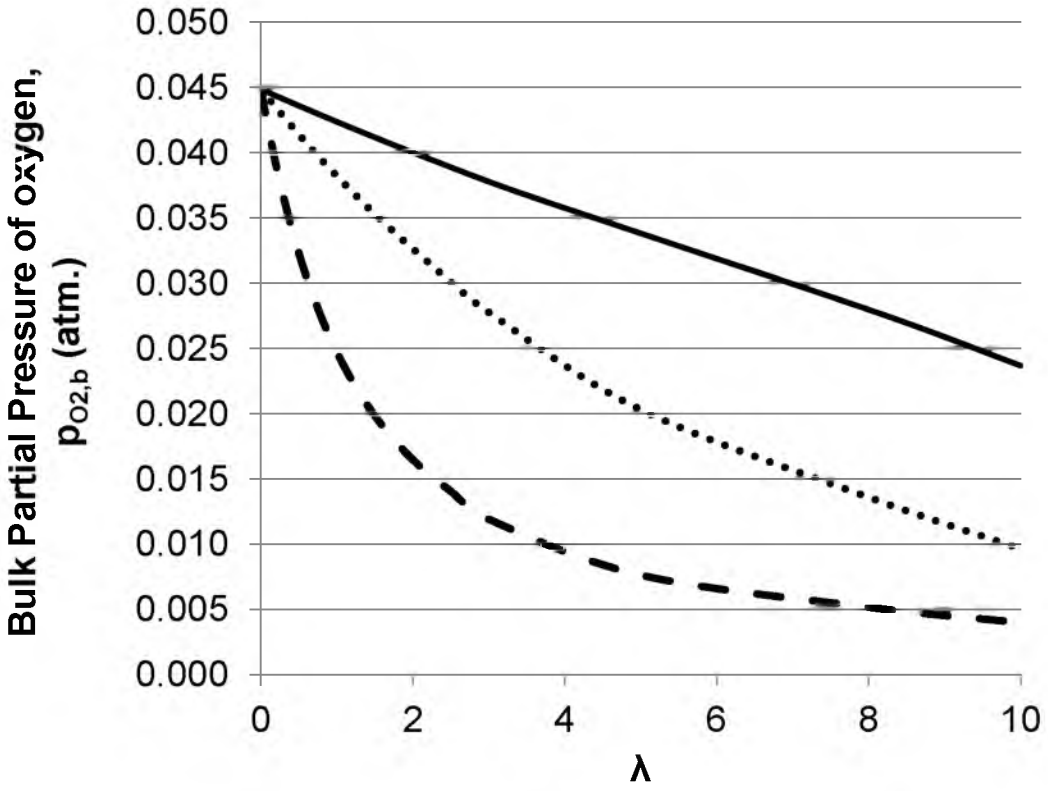

Figure C.2 Bulk partial pressure of oxygen vs. λ (— Pocahontas (Rate Equation from Hurt and Mitchell[8]), ··· Pittsburgh#8 (Rate Equation from Hurt and Mitchell[8]), - - Brown coal (Rate Equation from Hamor and Smith[9])

It captures the effect of the ratio of carbon particles introduced with respect to the CuO decomposing to release oxygen, and its sensitivity to the reactivity of coal. According to Donsi et al.[11] and Bittanti et al.[12], char loading is an important variable in fluidized-bed combustion systems as it is an indicator of the potential energy available. An excessive increase in bed temperature may occur if char or carbon loading increases. On the other end of the spectrum, low levels of char content causes difficulties in controlling combustion power. The combustion efficiency and NOx emissions are also affected by char loading.

As the reactivity of the coal increases, the bulk oxygen partial pressure decreases. With the decrease in the diameter of the coal particles, the bulk oxygen partial pressure approaches the equilibrium oxygen partial pressure conditions.

The preliminary evaluation based on simplified engineering approximations reiterates the need of adequately identifying the controlling factors in gas-solid reactions occurring in the CLOU process. The difference in the outlet oxygen profiles indicating a faster consumption of oxygen in highly reactive coals like lignite as compared to petcoke can be observed in experimental traces reported by experiments conducted at Chalmers University.[4,5] The role of reactivity of coal and its effect on oxygen carrier inventory for a CLOU process to attain 95% carbon capture efficiency at 925°C has been investigated at CSIC[13], with magnitudes ranging from 45 kg/MW_{th} using lignite to 490 kg MW_{th} for anthracite. The oxygen carrier employed in their study was 60% CuO supported on $MgAl_2O_4$.

C.1 Nomenclature

Symbols

A	surface area, cm^2
$k_{r,C}$	reaction rate constant for coal char oxidation, $g/cm^2 (atm)^{0.5} s$
k_m	mass transfer coefficient, cm/s
N	moles, mol
M	molecular weight, g/mol
p_{O_2}	partial pressure of oxygen, atm
$p_{O_{2,b}}$	partial pressure of oxygen at bulk, atm
$p_{O_{2,e}}$	partial pressure of oxygen at equilibrium, atm
$p_{O_{2,s}}$	partial pressure of oxygen at surface, atm
r	radius, cm
R	universal gas constant, cm^3 atm mol^{-1} K^{-1}
T	temperature, K
V_R	volume of reactor, cm^3

Greek Symbols

λ	parameter (Defined in equation C.6)
σ_P	number of particles
ρ	density, g/cm^3

Subscripts

b	bulk phase
C	carbon

CuO	cupric oxide
Cu_2O	cuprous oxide
e	equilibrium
O_2	oxygen
s	surface

C.2 References

1. Lewis, W. K.; Gilliland, E. R.; Sweeney, M. P., Gasification of Carbon, Metal Oxides in a Fluidized Powder Bed. *Chem. Eng. Prog.* **1951,** *47*, 251-256.

2. Lewis, W. K.; Gilliland, E. R., Production of pure carbon dioxide. U.S. Patent 2,665,971 and U.S. Patent 2,665,972, January 12,1954.

3. Mattisson, T.; Lyngfelt, A.; Leion, H., Chemical-looping with oxygen uncoupling for combustion of solid fuels. *International Journal of Greenhouse Gas Control* **2009,** *3* (1), 11-19.

4. Mattisson, T.; Leion, H.; Lyngfelt, A., Chemical-looping with oxygen uncoupling using CuO/ZrO_2 with petroleum coke. *Fuel* **2009,** *88* (4), 683-690.

5. Leion, H.; Mattisson, T.; Lyngfelt, A., Combustion of a German Lignite Using Chemical-looping With Oxygen uncoupling (CLOU). In *The 33rd International Technical Conference on Coal Utilization & Fuel Systems*, Clearwater,FL, 2008.

6. Leion, H.; Mattisson, T.; Lyngfelt, A., Solid fuels in chemical-looping combustion. *International Journal of Greenhouse Gas Control* **2008,** *2* (2), 180-193.

7. Leion, H.; Mattisson, T.; Lyngfelt, A., The use of petroleum coke as fuel in chemical-looping combustion. *Fuel* **2007,** *86* (12-13), 1947-1958.

8. Hurt, R. H.; Mitchell, R. E., Unified high-temperature char combustion kinetics for a suite of coals of various rank. *Symposium (International) on Combustion* **1992,** *24* (1), 1243-1250.

9. Hamor, R. J.; Smith, I. W.; Tyler, R. J., Kinetics of Combustion of a Pulverized Brown Coal Char between 630 and 2200 K. *Combust. Flame* **1973,** *21* (2), 153-162.

10. Poling, B. E.; Prausnitz, J. M.; O Connell, J. P., *The Properties of Gases and Liquids*. 5th ed.; Mc-Graw Hill: New York, 2001.

11. Donsi, G.; Massimilla, L.; Miccio, M.; Russo, G.; Stecconi, P., The Calculation of Carbon Load and Axial Profiles of Oxygen Concentration in the Bed of a Fluidized Combustor. *Combustion Science and Technology* **1979,** *21*(1-2), 25-33.

12. Bittanti, S.; Bolzern, P; Campi, M.C., A Model of a Bubbling Fluidized Bed Combustor Oriented to Char Mass Estimation. IEEE Transactions on Control Systems Technology **2000,***8*(2),247-256.

13. Adánez-Rubio, I.; Abad, A.; Gayán, P.; de Diego, L. F.; García-Labiano, F.; Adánez, J., Performance of CLOU process in the combustion of different types of coal with CO_2 capture. *International Journal of Greenhouse Gas Control* **2013,** *12* (0), 430-440.